International Geology Review

Vol. 1, No. 10 October 1959

Page

THE SYSTEM OF CARBONATE EQUILIBRIA
by A. V. Kazakov, M. M. Tikhomirova, and V. I. Plotnikova 1

VOLCANIC ACTIVITY ON THE MOON
by N. A. Kozyrev 40

CHRYSOLITES OF YAKUTIA'S KIMBERLITE PIPES AS PRECIOUS STONES FOR THE JEWELRY INDUSTRY
by I. V. Ilin, N. A. Kuryleva, L. A. Popugayeva, and Ya. B. Sigal 45

ON CENOZOIC VERTEBRATES IN KOREA
by Fuyuji Takai 47

THE MANGANESE ORES
by Paul Ramdohr 52

CONTRIBUTION TO THE STUDY OF SEDIMENTARY MANGANESE DEPOSITS
by H. Marchandise 73

REVIEW SECTION 78

- complete table of contents inside -

published by the
AMERICAN GEOLOGICAL INSTITUTE

The American Geological Institute operates under the National Academy of Sciences. It is governed by an Executive Committee and a Board of Directors composed of two directors from each of the fourteen Member Societies.

International Geology Review is published monthly by the American Geological Institute with the assistance of an initiating grant from the National Science Foundation. The journal will report, in English, significant contributions to pure and applied research in the earth sciences which appear in foreign-language journals, especially those published in the U.S.S.R.

The editors of International Geology Review will give consideration to full English translations, condensations, and reviews submitted voluntarily for publication. Translators will be appropriately credited.

Readers are invited to direct to the editors their comments and discussions of articles published in the International Geology Review. Readers are encouraged also to submit suggestions as to published foreign literature considered worthy of translation and publication. Such suggestions should relate to materials of broad, general interest, rather than materials of limited reader interest.

Address editorial and subscription inquiries to

AGI TRANSLATIONS OFFICE
AMERICAN GEOLOGICAL INSTITUTE
2101 Constitution Avenue, N.W., Washington 25, D. C.

The basic subscription rate for International Geology Review is $55 per year, 12 issues. A special subscription rate of $15 per year is available to members of AGI Member Societies who are on the GEOTIMES mailing list and who will pledge to restrict the journal to their personal use. The $15 per year subscription rate is also available to educational institutions and personnel. Foreign postage: No additional charge to Canada and Mexico; to Pan American Union countries add $0.50 per year; to all other foreign countries add $1.00 per year. Single copy price $5.00 ($1.50 to subscribers qualifying for special rates). Second class postage paid at Washington, D. C.

International Geology Review

published monthly by the
AMERICAN GEOLOGICAL INSTITUTE

Vol. 1, No. 10. October 1959

CONTENTS

	Page
IGR TRANSLITERATION OF RUSSIAN	ii
THE SYSTEM OF CARBONATE EQUILIBRIA, by A. V. Kazakov, M. M. Tikhomirova, and V. I. Plotnikova, translated by V. P. Sokoloff	1
VOLCANIC ACTIVITY ON THE MOON, by N. A. Kozyrev, translated by Edgar Huston	40
CHRYSOLITES OF YAKUTIA'S KIMBERLITE PIPES AS PRECIOUS STONES FOR THE JEWELRY INDUSTRY, by I. V. Ilin, N. A. Kuryleva, L. A. Popugayeva, and Ya. B. Sigal, prepared by the United States Joint Publications Research Service	45
ON CENOZOIC VERTEBRATES IN KOREA, by Fuyuji Takai, translated by the author	47
THE MANGANESE ORES, by Paul Ramdohr, translated by W. O. J. Groeneveld Meijer	52
CONTRIBUTION TO THE STUDY OF SEDIMENTARY MANGANESE DEPOSITS, by H. Marchandise, translated by W. O. J. Groeneveld Meijer	73

REVIEW SECTION

MIGRATION OF GAS AND OIL, by V. A. Sokolov, a synopsis by Paul A. Witherspoon and W. D. Romey	78
GEOLOGICAL STRUCTURE OF THE U. S. S. R., A. P. Markovsky, chief editor, a review by Eugene A. Alexandrov.	84
SOVIET BLOC INTERNATIONAL GEOPHYSICAL YEAR INFORMATION: ARCTIC AND ANTARCTIC, prepared by the U. S. Department of Commerce, Office of Technical Services	90

IGR TRANSLITERATION OF RUSSIAN

The AGI Translation Center has adopted the essential features of Cyrillic Transliteration recommended by the U. S. Department of the Interior, Board of Geographical Names, Washington, D. C.

Alphabet		transliteration
А	а	a
Б	б	b
В	в	v
Г	г	g
Д	д	d
Е	е	e, ye (1)
Ё	ё	ë, yë
Ж	ж	zh
З	з	z
И	и	i (2)
Й	й	y
К	к	k
Л	л	l
М	м	m
Н	н	n
О	о	o
П	п	p
Р	р	r
С	с	s
Т	т	t
У	у	u
Ф	ф	f
Х	х	kh
Ц	ц	ts
Ч	ч	ch
Ш	ш	sh
Щ	щ	shch
Ъ	ъ	" (3)
Ы	ы	y
Ь	ь	' (3)
Э	э	e
Ю	ю	yu
Я	я	ya

However, the AGI Translation Center recommends the following modifications:

1. Ye initially, after vowels, and after ъ, ь. Customary usage calls for "ie" in many names, e.g., SOVIET KIEV, DNIEPER, etc.; or "ye", e.g., BYELORUSSIA, where "e" follows consonants. "e" with dieresis in Russian should be given as "yo".

2. Omitted if preceding a y, e.g., Arkhangelsky (not iy; not ii).

3. Generally omitted.

NOTE: The well-known place and personnel names that have wide acceptance in international literature will be here adopted. However, German-type transliteration e.g., J for Y will not be used.

THE SYSTEM OF CARBONATE EQUILIBRIA[1]

by

A. V. Kazakov, M. M. Tikhomirova, and V. I. Plotnikova

• *translated by V. P. Sokoloff* •

ABSTRACT

The occurrence of dolomites with phosphorites in geosynclinal areas of the U. S. S. R., the wide distribution of dolomitic sediments in the Paleozoic and their absence in the Jurassic and Cretaceous of the Russian platform, and the absence of dolomite formation in modern marine sediments have led to the study of their origin. The possibility of a simultaneous (synchronous) development of phosphorites and dolomites (magnesites) is excluded. Concurrence is explained by subsequent impositions of diagenetic and epigenetic dolomites on previously deposited phosphate. Primary dolomites are negative prospecting indicators for phosphorites; secondary dolomites are not. Analysis of magnesite and dolomite systems at the 20°, 60°, and 150°C isotherms is offered in the experimental part of this report. Fields of crystallization and stability are defined for nesquehonite, magnesite, dolomite, basic magnesium carbonate (artinite and hydromagnesite), and brucite systems. --G. E. Denegar.

CONTENTS

TEXT

Abstract 1
Introduction 2
Field of high CO_2 concentrations (the nesquehonite field) 3
System of equilibria 3
Mineralogy of nesquehonite and lansfordite .. 7
Field of low CO_2 concentrations 12
Field of intermediate CO_2 concentrations 14
Method of magnesium supersaturation of solutions 14
Nesquehonite hydrolysis, procedure and results 15
Discussion 16
Effect of sea-water constituents on MgO-CO_2-H_2O system at 20°C 17
NaCl background 17
$MgSO_4$ background 17
Sea-water background 18
The 60°C isotherm (MgO-CO_2-H_2O system unconfined) 20
The 150°C isotherm (MgO-CO_2-H_2O system confined) 24
The dolomite system (CaO-MgO-CO_2-H_2O) 26
The method of slow mixing of Ca and Mg bicarbonate solutions while aerating with atmospheric air 26
The method of slow mixing of magnesium bicarbonate and calcium hydroxide solutions (using $Mg(HCO_3)_2 \cdot H_2O \cdot Ca(OH)_2$) 26
Effects of sea-water constituents on CaO-MgO-CO_2-H_2O system at 20°C 28
The 60°C isotherm in a semiopen CaO-MgO-CO_2-H_2O system and the 150°C isotherm in a closed system 28
Conditions of dolomite and magnesite formation in sedimentary rocks 30
Comparison of geochemical indices in environments of dolomite and magnesite sedimentation with those of apatite precipitated from sea water 30
Settling environment for apatite in natural basins 32
Conclusions 33
References 34

FIGURES

1. A review diagram of the MgO-CO_2-H_2O system equilibrium 6
2. Dynamics of system equilibria 7
3. Photomicrographs of nesquehonite particles 8
4. Nesquehonite thermogram 10
5. Ignition curve for Caucasian hydromagnesite 10
6. Differential ignition curves for basic magnesium carbonates 11
7. Lansfordite crystals 11
8. Equilibrium titration curve for $Mg(OH)_2$ ... 12
9. Dynamics of alkaline reserve of the MgO-CO_2-H_2O system during interactions between aqueous $Mg(OH)_2$ suspensions and increasing quantities of CO_2 12
10. Brucite thermogram 14
11. The rate of crystallization of basic magnesium carbonates from solutions supersaturated with magnesium ions 14
12. Dynamics of the alkaline reserve in the hydrolysis of nesquehonite 15
13. Dynamics of alkaline reserve in the MgO-CO_2-H_2O system 17
14. MgO-CO_2-H_2O and CaO-MgO-CO_2-H_2O systems in equilibrium 24
15. Magnesite rhombohedra 26

[1]Translated from Sistema karbonatnykh ravnovesy (dolomit, magnesit): Akademiya Nauk SSSR, Instituta Geologicheskikh Nauk, Trudy, 1957, no. 152, p. 13-58; Geologicheskaya Seriya no. 64.

16. Dolomite rhombohedra 30
17. Seasonal changes in the hydrochemical regimen of Lake Elton brine 30

TABLES

1. Analytical data on the $MgO-CO_2-H_2O$ system in equilibrium in the field of high concentrations of carbonic acid at 20^oC 5

2. Characteristics of the $CaO-CO_2-H_2O$ system in equilibrium 5

3. Specific gravity and optical characteristics of nesquehonite 8

4. Losses of CO_2 by air-dry coarsely crystalline nesquehonite and losses of H_2O by finely crystalline nesquehonite on heating 9

5. Debyeogram of nesquehonite, $MgCO_3 \cdot 3H_2O$ 9

6. Specific gravity and crystallographic and optical characteristics of lansfordite, $MgCO_3 \cdot 5H_2O$ 12

7. Results of analyses of liquid and solid phases of the $MgO-CO_2-H_2O$ system in the field of low carbonic acid concentrations 13

8. Results of analyses of liquid and solid phases of the $MgO-CO_2-H_2O$ system at assumed equilibria in the field of intermediate carbonic acid concentrations 15

9. Results of analyses of liquid and solid phases of $MgO-CO_2-H_2O$ system at assumed equilibrium in the field of intermediate carbonic acid concentrations.... 16

10. Results of analyses of liquid and solid phases in equilibrium in the $MgO-CO_2-H_2O$ system in a NaCl background 18

11. Results of analyses of liquid and solid phases of the $MgO-CO_2-H_2O$ system in equilibrium at 20^oC in a $MgSO_4$ background 19

12. Analyses of reagents used in $MgO-CO_2-H_2O$ system experiments in a background of sea water 20

13. Results of analyses of liquid and solid phases of $CaO-MgO-CO_2-H_2O$ in equilibrium in sea water at 150^oC 22

14. Results of analyses of liquid and solid phases at equilibrium in an open magnesium supersaturated $MgO-CO_2-H_2O$ system at 60^oC 21

15. Results of analyses of liquid and solid phases at equilibrium in a confined $MgO-CO_2-H_2O$ system at 150^oC 25

16. Results of analyses of liquid and solid phases at equilibrium in an open $MgO-CO_2-H_2O$ system at 20^oC 27

17. Results of analyses of liquid and solid phases at equilibrium in an open $CaO-MgO-CO_2-H_2O$ system at 20^oC 27

18. Results of analyses of the liquid phase at equilibrium in the $CaO-MgO-CO_2-H_2O$ system at 20^oC in a NaCl background..... 28

19. Results of analyses of liquid and solid phases in equilibrium in the $CaO-MgO-CO_2-H_2O$ system at 60^o and 150^oC 29

20. Characteristic geochemical indices for aqueous solutions from which dolomite and magnesite are crystallized (in equilibrium) 31

21. Hydrochemical indices of Lake Elton brine (monthly averages for 1934) 31

22. Hydrochemical indices of Lake Sakskoye brine for different degrees of salinity (evaporation) 32

23. Hydrochemical indices for marine waters of ordinary salinity and for fresh water ... 33

INTRODUCTION

Magnesium carbonates, dolomite and magnesite, are a tough riddle among carbonate sediments even now. The extensive distribution of dolomites in ancient sediments and their absence in modern marine sediments have led many investigators to conclude that "specific epochs of dolomitization" no longer occur.

The geosynclinal phosphate deposits in Karatau and layered phosphates on the western slope of the Urals in Bashkir A. S. S. R. are somewhat dolomitized. The platform-type phosphates in European U. S. S. R are devoid of traces of magnesium carbonates.

That dolomites are developed as saline residues in salinized marine basins is a common opinion among certain investigators; in 1939, we suggested that phosphorites are chemogenic sediments in marine basins of ordinary salinity. This has introduced a certain vagueness in the prospecting clues for phosphorites in dolomitic rock, inasmuch as we were still uncertain that dolomitization of sediments is a negative prospecting indicator in the exploration for phosphorites.

The commonly used geologic-lithologic methods of field investigation do not, without supporting activities, solve the problem of the origin of dolomites. For this reason, we had resorted to a comprehensive method primarily based on experimental studies dealing with Mg and Ca carbonate equilibria in physico-chemical systems. Therefore, we had performed the following investigations: 1) physico-chemical experiments of magnesitic and dolomitic systems, $MgO-CO_2-H_2O$ and $CaO-MgO-CO_2-H_2O$, respectively, at equilibria within the range of different isotherms (20^o and, in part, 60^o and 150^oC)-later, these systems were complicated by introduction of different "saline backgrounds" (additional components), chiefly marine salts (NaCl, $MgSO_4$, gypsum, and others); 2) systematic analyses of hydrochemical materials from modern basins and of subterranean and ground [Tr.: the aqueous phase or interstitial waters of sediments] waters in reference to settling of magnesium.

The literature on dolomites and magnesites in sedimentary rocks (about 110 articles) chiefly embracing geologic-genetic problems is extensive. Moreover, there are approximately 30 articles on the chemical and physico-chemical character of the carbonates. If we exclude studies made at high temperatures and at partial pressures of CO_2 in excess of atmosphere, 7 papers on the magnesite system remain. Of these 7, only 1 [87] really appears to be sufficiently complete to lay its formal claim as a finished piece of work. However, as it developed in the course of our investigations, the bottom phases within the fields of low and intermediate concentrations of carbonic acid were defined by Kline both incorrectly and incompletely, and he failed to detect magnesite and even the basic magnesium carbonates.

Our work was mainly conducted by the crystallization method (and not by the method of "solution" of natural carbonates). Also, we had established the highly developed metastability of carbonate-magnesium systems and the duration of the fall-off in the residual supersaturation, as opposed to the calcite system. This, in turn, had conditioned the prolonged "storage" of the systems, from one-half to 1 year.

The bulk of the experimental work was devoted to the magnesite system, in order to ascertain conditions of the crystallization of magnesite, $MgCO_3$, as well as prerequisites for the development of dolomite--an intermediate bottom phase. This system is here to be considered under three categories: high, low, and intermediate concentrations of CO_2, in correspondence with the experimental techniques and the nature of the bottom phases.

FIELD OF HIGH CO_2 CONCENTRATIONS (THE NESQUEHONITE FIELD)

System of Equilibria

For most of the experiments, a strong solution of magnesium bicarbonate was prepared in a 20-liter (1) bottle. Parts of this stock solution were subjected to ladderlike degasation in order to remove different proportions of CO_2 by aeration or by the addition of MgO. With the removal of CO_2 or with the addition of MgO, the system would become supersaturated and a settling of the corresponding bottom phase would begin. A third method of experimentation, the hydrolysis of $MgCO_3 \cdot 3H_2O$ (nesquehonite), is somewhat different.

Preparation and Analysis of $Mg(HCO_3)_2$ Solution

CO_2 from the storage tank or from the Kipp apparatus [Tr.: with a gas-atomizing nozzle of the kind used in aeration of aquariums] is passed through a suspension of $MgCO_3 + H_2O$ or $MgO + H_2O$ with a simultaneous agitation by a mechanical stirrer. Following the saturation and the period of "storage," the suspension is filtered (or, better, the clear supernatant solution is decanted after clarification by settling) and examined for MgO, CO_2, pH, and the alkaline reserve [Tr.: buffering capacity]. MgO and CO_2 are determined by the common gravimetric procedures.

The clear stock solution of magnesium bicarbonate is poured into vessels of 0.5 to 1 liter capacity where it is diluted with distilled water in order to obtain a series of solutions at 500 mg/l intervals in their zero-time CO_2 concentrations, for example, 7,000-6,500-6,000, and so forth mg CO_2/l. Then, the initial "alkaline reserve" and the pH are determined in the solutions. The series are ready for the decarbonization.

Decarbonization (partial)

For the partial removal of CO_2 from the system, the series of magnesium bicarbonate solutions can be aerated through a gas-atomizing nozzle connected to the compressor, or CO_2 can be evacuated by a vacuum oil pump ("cold boiling" of the system). Also, $Mg(OH)_2$ or MgO can be added to the system, resulting in low values of P_{CO_2}, or 10 to 20 percent of the original total CO_2 can be withdrawn by means of decarbonization [Tr.: means not given in original].

Placement of Stock Solution into Thermostat

The solution is placed into a thermostat. It is periodically mixed either manually or by a mechanical stirrer.

Periodic Control of System's Equilibrium

Periodic control of the system's equilibrium is maintained either by analytical control of the "alkaline reserve" (by titration with 0.1N HCl, with methyl orange) and pH determinations, or conductometrically or interferometrically (the most exact methods for determining small concentrations).

Filtration

Special precautions are required in the filtration process after the attainment of equilibrium in order to prevent the escape of CO_2 from the system into the air (or the reverse, a capture of CO_2 by the system from the air in experiments with low CO_2 concentrations). Decantation is especially convenient at times. The solid phase is filtered off rapidly in a Buchner funnel with a dry filter, and is washed with alcohol several times, or is simply pressed between sheets of dry filter paper. The solid phase is air-dried to a constant weight.

Analysis of the Equilibrium Liquid Phase

This analysis is made to determine the following indices of the control: 1) total CO_2, by the Fresenius method, gravimetrically; 2) titration with 0.1N HCl (methyl orange); 3) MgO content, by weight; 4) pH, electrometrically (glass electrode); and 5) specific gravity, by pycnometer.

Analysis of Solid Phase

The following determinations are made: 1) in aliquots of the air-dry residue, loss in weight at 105°C; 2) in aliquots residue dried at 105°C, loss on ignition at 800° to 900°C; 3) MgO content and CO_2 content; and 4) microscopic and crystal-optical investigations. Moreover, in special cases, thermograms and Debyeograms are obtained. In the instance of a two-phased residue, there is also a separation by gravity in heavy liquids in a centrifuge.

We had conducted 11 experiments by the degasation method. Their results are summarized in table 1 and are represented graphically in figures 1 and 2. As it is evident from table 1 and figure 1, the 11 experiments in the series lie within the nesquehonite field.

For a more complete presentation of relationships between magnesite and calcite systems and for comparing our results with the earlier investigations, the following is shown within the mg/l CO_2· MgO coordinates in figure 2: 1) the equilibrium curve for the CaO-CO_2-H_2O system, based on data shown in table 2; 2) Kline's curve [87] for the MgO-CO_2-H_2O system at 25°C; and 3) Kazakov's curve (1948) for the MgO-CO_2-H_2O system at equilibrium at 20°C. From these three equilibrium curves obtained at room temperature and ordinary pressures it follows that:

1. The curves for the carbonate-magnesium system at 20°C ("A," "B") appear as broken straight lines (the breaks come at the double points, nesquehonite-basic magnesium carbonate, "A," A_1," and "B") and represent no fewer than four bottom phases (the complex-forming tendency of basic magnesium carbonates is evident).

2. The "A" curve for the carbonate-calcium system has an entirely different shape and runs to the left when the MgO concentrations are lower and, consequently, when the alkaline reserve is also at its low levels. The curve, in fact, represents only one single equilibrium bottom phase, $CaCO_3$, through the entire range, up to 1 atm partial pressure of CO_2. This system, in a distinction from the magnesium carbonate system, is characterized by the absence of complex formation. It should be pertinent here to remark that all theoretical calculations (formulae) in regard to the state of saturation or unsaturation of calcium carbonate systems (and of natural waters) with respect to calcite, derived from dissociation constants and solubility products are by no means transferable to magnesium carbonate systems or to mixed calcium-magnesium carbonate systems, the way it has been done, not uncommonly, in the literature. In the present state of our knowledge, the very attempt to define the saturation state of natural waters, with respect to magnesite and dolomite, is devoid of any theoretical basis whatsoever and is false.

Let us consider now certain defects in Kline's diagram (fig. 1). For example, he regards the bottom phases at equilibrium as brucite, $Mg(OH)_2$, as represented by points 1 to 4, whereas, according to our findings, these points lie within the field of basic magnesium carbonates. Next, according to Kline, the nesquehonitic part of the curve descends to point 12, while, according to our findings, the entire range of the diagram, between points 12 and 17 lie within the field of basic magnesium salts and, consequently, the nesquehonitic part of the curve begins very much higher (the double point "A" of our diagram).

The paragenesis of brucite, $Mg(OH)_2$, and nesquehonite, $MgCO_3 \cdot 3H_2O$, alleged by Kline at the transitional point between 11 and 12 is crudely incorrect. Kline had missed the well-developed area of basic magnesium carbonates as a transition between brucite and nesquehonite.

Most defects in Kline's work are explained by the shortness of his "aging" period (3 to 5 days); ours lasted from 2 months to 1 year. Naturally, the short interval of time in Kline's experiments was insufficient for establishment of equilibria between the solution and the bottom

TABLE 1. Analytical data on the $MgO-CO_2-H_2O$ system in equilibrium in the field of high concentrations of carbonic acid at 20°C

Experiment	Initial Solution: CO_2 mg/l	Initial Solution: Alkaline Reserve meq/l[1]	Aeration time hr	Temperature °C	Storage time days	Liquid Phase at Equilibrium: MgO mg/l	MgO √	CO_2 mg/l	CO_2 √	CO_2 meq/l[1]	Alkaline Reserve meq/l[1]	Alkaline Reserve √
1	-	-	-	20	-	9,414	97.0	19,104	138.2	868.4	434.2	20.83
2	-	-	-	20	138	8,618	92.8	17,700	133.0	804.5	398.6	19.96
3	-	-	-	20	386	7,600	87.2	15,640	125.0	710.9	373.3	19.32
59	13,360	297.0	-	20	100	6,593	81.2	13,360	115.6	607.3	297.0	17.23
58	12,400	277.0	-	15	204	4,260	65.3	7,620	87.3	346.4	183.7	13.54
31	-	308.0	3	15	63	3,787	61.5	6,668	81.7	300.3	163.4	12.78
30	-	308.0	1	20	63	3,005	54.8	4,732	68.8	215.0	123.0	11.09
32	-	308.0	6	15	56	2,422	49.2	3,628	60.2	164.9	93.0	9.64
33	-	308.0	8	14	56	1,760	42.0	2,216	47.1	100.7	57.6	7.59
39	3,000	128.0	6	14	103	1,698	41.2	2,104	45.9	95.6	51.0	7.14
40	2,000	100.0	6	15	100	1,023	32.0	1,260	33.5	57.3	31.0	5.56

TABLE 1. Analytical data on the $MgO-CO_2-H_2O$ system in equilibrium in the field of high concentrations of carbonic acid at 20°C (Concluded)

Coefficients[2]: pH	Coefficients[2]: CO_2:MgO	Coefficients[2]: CO_2: alkaline reserve	Solid Phase at Bottom[3]: MgO	Solid Phase at Bottom[3]: CO_2	Solid Phase at Bottom[3]: Loss 105°/air dry	Solid Phase at Bottom[3]: Loss 900°/105°	Sum
			Percent of air-dry sample				
-	2.03	2.00	-	-	-	-	-
7.58	2.05	2.02	-	-	-	-	-
7.46	2.05	1.91	-	-	-	-	-
7.80	2.03	2.04	-	-	-	-	-
7.98	1.79	1.88	29.44	32.40	29.70	8.46	100.0
7.95	1.76	1.84	28.93	32.01	26.59	11.76	99.29
8.10	1.57	1.75	23.50	25.30	40.70	10.02	99.52
8.35	1.50	1.77	22.92	24.60	48.18	3.52	99.22
8.75	1.26	1.75	19.55	21.85	47.66	9.94	99.00
8.92	1.24	1.87	29.90	31.90	21.83	16.29	99.92
9.10	1.23	1.85	35.00	33.40	15.00	16.20	99.60

[1] Milliequivalents.

[2] [Tr.: Coefficients refer to liquid phase.]

[3] Minerals formed at the bottom, in the solid phase, are nesquehonite ($MgCO_3 \cdot 3H_2O$), except for experiments 30, 32, and 33, where they are lansfordite ($MgCO_3 \cdot 5H_2O$).

TABLE 2. Characteristics of the $CaO-CO_2-H_2O$ system in equilibrium

Concentration of CO_2 (mg/l)	Partial pressure P_{CO_2} (atm)	Temperature (°C)	Points	Reference
10.12-225	-	16-20	11-56	[90]
0.0313-44.820	$3.16 \cdot 10^{-14}$ $2.15 \cdot 10^{-14}$	16	1-10	[85]
up to 2,317	0.00031-0.9684	25	57-58	[81]

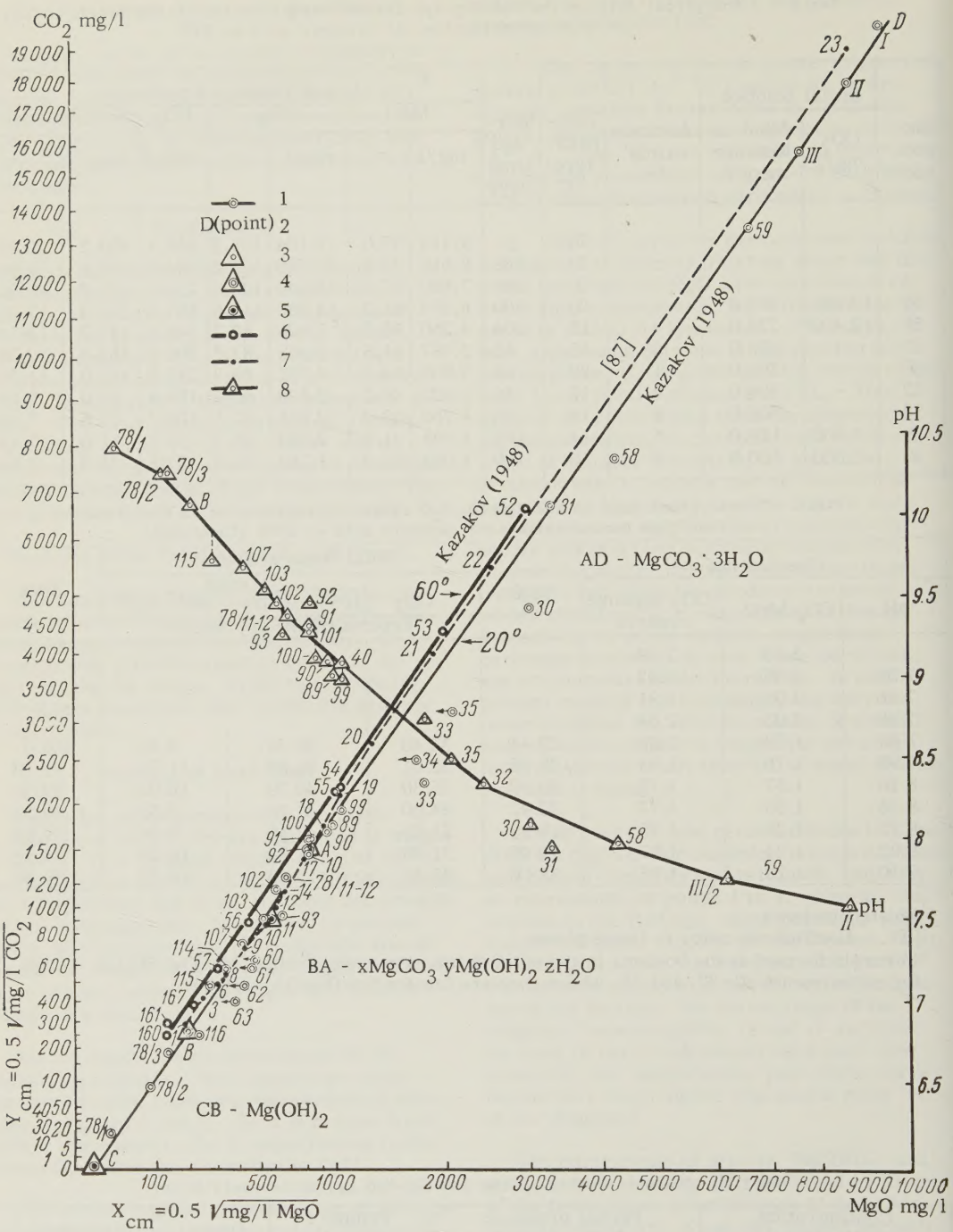

FIGURE 1. A review diagram of the $MgO-CO_2-H_2O$ system equilibrium (P_{CO_2} from 0 to 1 atm) 1) the 20° isotherm (A. V. Kazakov, 1948); 2) the figurative point "D" at P_{CO_2}= 1 atm (19,104 mg/l CO_2, 9,414 mg/l MgO, alkaline reserve 434.2 meq/l, bottom phase $MgCO_3 \cdot 3H_2O$); 3) the double point "A" ($MgCO_3 \cdot 3H_2O$ and basic magnesium carbonate); 4) the double point "B" (basic magnesium carbonate and $Mg(OH)_2$); 5) point "C" ($Mg(OH)_2$ at P_{CO_2} = 0 atm); 6) the 60°C isotherm (Kazakov, 1948); 7) the 25°C isotherm [87]; and 8) the pH curve of the $MgO-CO_2-H_2O$ system at 20°C (Kazakov, 1929).

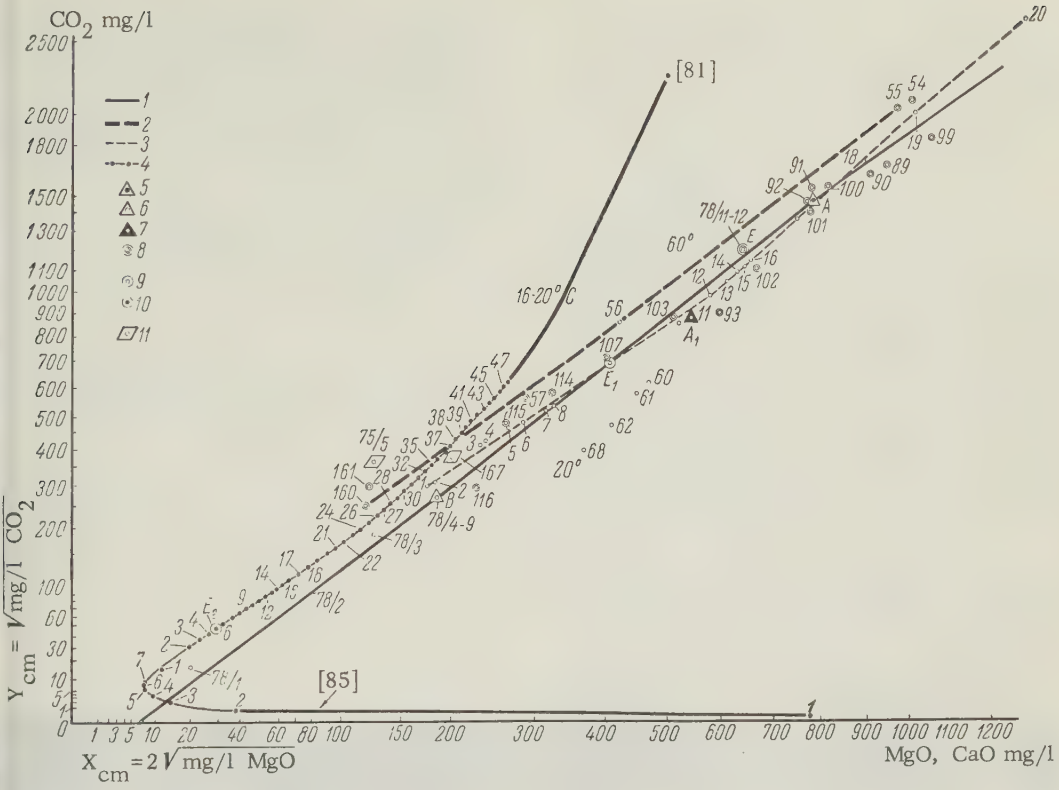

FIGURE 2. Dynamics of system equilibria

1) the equilibrium curve for $MgO-CO_2-H_2O$ system at 20°C (Kazakov, 1948); 2) the equilibrium curve for $MgO-CO_2-H_2O$ system at 60°C (Kazakov, 1948); 3) the equilibrium curve for $MgO-CO_2-H_2O$ system at 25°C [87]; 4) the equilibrium curve for $CaO-CO_2-H_2O$ system at 16° to 20°C [85, 90]; 5) the double point "A" ($MgCO_3 \cdot 3H_2O$ and basic magnesium carbonate); 6) the double point "B" (basic magnesium carbonate and $Mg(OH)_2$); 7) the double point "A_1" ($MgCO_3$ and basic magnesium carbonate[87]); 8) point "E" basic magnesium carbonate at equilibrium with CO_2 of air; Kazakov, 1948); 9) point "E_1" [87]; 10) the figurative point "E_2" of the $CaO-CO_2-H_2O$ system at equilibrium with CO_2 of the air[90]; and 11) the figurative points for magnesite in the $MgO-CO_2-H_2O$ system at 60°C.

hases (note our results on the rates of settling n the residual supersaturation fall-off cited in igure 7 and 11).

Mineralogy of Nesquehonite and Lansfordite

Nesquehonite ($MgCO_3 \cdot 3H_2O$)

In 1888, Genth and Penfield [41] discovered new mineral in stalactites in coal mines near ansford, Pennsylvania. They named this min- ral nesquehonite. The previously discovered nineral, lansfordite, in the same area [40] roved to be very unstable at higher tempera- ures and had decomposed in the summer of he same year at 32°C. It formed crypto- rystalline, opaline, chalklike nesquehonite ($MgCO_3 \cdot 3H_2O$).

Fundamental Properties of Nesquehonite: According to Genth and Penfield, nesquehonite crystallizes in rhombic prisms up to 10 mm long and 2 mm thick:

c(001)	d:d	49°6'
b(010)	d:b	65°27'
m(110)	m:m	65°36'
d(011)	m:m	114°24'

2E = 83°55' Li 2E = 84°15 Na

Its hardness is 2.5. The mineral is fairly stable in air. Even over H_2SO_4 the loss in weight amounted only to 0.1 percent after 3 days' exposure. The analysis is as follows

(averages from data on three specimens):

System Constituents	Weight	Molar proportions
MgO	29.22	1.06
CO_2	30.22	1.00
H_2O	40.32	3.26, therefore, $MgCO_3 \cdot 3H_2O$

Artificial crystals of nesquehonite were produced and described by Klaproth in 1808 and by Berzelius in 1835. Their more exact crystallographic description was given by Marignac in 1855. By the recent data of Genoglio, 1935; a:b:c = 0.6438:1:0.4518. Optical indices and specific gravity of nesquehonite are given in table 3.

TABLE 3. Specific gravity and optical characteristics of nesquehonite

Specific gravity	System	Optical sign	N_p	N_m	N_g	(N_g-N_p)	2V	References
1.83[1]	Rhombohedral	-	1.495	1.501	1.526	0.031	-	[41]
1.852[2]	-	-	-	-	-	-	-	[41]
1.875	-	-	-	-	-	-	-	Berkart (1881)[3]
1.808	-	-	-	-	-	-	-	[44]
1.84	Rhombohedral	negative	1.412	1.501	1.526	0.114	53°	[45]
1.854	-	negative	-	-	-	-	-	[46]
-	-	negative	-	1.474-1.557	-	-	-	Sallo (1922)
1.842	Rhombohedral	negative	1.417	1.503	1.527	0.110	53°3'	[36]

[1] Tule
[2] pycnometer, alcohol
[3] Antedating the discovery of this mineral by 7 years. --VPS.

FIGURE 3. Photomicrograph of nesquehonite particles (experiment 1, crossed nicols, X76)

In all 11 experiments (table 1), our observations and studies of the nesquehonite sediment had established the presence of well-developed translucent rhombic elongated prisms with weakly developed pyramidal faces (fig. 3). Pycnometrically, the specific gravity, D_{20°, of crystalline nesquehonite was determined in three experiments, 58, 38, and 6, as 1.823, 1.873, and 1.847, respectively. Losses of CO_2 on ignition were determined for the coarsely crystalline sediment of nesquehonite in experiment 58 (table 4). In such manner, carbonic acid is

TABLE 4. Losses of CO_2 by air-dry coarsely crystalline nesquehonite (experiment 58) and losses of H_2O by finely crystalline nesquehonite (experiments 38 and 59) on heating (% of air-dry sample)

Temp. (°C)	CO_2 (expt. 58)	H_2O (expt. 38)	H_2O (expt. 59)
60	0	2.3	-
80	-	14.3	-
100	0	16.5	-
105	-	17.3	-
110	0.20	19.0	14.5
140	2.04	-	-
900	-	33.6	-

molecularly more firmly bound than in low-temperature (110°C) water. The faces of nesquehonite crystals lose their original lustre and become opaque after drying at 110°C.

Nesquehonite Debyeogram: We have also obtained a debyeogram of nesquehonite, for diagnostic purposes. Our results are compared with the results by Handelt, Frimm, and Fremel [42] shown in table 5.

The Structural-Chemical Formula: Measurements of the crystal lattice structures of nesquehonite do not appear in the literature. Mineralogically, as a rule, the formula $MgCO_3 \cdot 3H_2O$ is ascribed to nesquehonite (magnesium carbonate trihydrate). However, Wells, an American chemist, in 1915, regarded nesquehonite as a basic magnesium carbonate, $MgOH \cdot HCO_3 \cdot 2H_2O$ [91]. Much later, in 1938, a well-known German chemist-halurgist, D'Ans, together with Gloss, published a report on the nature of nesquehonite and of basic magnesium carbonates. We are citing here their principal conclusions [75]:

1. The easily crystallizing $MgCO_3 \cdot 3H_2O$ is a metastable phase. It loses its CO_2 slowly at room temperature, in the air, and even under water and converts to the well-known basic magnesium carbonate of the artinite type, $MgCO_3 \cdot Mg(OH)_2 \cdot 4H_2O$. This process is accelerated significantly at higher temperatures. Thus, the conversion of 5 grams of crystalline $MgCO_3 \cdot 3H_2O$ into the basic magnesium carbonate was complete after 70 minutes of boiling with water.

TABLE 5. Debyeogram of nesquehonite, $MgCO_3 \cdot 3H_2O$ (a synthetic specimen from experiment 58, dried at 60°C)

Line no.	Kazakov		Handelt, Frimm, and Fremel [42]		Line no.	Kazakov		Handelt, Frimm, and Fremel [42]	
	I	d_{hkl}	I	d_{hkl}		I	d_{hkl}	I	d_{hkl}
1	strong	7.119	-	-	22	strong	1.549	0.12	1.55
2	very strong	6.351	1.00	6.5	23	medium	1.506	0.08	1.50
3	very weak	4.974	0.08	4.96	24	medium	1.460	0.08	1.450
4	strong	4.022	-	-	25	medium	1.434	0.08	1.430
5	very strong	3.807	0.80	3.86	26	medium	1.383	0.08	1.390
6	medium	3.548	0.16	3.58	27	weak	1.349	not measured	
7	medium	3.213	0.16	3.23	28	medium	1.332		
8	very strong	2.998	0.24	3.02	29	medium	1.284		
9	strong	2.772	0.16	2.77	30	medium	1.271		
10	strong	2.608	0.18	2.61		coalescent	1.257		
11	very strong	2.483	0.40	2.51		triple	1.247		
12	weak	2.339	0.80	2.35	31	weak	1.229		
13	weak, wide	2.244	-	-	32	weak, wide	1.177		
13	strong, wide	2.158	0.16	2.17			1.158		
13	weak, wide	2.114	-	-	33	weak	1.144		
14	medium	2.006	0.08	2.01	34	weak	1.121		
15	very strong	1.915	0.32	1.92	35	medium	1.108		
16	medium	1.833	0.08	1.83	36	medium	1.096		
17	strong	1.803	0.24	1.79	37	weak	1.081		
18	medium	1.715	0.16	1.71	38	weak, wide	1.070		
19	medium	1.672	-	-			1.057		
20	weak	1.620	0.80	1.64	39	medium	1.037		
21	weak	1.580	-	-					

2. The basic magnesium carbonate, $MgCO_3 \cdot Mg(OH)_2 \cdot 4H_2O$, according to D'ans, in turn, is also metastable. It is converted into a "well-crystallized magnesite," in an open vessel in a thermostat; the reaction is complete after 7 weeks at 65°C or after 4 months at 55°C.

3. In solving the problem of the structural formula, D'Ans was determining CO_2 pressures in nesquehonite crystals by the means of a differential tensiometer with a mercury lock (Bremer-Froveni design) in a thermostat at 34°C. After 208 days, the tensiometer registered CO_2 pressure at 950 mm of the mercury column. The residue was a mixture of basic magnesium carbonate and $MgCO_3$. The CO_2 pressure of the basic magnesium carbonate was very low at 34°C (a few millimeters of the mercury column). Magnesite (synthetic and natural), at the same time, had no measurable CO_2 tension and would not yield CO_2 even after a prolonged boiling with water.

4. D'Ans came to regard nesquehonite as a weakly explosive substance because of the rapid loss of CO_2. He assigned the following "basic magnesium carbonate" formula to this mineral:

$$Mg(OH \cdot HCO_3) \cdot 2H_2O,$$

that is, he supports the opinion of Wells.

Nesquehonite Thermograms: The differential thermogram (fig. 4) for fresh nesquehonite crystals (from experiment 1, table 1) proved to be very characteristic and it was deciphered as follows: 1) 220 to 222°C - an endothermal peak at the separation of the water of crystallization ($2H_2O$); 2) 508 to 525°C - an exothermal "explosive" effect (according to D'Ans, this effect is due to the separation of CO_2);

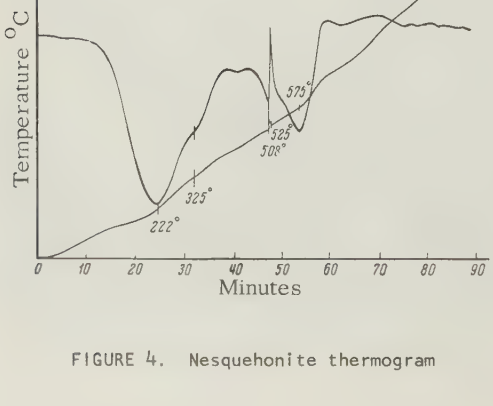

FIGURE 4. Nesquehonite thermogram

however, the withdrawal of CO_2 was, in reality, associated with an absorption of heat (endothermally); we cannot exclude the possibility that the exothermal effect was due to the formation of magnesite, according to the reaction:

$$Mg(OH \cdot HCO_3)MgCO_3 + H_2$$

The markedly expressed endothermal reaction, following the exothermal "explosive" effect, with the maximum at 575°C, was clearly connected with a disarrangement of the magnesite grouping among the products of the thermal transformations of nesquehonite. It should be noted that the same markedly endothermal reaction with the peak at 570 to 590°C is shown by the ignition curve of pure natural hydromagnesite (fig. 5) and it corresponds to the withdrawal of CO_2 [33].

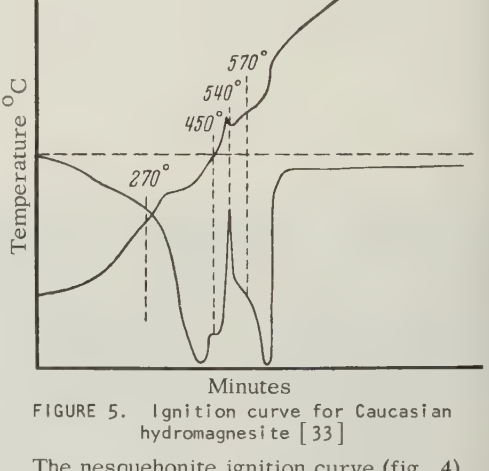

FIGURE 5. Ignition curve for Caucasian hydromagnesite [33]

The nesquehonite ignition curve (fig. 4) shows still another weakly endothermal reaction (the "saddle" with the peak at about 430°C) which represents the decomposition of the hydroxyl groups. This reaction is comparable to the endothermal reaction of the Caucasian hydromagnesite (with the maximum at 450°C) which loses its water at about this temperature (decomposition of the OH groups). At 520 to 540°C, the hydromagnesite in question has also a strongly expressed exothermal peak analogous to that of nesquehonite.

The great similarity in the thermal behavior of nesquehonite and hydromagnesite, $Mg_5(CO_3)_4(OH)_2 \cdot 4H_2O$, suggests that nesquehonite is a $Mg(OH)_2 \cdot Mg(HCO_3)_2 \cdot 4H_2O$ or $Mg(OH)(HCO_3) \cdot 2H_2O$.

After completion of the present studies, a report by Beck [34] was published. It contains data on thermal studies of magnesium hydrocarbons: nesquehonite, lansfordite, hydromagnesite, artinite, and others (fig. 6). The ignition curve of nesquehonite from Nesquehoning was analogous to the curve obtained by

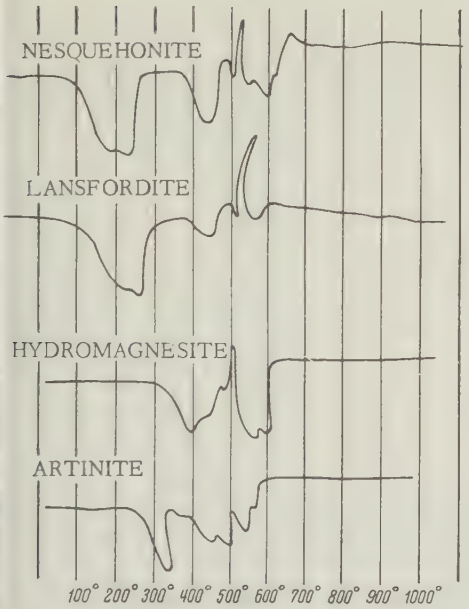

FIGURE 6. Differential ignition curves for basic magnesium carbonates [34]

Kazakov for his synthetic nesquehonite and had many points in common with thermal curves for lansfordite (kept in oil during the ignition), hydromagnesite, and artinite. The endothermal pause for these minerals at about 400°C is characteristic, corresponding to a decomposition of the Mg-OH groups, in addition to the endothermal withdrawals of the water of hydration. The major endothermal effects in the 470 to 610°C range are also characteristic, as they represent the separation of carbonic acid and are interrupted by high exothermal peaks in nesquehonite, lansfordite, and hydromagnesite and by a weak peak in artinite.

Beck also believes nesquehonite to be a basic carbonate of magnesium and thinks that the crystallization of periclase from amorphous (?) MgO derived from the decomposition of Mg-OH groups is responsible for abrupt exothermal reactions at about 500°C. Roentgenograms of the ignition products at 515°C showed a development of periclase among the products.

It should be noted the exothermal "explosions" accompanied by a formation of periclase are not characteristic of hydroxyl-bearing magnesium minerals containing but little carbonic acid (hydroalcite, pyroaurite, and stichtite) or of those where none is present (brucite). On the other hand, the exothermal reaction itself takes its place commonly only after the evolution of carbonic acid has begun. It is entirely possible that, in this case, it was crystallized in the presence of carbon dioxide gas.

Lansfordite ($MgCO_3 \cdot 5H_2O$)

Coarsely crystalline lansfordite is the earliest among the bottom phases, with the formation of stable nesquehonite, in all 11 experiments. Figure 7 is a sketch of the microscopic observations. Average size of the crystals was 80 to 200 microns. This particular bottom phase proved to be highly unstable at room temperatures (15° to 20°C). It would generally pass into solution within 1 or 2 days, to be replaced by the newly settled stable nesquehonite crystals.

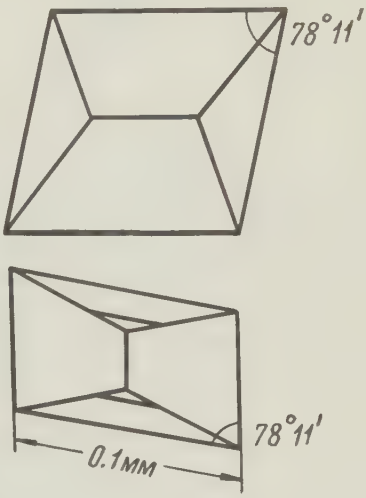

FIGURE 7. Lansfordite crystals

Young [52] had investigated hydromagnesite deposits at Atlin, Canada, and had found a very thin (about 1 mm) crust of white crystalline mineral, lansfordite, in vugs and also on the surface of a number of specimens. Goniometric measurements of this mineral had served to establish its monoclinic syngony. The forms found were: (100), (010), (120), (111), (101), (102), (302), (011), (321), (328), and (001).

From the very scanty data on lansfordite in the literature, as well as on the basis of our own observations, the following reliable generalizations can be made:

1. Paragenetically, lansfordite has been found with nesquehonite in stalactites, in anthracite coal mines at Nesquehoning near Lansford, Pennsylvania; and also in thin crusts on hydromagnesite at Atlin, Canada.

2. Lansfordite cannot possibly be a phase adjoining magnesite.

3. Lansfordite stability field can lie in some lower temperature ranges (table 6).

TABLE 6. Specific gravity and crystallographic and optical characteristics of lansfordite, ($MgCO_3 \cdot 5H_2O$)

Characteristics	Specimens Synthetic	Atlin, Canada	Atlin, Canada
System	Monoclinic		Monoclinic
a	1.632		1.6529
b	1		1
c	0.968		0.9722
Beta-angle	$78^{o}11'$		
Specific gravity	1.73	1.692 to 1.688	1.688
N_g	1.508	1.507	1.508 (at $15^{o}C$, 1.502)
N_m	1.470	1.468	1.476 (at $15^{o}C$, 1.469)
N_p	1.457	1.456	1.456 (at $15^{o}C$, 1.456)
N_g-N_p	0.051	0.051	0.046 (at $15^{o}C$, 0.052)
$2V$	$60^{o}37'$	$59^{o}30'$	$59^{o}48'$
References	[36]	[48]	[Gapon, 1928; Fenoglio, 1936; 46, 52]

FIELD OF LOW CO_2 CONCENTRATIONS

After it was established that nesquehonite is the stable bottom phase within fields of high CO_2 concentrations at equilibrium (260 mg/1 and higher) and of high alkaline reserve (31 meq/1 and higher), it was decided to investigate the marginal fields of low CO_2 concentrations and low alkaline reserve in order to ascertain the fields of stability of $Mg(OH)_2$ and of basic magnesium carbonates.

An aqueous suspension of $Mg(OH)_2$ was prepared at 22.4 g MgO/l. In every experiment, to 50 ml of this suspension (total MgO, 1,120 mg) were added increasing amounts of CO_2 water, at 1,400 mg CO_2/1. The vessels containing different dosages of CO_2 were shaken and were set aside, to attain equilibrium. The analytical control consisted of the determination of pH and the alkaline reserve. "Aging" of the systems was continued generally from 1 to 2 months, which was sufficient for attainment of the physico-chemical equilibria (figs. 8 and 9).

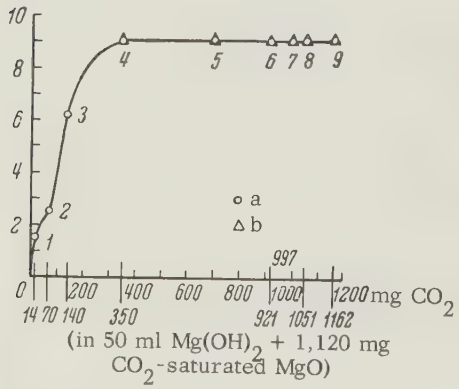

FIGURE 8. Equilibrium titration curve for $Mg(OH)_2$ (suspension by aqueous CO_2) a) $Mg(OH)_2$; b) $Mg(OH)_2 \cdot MgCO_3 \cdot Mg(OH)_2 \cdot 4H_2O$) (double points); 1) 78/1, pH 10.46; 2) 78/2, pH 10.40; 3) 78/3, pH 10.00; 4) 78/4, pH 10.17; 5) 78/5, pH 10.00; 6) 78/6, pH 10.18; 7) 78/7, pH 9.86; 8) 78/9, Ed.: pH value not given ; 9) 78/6, average pH 10.06.

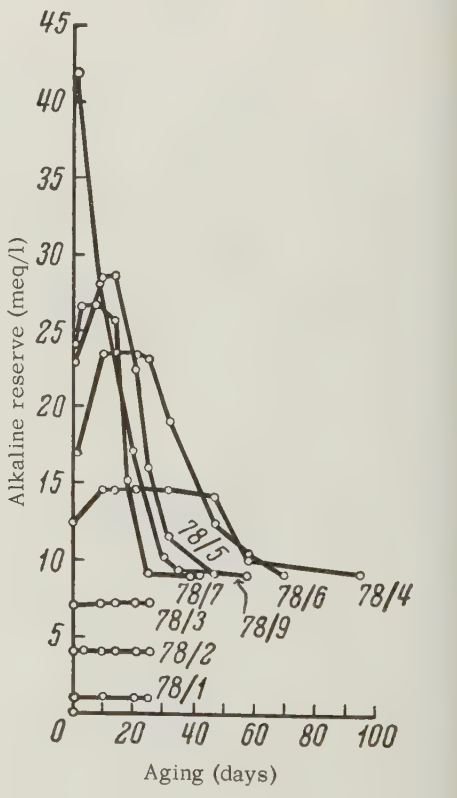

FIGURE 9. Dynamics of alkaline reserve of the $MgO-CO_2-H_2O$ system during interactions between aqueous $Mg(OH)_2$ suspensions and increasing quantities of CO_2

TABLE 7. Results of analyses of liquid and solid phases of the $MgO-CO_2-H_2O$ system in the field of low carbonic acid concentrations (temperature 20°C)

Experiment	Reagents: $Mg(OH)_2$ suspension (ml)	Reagents: H_2O (ml)	Reagents: CO_2+H_2O (ml)	Reagents: CO_2 (mg)	Aging (days)	Liquid phase at equilibrium: MgO (mg/l)	MgO: √	CO_2 (mg/l)	CO_2: √	CO_2 (meq/l)
78/0	50	-	0	0	-	6.9	2.627	0	-	0
78/1[1]	50	740	10	14	25	20	4.47	16	4.00	0.73
78/2	50	700	50	70	25	80	8.84	88	9.38	4.0
78/3	50	650	100	125	25	125	11.18	184	13.56	8.36
78/4	50	500	250	350	64	180	13.40	296	16.43	
78/5[2]	50	250	500	700	54	180	13.40	296	16.43	
78/6[2]	50	750	800	560	42	180	13.40	100	17.13	Avg.
78/7[2]	50	550	700	494	42	196	14.00	-	-	9.06
78/8	50	25	650	1,038	58	180	13.40	264	15.68	
78/9	50	0	350	1,118	58	195	14.00	244	15.62	
78/11[3]	400 mg MgO	500	aeration		80	640	25.30	1,152	35.39	52.3
78/12[3]					81					

TABLE 7. Results of analyses of liquid and solid phases of the $MgO-CO_2-H_2O$ system in the field of low carbonic acid concentrations (temperature 20°C) (Concluded)

Experiment	Liquid phase at equilibrium (cont'd): Alkaline reserve meq/l	Alkaline reserve √	Coefficients: pH	CO_2:MgO	CO_2 alkaline reserve	Solid-bottom phase (% dry-air sample): MgO	CO_2	Loss on ignition 900°:105°	Total
78/0	0.35	0.59	-	0	0	-	-	-	-
78/1[1]	1.51	1.23	10.46	0.80	0.48	65.66	1.02	33.40	100.08
78/2	4.03	2.01	10.30	1.10	0.99	67.64	0.89	31.43	99.96
78/3	6.25	2.50	10.30	1.47	1.34	67.53	1.43	31.04	100.00
78/4	9.09	3.01	10.17	-	-	-	-	-	-
78/5[2]	9.06	3.01	10.00			57.52	14.64	27.84	100.00
78/6[2]	9.06	3.01	10.06		Avg	-	-	-	-
78/7[2]	9.06	3.01	9.86	1.46	1.00		-	-	-
78/8	9.07	3.01	10.18			-	-	-	-
78/9	9.07	3.01	10.25			-	-	-	-
78/11	27.1	5.19	9.39	1.80	1.94	43.25	37.66	19.10	100.01
78/12[3]	26.7								

brucite ($Mg(OH)_2$)
double point: $Mg(OH)_2$ plus basic magnesium carbonate (artinite type)
hydromagnesite ($4MgCO_3 \cdot Mg(OH)_2 \cdot 4H_2O$)

esults of the nine experiments are presented table 7.

The following conclusions may be drawn om the data obtained:

1. In the equilibrium concentrations of O_2 from 0 to 270 mg/l. as CO_2 increases a solution at equilibrium, its excess ecipitates in the form of basic magnesium rbonate (extinite) which forms a two-ased sediment with brucite. The ignition rve of brucite is given in figure 10.

2. Hydrochemical indices for the equilib-um of $MgO-CO_2-H_2O$ at 20°C, in solution, ith the two-phased sediment of $Mg(OH)_2$ us basic magnesium carbonate (artinite) e represented by the following averages of ve experiments.

Double point	"B" (fig. 1)
MgO (mg/l)	185
CO_2 (mg/l)	270
Alkaline reserve (meq/l)	9.06
pH	10.10

Moreover, partial pressures of CO_2 were determined in the gaseous phase of the $MgO-CO_2-H_2O$ system, in experimental vessels, over the solutions at equilibrium:

Experiment	CO_2 in gaseous phase: mg/l	% volume
78/4	0.12	0.006
78/6	0.20	0.010
78/8	0.20	0.011
78/9	0.22	0.011

The CO_2 content of the gaseous phase is one third its content in air, as the gaseous phase corresponds to the equilibrium of the $MgO-CO_2-H_2O$ system the bottom phase of which represents the para-

FIGURE 10. Brucite thermogram

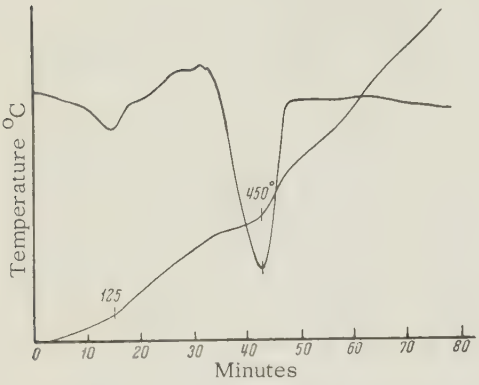

Calculations of the chemical composition of brucite-basic magnesium carbonate mixture show that the moisture consists of three parts of $Mg(OH)_2$ and one part of $MgCO_3 \cdot Mg(OH)_2 \cdot 1.5H_2O$. The latter mineral contains one-half of the water of crystallization of the typical artinite, although Beck [34] cites the formula for artinite from Nevada as $MgCO_3 \cdot Mg(OH)_2 \cdot 2H_2O$. D'Ans and Glass [75] note the transition of nesquehonite into basic magnesium carbonate ($MgCO_3 \cdot Mg(OH)_2 \cdot 4H_2O$).

genesis of $Mg(OH)_2$ plus basic magnesium carbonates. This predetermines the impossibility of stability of brucite, $Mg(OH)_2$ in open bodies of water, in which gas exchanges directly with the atmosphere, and also the inevitability of the carbonization of brucite into basic magnesium carbonates.

3. In order to define the equilibrium system $MgO-CO_2-H_2O$ at its contact with carbonic acid of the atmospheric air, we had performed two experiments with the aeration of the $Mg(OH)_2$ suspension (78/11 and 78/12). These experiments lasted for about 3 months. As expected, both experiments had yielded the same figurative point for composition (table 7). The relatively high alkaline reserve so attained, the pH, and the CO_2 and MgO concentrations should be noted.

The bottom phase in experiments 78/11 and 78/12 is a weakly polarizing homogeneous fine-grained scaly mass, with N_m higher than 1.507 and lower than 1.517.

FIELD OF INTERMEDIATE CO_2 CONCENTRATIONS

Two different procedures were employed in experiments with the crystallization of the bottom phases: 1) a supersaturation of the solution with respect to manganese (experiments 60-63); 2) a hydrolysis of nesquehonite (experiments 89-93, 99-116).

Method of Magnesium Supersaturation of Solutions

The equilibrium solution from experiment 58 was diluted by water (table 8) and 1 g of powered MgO was added to 2 liters of the dilute solution. The resulting suspension was agitated for 30 minutes and filtered. The magnesium-supersaturated clear filtrate (table 8) was set aside for crystallization. Special experiments had shown that this process of saturating the system with Mg ions may be continued longer - up to 2 hours inasmuch as the reverse process of crystallization, in such conditions, becomes operative not earlier than 4 hours after the beginning of the magnesium oxide-treatment of the test solution.

Determinations of the indices of the liquid phase and of the figurative points on the diagram (fig. 11) had shown clearly that the filtration in experiments 60-63 was performed too soon; the system was but slightly supersaturated with Mg ions and, as a consequence, the MgO, pH, and alkaline-reserve levels were rather too high in comparison with their equilibrium levels.

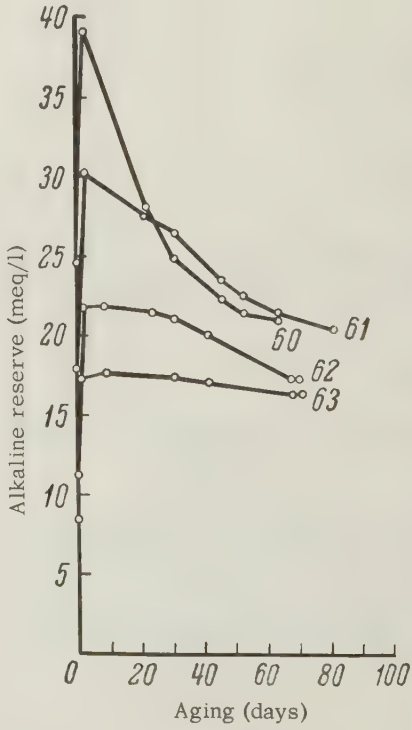

FIGURE 11. The rate of crystallization of basic magnesium carbonates from solutions supersaturated with magnesium ions (the $MgO-CO_2-H_2O$ system at 20°C in the fields of intermediate concentration)

TABLE 8. Results of analyses of liquid and solid phases of the $MgO-CO_2-H_2O$ system at assumed equilibria in the field of intermediate carbonic acid concentrations (the magnesium-supersaturation method at 20°C)

Results	Experiments			
	60	61	62	63
Initial solution before treatment with MgO powder				
Dilution of equilibrium phase with water (58)	1:7.52	1:10	1:15	1:20
MgO (mg/l)	566	426	284	213
CO_2 (mg/l)	1013	762	508	381
Alkaline reserve (meq/l)	24.6	18.4	-	-
Initial liquid phase after treatment with MgO powder				
MgO (mg/l)	876	695	496	380
CO_2 (mg/l)	940	740	532	402
Alkaline reserve (meq/l)	39.2	30.2	21.8	17.6
Assumed equilibrium solution				
Duration of "aging" (days)	93	82	71	71
MgO (mg/l)	463	449	412	369
MgO ($\sqrt{-}$/l)	21.52	21.19	20.30	19.21
CO_2 (mg/l)	636	588	480	402
CO_2 ($\sqrt{-}$/l)	25.22	24.25	21.21	20.05
CO_2 (meq/l)	28.9	26.7	21.8	18.3
Alkaline reserve (meq/l)	20.8	20.3	17.3	16.3
Alkaline reserve ($\sqrt{-}$/meq/l)	4.56	4.51	4.16	4.04
Indices				
pH	10.02	10.06	10.24	10.46
CO_2:MgO	1.37	1.31	1.14	1.09
CO_2:alkaline reserve	1.39	1.32	1.26	1.12
Bottom phase	Basic magnesium carbonates			

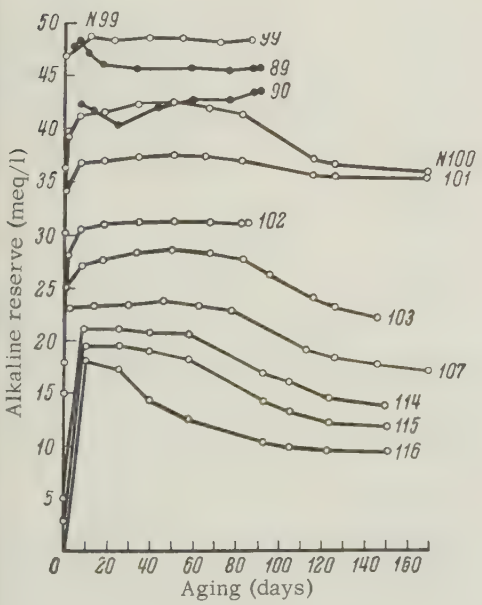

FIGURE 12. Dynamics of the alkaline reserve in the hydrolysis of nesquehonite

Magnesite could not be detected in the solid phase in any of the experiments. Some rhombohedral crystals, from 3 to 22 microns in diameter, were seen in experiment 62, for which the N_p value equaled 1.631 and the N_g value equaled 1.646.

Nesquehonite Hydrolysis, Procedure and Results

Hydrolysis of nesquehonite (experiments 99-116) were conducted by adding 1-liter lots of magnesium bicarbonate solutions, in diminishing concentrations, to distilled water, resulting in 1.5 g aliquots of nesquehonite (table 9). The solutions were "aged" for 84 to 169 days, with two daily shakings (once in the morning and once at evening). The solution was analyzed periodically (in order to determine the alkaline reserve and the pH) and the bottom phase was examined microscopically. On attainment of equilibrium in each solution, the systems were filtered and were subjected to the terminal analysis (table 9; fig. 12). Experiments 89-93 involved the supplementary saturation of the initial solutions with additional magnesium (experiments 60-63, table 8).

TABLE 9. Results of analyses of liquid and solid phases of $MgO-CO_2-H_2O$ system at assumed equilibrium in the field of intermediate carbonic acid concentrations

Initial Solution					With added $MgCO_3 \cdot 3H_2O$	Duration of aging (days)	MgO		CO_2	
Experiment	Stock solution: water	MgO (mg/l)	CO_2 (mg/l)	Alkaline reserve (meq/l)			mg/l	$\sqrt{}$	mg/l	$\sqrt{}$
99	1:9	760	1564	36.4	1.5 g/l	87	1020	31.24	1905	43.7
100	1:11	633	1302	30.2	1.5 g/l	169	816	28.56	1610	40.1
101	1:14	507	1042	25.2	1.5 g/l	168	780	27.93	1450	38.1
102	1:19	380	782	18.1	1.5 g/l	84	670	25.88	1236	35.1
103	1:24	304	626	15.1	1.5 g/l	145	512	22.63	910	30.2
107	1:39	190	391	14.8	1.5 g/l	169	404	20.10	707	26.5
114	1:59	126	261	5.0	1.5 g/l	149	324	18.00	567	23.8
115	1:99	76	156	3.0	1.5 g/l	150	264	16.25	449	21.0
116	Dist. water only	0	0	0	1.5 g/l	150	228	15.10	296	17.0
89	1:9	760	1564	-	1 g/l $MgCO_3 \cdot 3H_2O$ + 100 mg/l MgO	90	950	30.82	1735	41.7
90	1:9	760	1564	-	1 g/l $MgCO_3 \cdot 3H_2O$ + 200 mg/l MgO	90	910	30.16	1680	41.0
91	1:9	760	1564	-	1 g/l $MgCO_3 \cdot 3H_2O$ + 300 mg/l MgO	92	780	27.93	1590	39.9
92	1:9	760	1564	-	1 g/l $MgCO_3 \cdot 3H_2O$ + 400 mg/l MgO	140	771	27.77	1510	38.9
93	1:9	760	1564	-	1 g/l $MgCO_3 \cdot 3H_2O$ + 500 mg/l MgO	48	620	24.90	1159	30.5

TABLE 9. Results of analyses of liquid and solid phases of $MgO-CO_2-H_2O$ system at assumed equilibrium in the field of intermediate carbonic acid concentrations (Concluded)

Experiment	Alkaline reserve meq/l	Alkaline reserve $\sqrt{}$	pH	Coefficients CO_2:MgO	Coefficients CO_2:alkaline reserve	Bottom phase
99	48.5	6.96	8.48	1.87	1.78	$MgCO_3 \cdot 3H_2O$
100	41.4	6.00	9.14	1.97	1.77	Double points: nesquehonite and basic magnesium carbonate
101	35.6	5.97	9.30	1.86	1.85	
102	31.2	5.59	9.22	1.84	1.80	
103	22.3	1.72	9.58	1.78	1.85	The field of basic magnesium carbonates
107	17.1	4.14	9.70	1.75	1.88	
114	13.8	3.72	-	1.75	1.87	
115	11.8	3.44	9.76	1.70	1.73	
116	9.6	3.02	-	1.30	1.41	
89	45.9	6.78	9.03	1.82	1.72	$MgCO_3 \cdot 3H_2O$
90	43.7	6.61	9.12	1.73	1.75	
91	36.3	6.03	9.34	2.04	1.99	Double points: nesquehonite and basic magnesium carbonate
92	34.0	5.83	9.30	1.96	1.93	
93	28.5	5.34	9.42	1.87	1.85	Basic magnesium carbonate

Discussion

It is evident from the data presented that the nesquehonite field in the $MgO-CO_2-H_2O$ system at 20°C begins at the double point "A" corresponding to the following parameters of the liquid phase:

Double point	"A"
MgO (mg/l)	784
CO_2 (mg/l)	1,521
Alkaline reserve (meq/l)	36.0
pH	approx. 9.26

and continues toward higher concentrations, for example, in experiment 1:

MgO (mg/l)	9,414
CO_2 (mg/l)	19,104
Alkaline reserve (meq/l)	434.2
pH	approx. 9.26

From the extreme (double) point "A" in the nesquehonite field, the field of basic magnesium carbonates begins; it continues downward to double point "B" which represents the following parameters of the liquid phase:

Double point	"B"
MgO (mg/l)	185
CO_2 (mg/l)	270
Alkaline reserve (meq/l)	9.06
pH	10.1

The possibility that there may be not one but two phases of basic magnesium carbonates along the "AB" line (for example, of the artinite and of the hydromagnesite types) is not excluded. Magnesite, as such, could not be detected to this part of the field. Finally, from point "B" to still lower concentrations lies the brucite, $Mg(OH)_2$ line.

Both alkaline reserves in magnesium carbonate systems (figs. 8, 12, and 13) during their interactions with the introduced solid phase at a disequilibrium show that the solution and the crystallization processes are independent from each other. When the solution rate exceeds the rate of crystallization, a "jump" of the liquidus of the system into the supersaturation field may be observed, generally during the first moment of the reaction. After a certain stage, the so-called "induction period," the period of crystallization sets in and the figurative point of the system on the hyperbolic curve descends towards the fall-off of the supersaturation. This regularity is shown by all curves in figures 8, 12, and 13.

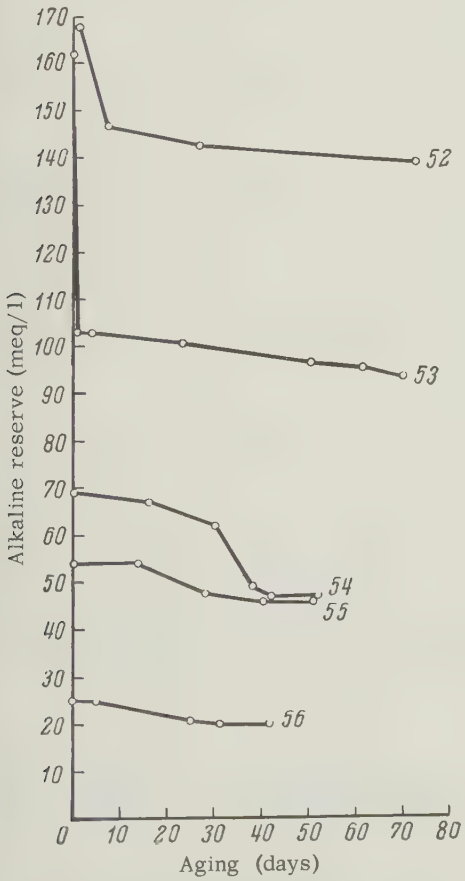

FIGURE 13. Dynamics of alkaline reserve in $MgO-CO_2-H_2O$ system

From this point of view, the equilibrium systems should be regarded dynamically and not statically, considering the mass of substance (molecules, ions), at any given moment, passing from the solid to the liquid phase (the process of solution) as well as in the opposite direction (the process of condensation, of precipitation). Thus the very concept of "solution" of a solid in a liquid phase here acquires a different physical sense.

All curves in figures 8, 12, and 13 give single-value indications to the effect that a definite period of time is required for the initially unbalanced systems to pass to their equilibrium balance. Theoretically, from this point of view, the salt-solubility "jumps" previously noted, with the subsequent (slower) precipitation in the course of the flotation process, should be quite well developed in the relatively rapid salt-flotation methods (potassium salts).

EFFECT OF SEA WATER CONSTITUENTS ON $MgO-CO_2-H_2O$ SYSTEM AT 20°C

NaCl Background

Only two experiments, 34 and 35, were conducted in the fields of high CO_2 concentrations; they have an orientation significance (table 10).

$MgSO_4$ Background

Eight experiments, 152-159, were conducted in a background of 25 g/l $MgSO_4$ and three, 36-38, at high $MgSO_4$ concentrations. As the concentration of $MgSO_4$ increases in the system, $Mg(OH)_2$ becomes captured by the sediment, at relatively high rates of crystallization conditioned by the experiments. There is also a weak capture (coprecipitation) of sulfate ion.

The equilibrium figurative points obtained in experiments reported in tables 10 and 11 are plotted on the diagram (fig. 2).

All experiments with the $MgO-CO_2-H_2O$ system containing added NaCl and $MgSO_4$ were within the nesquehonite field at 20°C. Crystallization of the $MgCO_3 \cdot 3H_2O$ sediment is affected adversely by the addition of $NaCl-MgSO_4$ salts to the system. Addition of NaCl causes an increase in the solubility of magnesium carbonates which leads to an adverse decrease in the CO_2:MgO and the CO_2:alkaline reserve coefficients (down to 1.52 in the equilibrium liquid phase, experiment 34). Addition of 25 g/l

TABLE 10. Results of analyses of liquid and solid phases in equilibrium in $MgO-CO_2-H_2O$ system in a NaCl background (figs. 1 and 2)

Results	Experiments	
	34	35
Initial solution		
MgO (mg/l)	5,983	3,989
CO_2 (mg/l)	12,400	8,267
Alkaline reserve (meq/l)	277	185
pH	-	-
NaCl added (g/l)	135	200
Length of aeration (hours)	12	6
Duration of aging (days)	2	2
Equilibrium solution		
MgO (mg/l)	1,788	2,071
MgO (√ of mg/l)	42.3	45.5
CO_2 (mg/l)	2,504	3,122
CO_2 (√ of mg/l)	50.0	55.9
CO_2 (meq of mg/l)	113.8	141.9
Alkaline reserve (meq/l)	74.8	84.2
Alkaline reserve (√ of meq/l)	8.65	9.18
pH	9.0	8.5
Coefficients		
CO_2:MgO	1.40	1.51
CO_2:alkaline reserve	1.52	1.68
Bottom phase*		
MgO (% air-dry sample)	29.83	29.54
CO_2 (% air-dry sample)	32.60	32.25
100° (% air-dry sample)	20.94	24.36
H_2O (900°:100°)	16.91	14.08
Total	100.28	100.23
Formula	$MgCO_3 \cdot 3H_2O$	

* Bottom phase of both experiments 34 and 35 consisted of a highly dispersed nesquehonite sediment.

$MgSO_4$ causes practically no displacement of figurative points from their normal positions in the $MgO-CO_2-H_2O$ system (experiments 152-159) and practically no change in the CO_2:alkaline reserve coefficients (1.6-1.8).

Sea-Water Background

Eighteen experiments were performed against the background of sea water of ordinary salinity, all in the early stage of our work when it still seemed possible that a development of the equilibrium sediments of magnesite and dolomite in calcium-magnesium-carbonate systems was a simple straightforward proposition. Our complete failure in obtaining the intermediate-salt sediments, $MgCO_3$ and $CaMg(CO_3)_2$, from unconfined Ca-Mg-carbonate systems at room temperature led us to prolonged systematic studies of simpler systems and, first of all, of the magnesite system, $MgO-CO_2-H_2O$, within a wide range of concentrations and thermodynamic potentials of carbonic acid.

Sea water (SW) was prepared artificially, according to the well-known recipe of Bruyevich. The salts were dissolved in distilled water in the following sequence, g/l: 27.021 NaCl; 0.085 NaBr; 0.206 $NaHCO_3$; 0.739 KCl; 2.493 $MgCl_2$; 3.368 $MgSO_4$; and 1.163 $CaCl_2$. This corresponds, by conversion to the oxides, 558 mg/l CaO, 108 mg/l CO_2, 2,851 mg/l MgO, and 2,250 mg/l SO_3.

For most of the experiments in these series, solutions of calcium bicarbonate, $Ca(HCO_3)_2$, and of magnesium bicarbonate, $Mg(HCO_3)_2$, were added slowly, from burettes, simultaneously or separately, to sea-water solutions of the composition as previously stated, with a continuous aeration by air of the atmosphere through a porous nozzle by which the air was atomized into very small bubbles. The purpose of the aeration was to keep the system mixed, to blow out the excess of CO_2 introduced with the bicarbonate solutions, and to facilitate attainment of the equilibrium with the atmosphere. The systems were impoverished generally with respect to CO_2 in the course of the aeration, passing into a supersaturated state with respect to Ca and Mg. Carbonate sediments of calcium and magnesium would begin to form in a few hours, as a rule.

In order to avoid dilution of the SW salts by the Ca and Mg bicarbonates, the bicarbonate solutions were prepared from the sea-water stock, by additions of solid $CaCO_3$ and MgO and by passing CO_2 from a tank through the resulting suspensions. The systems were filtered afterwards. Analytical control data on the reagents used in the experiments are presented in table 12 (see p. 20).

The results of our experiments are summarized in table 13 (see p. 22). From these analyses, it is concluded that:

1. Nesquehonite and calcite are the bottom phases of the $CaO-MgO-CO_2-H_2O$ system in a sea-water background at $15^{\circ}C$ in the fields of high concentrations (alkaline reserve = 41 meq/l). The intermediate salts, $MgCO_3$ and $CaMg(CO_3)_2$, are absent. The paragenesis of nesquehonite and calcite is common.

2. In the fields of intermediate and low concentrations (alkaline reserve = 24 to 4.7 meq/l), all seven experiments had yielded only calcite in the bottom phases.

3. The CO_2:alkaline reserve ratio fluctuates between 1.6 and 2.0 in all 18 experiments with the unconfined system in question at relatively low partial pressures of carbonic acid.

TABLE 11. Results of analyses of liquid and solid phases of the $MgO-CO_2-H_2O$ system in equilibrium at 20°C in a $MgSO_4$ background

Experiment	Initial Solution: MgO (mg/l)	Initial Solution: CO_2 (mg/l)	Initial Solution: Alkaline reserve (meq/l)	Initial Solution: pH	Initial Solution: Additions of NaCl or $MgSO_4$[1]	Length of aeration (hours)	Duration of aging (hours)	Solution at equilibrium: MgO (mg/l)	Solution at equilibrium: CO_2 (mg/l)	Solution at equilibrium: CO_2 (meq/l)	Solution at equilibrium: Alkaline reserve (meq/l)	Solution at equilibrium: pH	Solution at equilibrium: Coefficient CO_2:alkaline reserve
152	0	11,740	240.8	-		-	188	13,400	9,230	419.6	239.8	7.70	1.75
153	0	5,870	119.4	-		-	188	11,297	5,400	245.5	132.8	8.04	1.85
154	0	3,913	91.4	-	$MgSO_4$, at the rate of 25 g/l + 2 g/l $MgCO_3 \cdot 3H_2O$	-	188	10,680	4,000	181.8	101.6	8.19	1.79
155	0	2,935	69.5	-		-	188	10,200	3,050	138.7	80.9	8.27	1.71
156	0	2,348	51.3	-		-	200	9,770	2,633	119.7	69.2	8.38	1.73
157	0	1,677	44.9	-		-	200	9,520	2,000	90.9	55.0	8.51	1.65
158	0	1,304	36.2	-		-	200	9,300	1,600	72.7	45.0	8.63	1.62
159	0	1,067	32.1	-		-	200	9,270	1,510	68.6	41.0	8.71	1.67
36[3]	0	-	288	9.24	NaCl 390 g/l	17	133	101,388	4,040	183.6	126.0	7.46	1.46
37[3]	0	-	224	9.24	NaCl 195 g/l	12	122	57,300	4,200	190.9	100.8	8.10	1.89
38[3]	0	-	287	9.0	NaCl 97 g/l	6	118	30,900	4,104	-	72.	9.10	-

TABLE 11. Results of analyses of liquid and solid phases of the $MgO-CO_2-H_2O$ system in equilibrium at 20°C in a $MgSO_4$ background (Concluded)

Experiment	Bottom phases: MgO[2]	CO_2[2]	100°:air-dry[2]	H_2O (900° : 100°)	SO_4 (mg/l)	Total	N_g	N_p	$N_g - N_p$	D 20/4 (specific gravity)
No data available for experiments 152-159										
36[3]	39.70	35.50	10.05	17.00	0.96	100.21	-	1.480	-	2.067
37[3]	39.11	37.80	8.28	14.07	0.80	100.06	-	-	-	2.561
38[3]	32.84	33.50	18.71	15.14	trace	100.19	1.500	1.484	0.016	1.873

[1] This column is labeled "Added NaCl, g/liter" in the original. However, no NaCl was added in Expts. 152-159 but $MgSO_4$ was added instead. It is not clear from the Table or the context whether $MgCO_3 \cdot 3H_2O$ was added to No. 's 156-159 only or to No. 's 152-159, alongside $MgSO_4$ or whether the rate of addition of the sulfate had a relation to the carbonate expected to develop in the solid phase. VPS

[2] Expressed in percent of air-dry sample.

[3] The empirical formulae for the sediments from the last three experiments, not including percent H_2O lost at 110°C, are: 36, $MgCO_3 \cdot 0.24Mg(OH)_2 \cdot 1.70H_2O$; 37, $MgCO_3 \cdot 13Mg(OH)_2 \cdot 1.29H_2O$; and 38, $MgCO_3 \cdot 0.05Mg(OH)_2 \cdot 1.82H_2O$.

TABLE 12. Analyses of reagents used in $MgO-CO_2-H_2O$ system experiments in a background of sea water (mg/l)

Reagent	CaO	MgO	CO_2	Alkaline reserve (meq/l)	pH	Cl^-	SO_4^{2-}	Experiments
Sea Water	580	2,170	108	2.6	-	18,940	2,540	1-11
	610	2,140	108	2.6	-	19,040	2,650	12-13
	610	2,200	108	2.6	-	19,170	2,690	14-19
$Ca(HCO_3)_2$ and sea water	1,380	2,014	-	30.9	6.8	-	-	1-11
	1,570	2,150	-	34.9	-	-	-	14-19
	2,050	-	-	48.0	-	-	-	12-13
$Mg(HCO_3)_2$ and sea water	540	6,080	-	186.3	7.1	-	-	1-3
	-	6,338	-	196.1	-	-	-	4-10
	300	6,573	-	210.5	-	-	-	11-13
	-	7,560	-	264.8	-	-	-	14-19

THE 60°C ISOTHERM ($MgO-CO_2-H_2O$) SYSTEM UNCONFINED

The absence of magnesite - as the equilibrium bottom phase - in our experiments with the 20°C isotherm of the unconfined $MgO-CO_2-H_2O$ system has led us to a consideration of thermodynamic factors of the magnesite system, that is, temperature and partial pressures of CO_2. Because these two magnitudes are interrelated functionally in our system, their mutual effect in confined systems (like natural deep waters and ground waters) was designated by us as "the thermodynamic factor." In the instance of open systems, where the partial pressure of CO_2 is determined chiefly by the atmospheric air, the temperature factor acquires an independent significance, for all practical purposes, and may be regarded independently from the pressure.

However, in open systems of the relatively deep basin type, where there is a continuous production of CO_2 in the bottom silts, the environment is created which is intermediate between confined and open systems, for the carbonic acid secreted during the diagenesis of bottom silts is, first of all, under a pressure of a column of water in the given basin.

The foregoing considerations have led us to a series of experiments in open vessels, as well as in ampules at varying temperatures and pressures of the gaseous phase.

The Method of Crystallization from Magnesium-Supersaturated Solutions by the Means of a Partial Removal of CO_2 (degasation).

Six experiments (52-57) were performed at 60°C, involving one to two months' "aging" of the solutions. The experiments were in the fields of high and intermediate CO_2 concentrations. Their results are summarized in table 14 and are represented also by figures 2 and 14.

The bottom phase, in all experiments, was a fine-grained crystalline sediment of the empirical formula $4MgCO_3 \cdot Mg(OH)_2 \cdot 4H_2O$ (hydromagnesite).

In the crystallogenetic process, in systems at high concentrations (experiments 52 and 53), nesquehonite of the needle habit (length of the needles commonly 100 microns; width, 10 to 20 microns) was the earliest bottom phase. However, after a few days, a degeneration of the nesquehonite crystals would begin, with a transition toward a stable equilibrium phase; basic magnesium carbonate with the composition formula of hydromagnesite, as given above; hence the formula: $834\ MgCO_3 \cdot 129\ Mg(OH)_2 \cdot 808H_2O$ or, disregarding the insignificant admixtures of nesquehonite and magnesite, $4MgCO_3 \cdot Mg(OH)_2 \cdot 4H_2O$. Coefficients of the liquid phase at equilibrium, CO_2:MgO and CO_2:alkaline residue are given in milligrams and milliequivalents per liter respectively.

Sediments obtained at 60°C are almost entirely of the $4MgCO_3 \cdot Mg(OH)2 \cdot 4H2O$ type. They are closer to the intermediate salt (magnesite) than are the sediments of the 20°C isotherm which are chiefly brucite, $mg(OH)_2$; artinite, $MgCO_3 \cdot Mg(OH)_2 \cdot 1.5H_2O$; and, in part, hydromagnesite, $4\ MgCO_3 \cdot Mg(OH)_2 \cdot 4H_2O$. Because of this, relative partial pressure of carbonic acid (with respect to magnesium, CO_2:MgO was greatly increased, requiring aeration of the system (evaporating) by atmospheric air conditioning definite quantities of CO_2.

The Method of Evaporation of Unsaturated Solutions with Continuous Blowing of Atmospheric Air

Experiments 160, 161, and 167 (table 14, p. 21, fig. 1) were made at 60°C. In 160, the evaporated volume was being replaced by distilled water. The alkaline reserve fell to 5.0 to 5.6 from the original 24.9. The bottom phase was basic magnesium carbonate.

TABLE 14. Results of analyses of liquid and solid phases at equilibrium in an open magnesium-supersaturated $MgO-CO_2-H_2O$ system at 60°C (partial-CO_2-removal method)

Experiment	Initial Solution			pH	CO_2-degas-ation in vacuum (minutes)	Length of aging (days)	Solution at equilibrium							
	MgO (mg/l)	CO_2 (mg/l) $Mg(OH)_2$	Alkaline reserve (meq/l)				MgO		CO_2			Alkaline reserve		pH
							(mg/l)	√	(mg/l)	√	(meq/l)	(meq/l)	√	
52	6,180	13,360	297	7.80	15	75	2,962	54.4	6,610	81.3	300.5	139	11.79	8.34
53	3,534	7,128	162	8.3	18	70	1,963	44.3	4,360	66.0	198.2	94	9.69	8.2
54	2,140	4,672	106	8.4	40	52	1,003	31.7	2,162	46.5	98.3	47.0	6.85	8.54
55	1,650	-	76.1	8.4	60	51	970	31.1	2,100	45.9	95.5	46.0	6.78	8.68
56	1,060	-	48.0	8.4	130	42	427	20.7	890	29.8	40.5	20.0	4.47	8.75
57	615	1,232	28.0	8.4	240	40	289	17.0	573	23.9	26.1	13.0	3.60	8.96
160	590	1,230	24.9	-	continuous	27	120	10.9	250	15.8	11.4	5.0	2.24	8.71
161	530	$Mg(OH)_2$ suspension		-	aeration with air of the atmosphere	41	120	10.9	300	17.3	13.6	6.0	2.45	9.26
167	240	490	10.9	-		36	200	14.1	380	19.5	17.3	8.0	2.83	9.43

TABLE 14. Results of analyses of liquid and solid phases at equilibrium in an open magnesium-supersaturated $MgO-CO_2-H_2O$ system at 60°C (partial-CO_2-removal method) (Concluded)

Experiment	Coefficients		Bottom phases[1]					Optics[2]		
	CO_2:MgO	CO_2:alkaline reserve	MgO	CO_2	H_2O:110° (air-dry)	H_2O (900°:100°)	Total	N_g	N_p	N_g-N_p
52	2.23	2.16	41.29	37.4	4.09	17.27	100.05	1.518	1.417	0.101
53	2.22	2.11	41.55	36.20	3.80	18.64	100.19	-	-	-
54	2.16	2.09	40.94	37.40	4.37	17.71	99.39	-	-	-
55	2.16	2.07	41.59	36.20	3.84	18.73	100.36	1.516	1.419	0.097
56	2.08	2.02	41.22	36.20	4.44	18.17	100.03	1.516	1.419	0.097
57	1.98	2.00	41.49	36.60	4.76	17.21	100.05	1.516	1.419	0.097
160	2.09	2.27	-	-	-	-	-	-	-	-
161	2.50	2.27	Double point $Mg(OH)_2$ basic magnesium carbonate							
167	1.90	2.16	Magnesite					1.710	1.515	0.195

[1]Chemical analyses represent principal nearly monominerallic mass of hydromagnesite (experiments 52-57)

[2]Single well-defined individuals of nesquehonite within the matrix of a very fine and poorly definable hydromagnesite were optically investigated (experiments 52-57)

TABLE 13. Results of analysis of liquid and solid phases of $CaO-MgO-CO_2-H_2O$

Experiment	Experimental design	Rate of addition (ml/hr)		Initial solution				
		Ca	Mg	CaO (mg/l)	MgO (mg/l)	CO_2 (mg/l)	Alkaline reserve (meq/l)	pH
4		-	-	1, 380	2, 014	-	30.9	-
9	$Ca(HCO_3)_2 \rightarrow$ SW	-	-	-	-	-	-	-
8		-	-	-	-	-	-	-
16		350	20	-	2, 442	-	-	-
15	$Ca(HCO_3)_2$ + $Mg(HCO_3)_2 \rightarrow$ SW	400	50	-	2, 751	-	25. 2	-
14		275	50	-	2, 996	-	23. 6	-
6	$Mg(HCO_3)_2 \rightarrow$ SW	-	-	-	-	-	-	-
19	$Ca(HCO_3)_2$ + $Mg(HCO_3)_2 \rightarrow$ SW	40	20	-	3, 953	-	-	-
3	$Mg(HCO_3)_2 \rightarrow$ SW	-	20	-	6, 080	-	58. 0	-
13	$Ca(HCO_3)_2$ + $Mg(HCO_3)_2 \rightarrow$ SW	250	120	-	3, 585	-	-	-
18		50	60	-	-	-	-	-
10	$Mg(HCO_3)_2 \rightarrow$ SW	-	150	-	-	-	-	-
2	Aerated SW saturated with $Mg(HCO_3)_2$	-	-	160	4, 070	-	73. 0	8. 4
11	$Mg(HCO_3)_2 \rightarrow$ SW	-	50	-	-	-	-	-
12	$Ca(HCO_3)_2$ + $Mg(HCO_3)_2 \rightarrow$ SW	120	120	-	4, 361	-	-	-
1	Aerated SW	-	-	540	6, 080	-	186. 3	7. 1
5	saturated with	-	-	-	6, 338	-	196. 1	-
7	$Mg(HCO_3)_2$	-	-	-	-	-	-	-

TABLE 13. Results of analysis of liquid and solid phases of $CaO-MgO-CO_2-H_2O$

Experiment	Experimental design	Solution at equilibrium				Solid-bottom phase (percent air-dry sample)		
		Alkaline reserve		pH	Coefficient			
		meq/l	$\sqrt{\ }$		CO_2: alk. r.	CaO	MgO	CO_2
4		4. 7	-	7. 30		53. 33	none	42. 00
9	$Ca(HCO_3)_2 \rightarrow$ SW	7. 7	2. 77	7. 30	1. 71	53. 53	0. 36	42. 37
8		7. 7	2. 77	7. 5	1. 77	54. 45	0. 45	43. 21
16		15. 0	3. 87	7. 4	2. 00	53. 90	0. 94	42. 98
15	$Ca(HCO_3)_2$ + $Mg(HCO_3)_2 \rightarrow$ SW	18. 1	4. 26	7. 2	1. 95	54. 10	0. 86	43. 20
14		24. 0	4. 90	7. 7	1. 90	54. 20	0. 86	43. 46
6	$Mg(HCO_3)_2 \rightarrow$ SW	41. 0	6. 40	8. 4	2. 00	0. 08	29. 00	32. 10
19	$Ca(HCO_3)_2$ + $Mg(HCO_3)_2 \rightarrow$ SW	47. 2	6. 87	8. 4	1. 93	48. 0	3. 25	41. 30
3	$Mg(HCO_3)_2 \rightarrow$ SW	53. 0	7. 28	8. 4	1. 70	9. 45	24. 47	32. 00
13	$Ca(HCO_3)_2$ + $Mg(HCO_3)_2 \rightarrow$ SW	53. 2	7. 29	8. 4	1. 71	51. 80	1. 23	42. 30
18		60. 2	7. 76	8. 4	2. 00	18. 70	22. 0	38. 60
10	$Mg(HCO_3)_2 \rightarrow$ SW	60. 9	7. 80	-	1. 73	21. 0	18. 90	37. 07
2	Aerated SW saturated with $Mg(HCO_3)_2$	62. 7	7. 92	8. 4	1. 62	1. 95	27. 41	33. 00
11	$Mg(HCO_3)_2 \rightarrow$ SW	72. 0	8. 48	8. 4	1. 74	9. 44	24. 26	34. 08
12	$Ca(HCO_3)_2$ + $Mg(HCO_3)_2 \rightarrow$ SW	78. 7	8. 8	8. 3	1. 84	46. 44	4. 40	40. 80
1	Aerated SW	88. 4	9. 4	8. 3	2. 00	2. 95	26. 08	32. 00
5	saturated with	96. 4	19. 8[1]	8. 3	1. 89	0. 16	28. 57	31. 80
7	$Mg(HCO_3)_2$	228. 0	15. 1	8. 1	1. 84	0. 08	28. 4	31. 01

[1]Value should be 9. 3 --VPS.

Experiment 167 was most interesting after 36 days of the continuous blowing of the atmospheric air, it became possible to obtain an equilibrium system containing 200 mg/l MgO in solution, together with 380 mg/l CO_2, and the alkaline reserve of 8. 0 meq/l at pH 9. 43. Under such conditions, the sediment was a two-phased system: a) magnesite rhombohedra,

system at equilibrium against the background of sea water (SW), at 15°C

Solution at equilbrium								
Duration of aeration (mixing)		Temperature (°C)	Length of aging (days)	CaO (mg/l)	MgO (mg/l)	CO_2		
(days)	(hours)					(mg/l)	$\sqrt{}$	(meq/l)
11	-	15	23	780	2, 200	-	-	-
11	-	-	76	660	2, 220	290	17.03	13.18
11	-	-	80	150	2, 550	300	17.32	13.64
11	-	-	45	420	2, 470	660	25.69	30.0
11	-	-	85	300	2, 790	776	27.85	35.3
11	-	-	84	140	3, 050	1, 003	30.98	45.6
-	8	-	32	trace	3, 400	1, 800	42.42	82.0
-	8	-	67	180	3, 460	2, 000	44.72	91.0
-	8	15 ± 1	24	40	3, 650	1, 980	43.8	90.0
-	8	-	60	20	3, 520	2, 000	44.72	91.0
-	8	-	67	60	3, 740	2, 464	49.6	112.0
-	8	-	64	30	3, 720	2, 320	48.2	105.5
-	10	14	30	120	3, 880	2, 240	47.3	101.8
-	10	-	60	50	4, 010	2, 750	52.4	125.5
-	10	-	60	30	4, 170	3, 190	-	145.0
-	15	14	32	160	4, 310	3, 000	-	177.3
-	2	-	32	trace	4, 100	4, 004	-	182.0
-	0.5	-	32	trace	4, 374	5, 200	-	236.4

system at equilibrium against the background of sea water (SW), at 15°C (Concluded)

Solid-bottom phase (concluded)				
110°: air-dry	H_2O (900°:100°C	Insoluble residue	Total	Minerals (formulae)
3.04	42.76	0.14	99.27	$CaCO_3$
4.40	0.03	trace	100.69	
0.90	0.74	trace	99.75	
1.38	1.23	-	100.43	
1.23	0.90	-	100.29	
1.12	0.96	-	100.60	
21.05	18.30	0.02	100.55	$MgCO_3 \cdot 3H_2O$; D16/4 = 1.847
3.71	4.20	0.02	100.46	$CaCO_3 + MgCO_3 \cdot 3H_2O$
16.37	18.42	-	100.71	
3.18	1.26	trace	99.77	
15.06	4.74	-	99.10	
14.81	8.87	trace	100.65	
21.26	17.10	0.08	100.80	
18.58	14.44	trace	100.72	
5.06	3.08	trace	99.78	
19.76	18.92	0.02	99.73	
20.12	20.00	0.02	100.67	$MgCO_3 \cdot 3H_2O$
22.05	19.00	0.04	100.57	

rom 3 to 12 microns in diameter, with the efraction indices N_g = 1.710, N_p = 1.515. $_g$-N_p = 0.195 (experiment 167); b) a scaly fine- crystalline mass (possibly of the hydromagne- ite type (?) with the following refraction indices: N_g = 1.527, N_p = 1.501, and N_g-N_p = 0.026.

It was very characteristic for experiments 160-167 that the partial pressure of CO_2 was relatively high (the CO_2:alkaline reserve

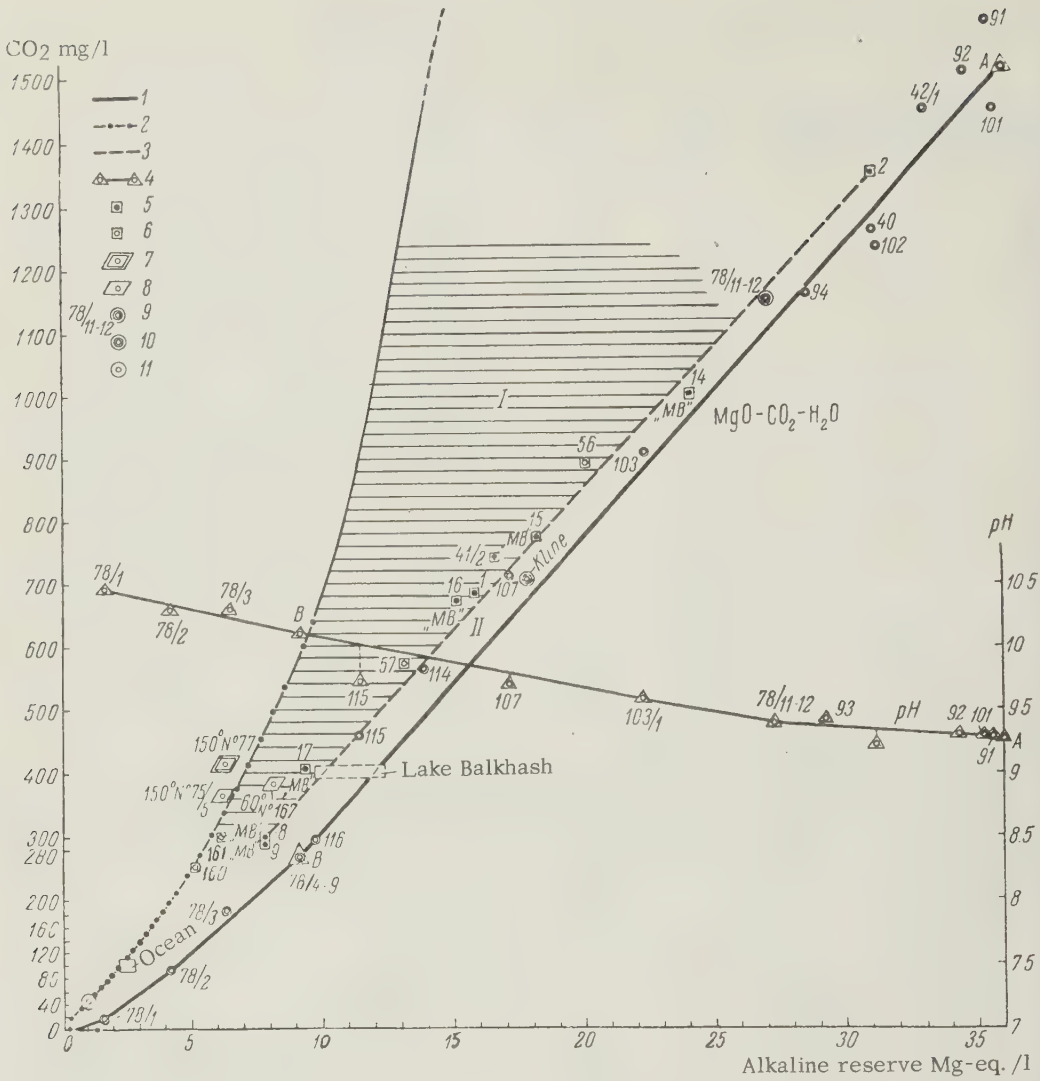

FIGURE 14. $MgO-CO_2-H_2O$ and $CaO-MgO-CO_2-H_2O$ systems at equilibrium
1) $MgO-CO_2-H_2O$ system equilibrium curve at 20°C; 2) $CaO-MgO-CO_2-H_2O$ system equilibrium curve at 20°C; 3) boundary between $CaCO_3$ and magnesium carbonate fields; 4) pH curve for $MgO-CO_2-H_2O$ system at 20°C; 5) bottom phases of $CaCO_3$ at 20°C; 6) bottom phases of $MgO-CO_2-H_2O$ system at 60°C; 7) bottom phase of dolomite at 150°C; 8) bottom phases of magnesite at 60° and 150°C; 9) the (Kazakov) point of basic magnesium carbonate at equilibrium with CO_2 of the atmosphere at 20°C; 10) the point of basic magnesium carbonate at equilibrium with CO_2 of the atmosphere at 20°C [87]; and 11) the point of $CaCO_3$ in the $CaO-CO_2-H_2O$ system at 16° to 20°C at equilibrium with CO_2 of the atmosphere [85].

coefficient was from 2.16 to 2.27). Experiment 167 serves to define apparently the lower boundary of the magnesitic field of the 60°C isotherm (by the alkaline reserve), confirming the previously indicated importance of the thermodynamic factor in the formation of magnesite.

THE 150°C ISOTHERM ($MgO-CO_2-H_2O$ SYSTEM CONFINED)

The beneficial effect of the increased thermodynamic factor on crystallization of magnesite of the 60°C isotherm, the $MgO-CO_2-H_2O$ system, led us to further elaborations of this factor and to experiments in ampules at 150°C in a thermostat. We had performed nine such experiments. Well crystallized sediments (rhombohedra) of magnesite were obtained in all, except experiment 73/9 (table 15 and fig. 15).

These experiments have served clearly to delineate the magnesite field in the $MgO-CO_2-H_2O$ system at 150°C. The lower boundary of the field may be taken as the line corresponding to 6.0 meq/l alkaline reserve; the upper boundary is about 15. The pH level is not particularly high in this field; it falls between 6.8 and 7.8.

TABLE 15. Results of analyses of liquid and solid phases at equilibrium in a confined $MgO-CO_2-H_2O$ system at 150°C

Experiment	Initial Solution				Solution at equilibrium									Bottom phases
	MgO (mg/l)	CO_2 (mg/l)	Alkaline reserve (meq/l)	pH	Aging (hrs)	MgO (mg/l)	CO_2 (mg/l)	CO_2 Mg- (meq/l)	Alkaline reserve (meq/l)	pH	CO_2:MgO	CO_2: a. r.*	Temperature (°C)	
73/5c	1,231	2,528	57.0	-	15	-	-	-	17.3	-	-	-	150	Metastable nesquehonite and rare rhombohedral magnesite; 5 to 10 microns; $N_g = \pm 1.700$.
73/6b	783	1,609	36.0	-	18	-	-	-	13.2	-	-	-	150	Stable, coarse rhombohedral $MgCO_3$ (up to 25 microns). About 85 percent degenerate metastable needles of $MgCO_3 \cdot 3H_2O$
75/1	696	1,522	34.6	8.30	16	-	-	-	17.3	7.88	-	-	150	Sparse $MgCO_3$ rhombohedra; and metastable needles of $MgCO_3 \cdot 3H_2O$
75/2	696	1,522	34.6	8.30	40	-	-	-	10.1	7.36	-	-	158	Stable $MgCO_3$ rhombohedra $N_g > 1.694 < 1.708$; $N_p = 1.512$
75/3	696	1,522	34.6	8.30	60	-	-	-	6.1	6.74	-	-	158	$MgCO_3$ rhombohedra
75/4	696	1,522	34.6	8.30	100	-	-	-	6.1	6.80	-	-	158	$MgCO_3$ rhombohedra
75/5	696	1,522	34.6	8.30	115	126	366	16.6	6.1	6.87	2.91	2.73	158	$MgCO_3$ rhombohedra
73/7	410	843	18.3	-	-	-	-		-	-	-	-	150	Small rhombohedra of $MgCO_3$ (approximately 3 microns)
73/9	210	432	9.2	7.5	-	-	-		-	-	-	-	150	No $MgCO_3$ rhombohedra detected

* alkaline reserve

The relatively high partial pressures of CO_2 of the liquid phase at equilibrium are very typical for the high-temperature magnesite systems. They are characterized by the coefficients CO_2:MgO = 2.91, which coincides with the same coefficients of low-temperature magnesite systems (at 20° and even at 60°C).

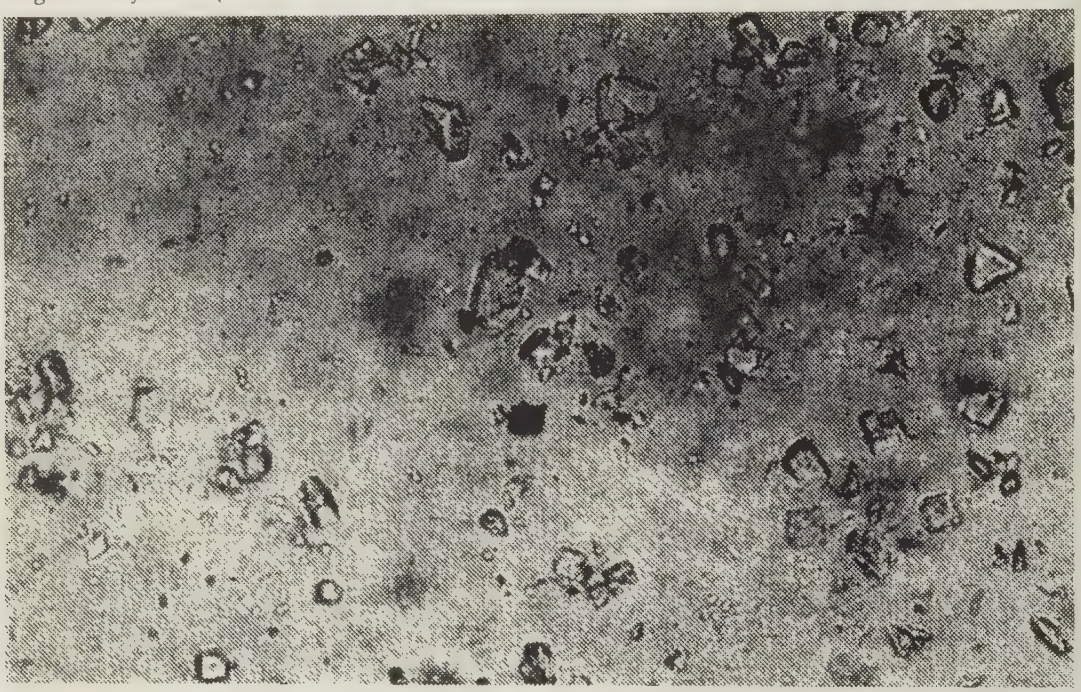

FIGURE 15. Magnesite rhombohedra (experiment 75/5, X368)

Having ascertained the major role of the thermodynamic factor in the development of magnesite, with the examples of the 60° and the 150°C isotherms, it becomes possible to suppose that stable magnesite fields in MgO-CO_2-H_2O systems may also exist at temperatures lower than 60°C, under appropriately increased partial pressures of CO_2 in the systems.

THE DOLOMITE SYSTEM CaO-MgO-CO_2-H_2O: THE 20°C ISOTHERM

Method of Slow Mixing of Ca and Mg Bicarbonate Solutions while Aerating with Atmospheric Air

This method is analogous to the one that was used in our studies of the unconfined MgO-CO_2-H_2O system in a sea-water background. This method was employed in seven experiments and the results are given in table 16. Particularly, table 16 shows that, in all cases, the solid bottom phases were either calcite nesquehonite or calcite with an admixture of basic magnesium carbonate.

The Method of Slow Mixing of Magnesium Bicarbonate and Calcium Hydroxide Solutions (using $Mg(HCO_3)_2 \cdot H_2O \cdot Ca(OH)_2$)

Two experiments (41/1 and 41/2) were performed with a slow concurrent mixing of a solution of $Mg(HCO_3)_2$ and a saturated $Ca(OH)_2$ solution containing 1,525 mg CaO per liter (table 17). The bottom phases, in both experiments, were calcite mixed with a basic magnesium carbonate.

All nine experiments with the CaO-MgO-CO_2-H_2O system at 20° to 24°C in the fields of high and intermediate CO_2 concentrations enable us to make the following conclusions:

1. Figurative points of the given quaternary system, in the diagram with the CO_2:alkaline reserve parameters, fall along the nesquehonite line of the MgO-CO_2-H_2O system and of its basic magnesium carbonates.

2. Calcite with a small admixture of basic magnesium carbonate are the bottom phases of the system within the alkaline reserve fields from 16.5 to 38.0. In the alkaline reserve fields of 54 meq/l and higher the bottom phase is a mixture of calcite and nesquehonite. In such manner, all of these nine points are essentially double points which form a line separating the field of pure calcite from the field of magnesium carbonates. Dolomite and magnesite were not detected in these experiments.

The CO_2 partial pressure index, CO_2: alkaline reserve, was 1.8 to 2.0 in all experiments with the system in question; it was not different from the index of the MgO-CO_2-H_2O system at 20°C previously examined.

TABLE 16. Results of analyses of liquid and solid phases at equilibrium in an open $MgO-CO_2-H_2O$ systems at 20°C(mixed solutions of $Ca(HCO_3)_2$ and $Mg(HCO_3)_2$)

Experiment	Initial Solution				Rate of Mixing (ml/hr)		Aging (days)
	CaO (mg/l)	MgO (mg/l)	CO_2 (mg/l)	Alkaline reserve (meq/l)	Ca	Mg	
5	199	1,519	3,733	-	100	200	92
6	120	1,822	4,251	-	100	400	102
4	296	1,139	3,086	-	100	100	141
4a	296	1,139	3,086	-	100	100	6
3	395	760	2,439	36.2	100	50	8
2	474	456	1,921	-	100	25	146
1	539	207	1,497	-	100	10	153

TABLE 16. Results of analyses of liquid and solid phases at equilibrium in an open $MgO-CO_2-H_2O$ systems at 20°C(mixed solutions of $Ca(HCO_3)_2$ and $Mg(HCO_3)_2$) (Continued)

Experiment	Solution at equilibrium								
	CaO (mg/l)	MgO (mg/l)	CO_2			Alkaline reserve		pH	CO_2:alk. reserve
			(mg/l)	$\sqrt{\ }$	(meq/l)	(meq/l)	$\sqrt{\ }$		
5	-	955	3,040	55.1	138.2	80.5	8.97	8.75	1.72
6	-	1,038	2,710	52.1	123.2	74.0	8.60	9.11	1.66
4	22	985	2,318	48.1	105.3	59.0	7.68	8.41	1.78
4a	22	-	2,196	46.9	99.8	54.0	7.35	-	1.85
3	25	623	1,492	38.6	67.8	36.0	6.0	8.20	1.88
2	37	401	1,352	36.8	61.5	31.0	5.57	8.08	1.98
1	50	-	684	26.2	31.1	15.7	3.96	8.08	1.98

TABLE 16. Results of analyses of liquid and solid phases at equilibrium in an open $MgO-CO_2-H_2O$ systems at 20°C(mixed solutions of $Ca(HCO_3)_2$ and $Mg(HCO_3)_2$) (Concluded)

Experiment	Bottom phases	Analysis of bottom phases (percent of air-dry sample)			
		CaO	MgO	CO_2	110°:air-dry
5	$CaCO_3$ and some $MgCO_3 \cdot 3H_2O$	53.44	2.13	-	-
6	$MgCO_3 \cdot 3H_2O$ and $CaCO_3$	3.90	-	42.15	-
4	$CaCO_3$ and some $MgCO_3 \cdot 3H_2O$	53.73	1.27	44.15	0.37
4a	$CaCO_3$ and some $MgCO_3 \cdot 3H_2O$	-	-	-	-
3	$CaCO_3$ and some basic magnesium carbonate	-	-	-	-
2	$CaCO_3$ and some basic magnesium carbonate	-	-	-	-
1	$CaCO_3$ and some basic magnesium carbonate	-	-	-	-

TABLE 17. Results of analyses of liquid and solid phases at equilibrium in an open $CaO-MgO-CO_2-H_2O$ system at 20°C (in a solution of $Mg(HCO_3)_2$ and a saturated $Ca(OH)_2$ solution)*

Experiment	CaO (mg/l)	MgO (mg/l)	CO_2 (mg/l)	Alkaline reserve (meq/l)	Rate of Mixing (ml/hr)		Aging (days)
					Ca	Mg	
41/1	243	5,200	2,521	64.5	19	100	106
41/2	762	3,090	1,500	-	100	100	104

TABLE 17. Results of analyses of liquid and solid phases at equilibrium in an open $CaO-MgO-CO_2-H_2O$ system at 20°C (in a solution of $Mg(HCO_3)_2$ and a saturated $Ca(OH)_2$ solution)* (Concluded)

Experiment	Solution at equilibrium							pH	CO_2:alkaline reserve
	CaO (mg/l)	MgO (mg/l)	CO_2			Alkaline reserve			
			(mg/l)	$\sqrt{\ }$	(meq/l)	(meq/l)	$\sqrt{\ }$		
41/1	trace	1,209	1,672	40.9	76.0	38.0	6.16	8.4	2.00
41/2	trace	456	740	27.2	33.6	16.5	4.06	8.4	2.04

* Bottom phase is represented by $CaCO_3$ and basic magnesium carbonates

Effects of Sea-Water Constituents on CaO-MgO-CO_2-H_2O System at 20°C

NaCl Background

Three experiments were made with the addition of NaCl, as the background, by analogy with the magnesite system. The results are summarized in table 18 and represented in figures 1 and 14.

TABLE 18. Results of analyses of the liquid phase at equilibrium in the CaO-MgO-CO_2-H_2O system at 20°C in a NaCl background

Experiment	Initial solution					Aging (days)	Temperature (°C)
	CaO (mg/l)	MgO (mg/l)	CO_2 (mg/l)	Alkaline reserve (meq/l)	NaCl (g/l)		
42/2	250	-	2,383	68.0	289	90	20
43	250	-	2,383	68.0	289	90	20
42/1	250	-	2,383	68.0	289	90	20

TABLE 18. Results of analyses of the liquid phase at equilibrium in the CaO-MgO-CO_2-H_2O system at 20°C in a NaCl background (Concluded)

Experiment	Solution at equilibrium									
	CaO (mg/l)	MgO (mg/l)	CO_2			Alkaline reserve		NaCl (g/l)	pH	CO_2:alk. reserve
			(mg/l)	$\sqrt{}$	(meq/l)	(meq/l)	$\sqrt{}$			
42/2	trace	2,020	2,040	45.0	92.0	46.0	6.78	289	8.34	2.00
43	trace	1,873	1,700	41.2	77.3	40.0	6.32	289	9.20	1.93
42/1	trace	1,423	1,452	38.1	66.0	33.0	5.74	289	8.78	2.00

As evident from the figurative points in figure 2 no important displacement or changes in the CaO-MgO-CO_2-H_2O system at 20°C are caused by the addition of NaCl. Magnesite could not be detected in these experiments, and the bottom phase was represented chiefly by calcite.

Sea-Water Background

The absence of magnesite and dolomite sediments in open MgO-CO_2-H_2O and CaO-MgO-CO_2-H_2O systems at 20° to 24°C has prompted us to investigate a quaternary system of dolomite in a sea-water background, by way of a reconnaissance, within a wide range of the alkaline-reserve levels from 7 to 120.

By adding solutions of Ca and Mg bicarbonates to artificial sea water, prepared according to the Bruyevich method, and by the subsequent blowing of atmospheric air through the system (the degasation of CO_2), the crystallization of the CaO-MgO-CO_2-H_2O system was induced (the SW background). After sufficient aging, the equilibrium liquid and solid phases were examined. Altogether, there were 19 long experiments (1-19).

The bottom phases in experiments 1-19 were chiefly calcite, $CaCO_3$, and nesquehonite, $MgCO_3 \cdot 3H_2O$, separately or as two-phased sediments. Dolomite and magnesite sediments were not detected in the open CaO-MgO-CO_2-H_2O system in a sea-water background.

In all experiments with the open system here discussed, a relatively low partial pressure of carbonic acid at equilibrium (the CO_2:alkaline reserve coefficient was 2.0) was observed. The sea-water background produced no appreciable increase in the CO_2 tension of the system.

THE 60°C ISOTHERM IN A SEMIOPEN CaO-MgO-CO_2-H_2O SYSTEM AND THE 150°C ISOTHERM IN A CLOSED SYSTEM

The following experiments were conducted to determine the thermodynamic potential of CO_2: 2 at 60°C, aerated with atmospheric air; 1 at 100°C, aerated with CO_2 from a cylinder; and 9 at 150°C in ampules. Of these, 8 were completed. Their results are summarized in table 19 and represented in figures 1 and 16.

Analogously to magnesite, dolomite is developed easily in a carbonate system at an elevated thermodynamic potential (the type of closed systems at an elevated partial pressure of CO_2) but is not formed in open systems where the partial pressure of carbonic acid is similar to that of normal atmospheric air. The indirect index of the relative partial pressure of carbonic acid in the system, by reference to the alkaline reserve (CO_2:alkaline reserve), serves to define rather clearly the alkaline-reserve contours of the magnesite-dolomite field of the flat diagram, with the CO_2:alkaline reserve as 2.3 to 2.6 at at 60°C and 2.7 to 3.0 for the 150°C isotherm.

In the field of dolomite and magnesite crystallization, in the quaternary CaO-MgO-CO_2-H_2O system, magnesite begins to pass into the sediment after the Ca-ion impoverishment of the

TABLE 19. Results of analyses of liquid and solid phases in equilibrium in the CaO-MgO-CO_2-H_2O system at 60° and 150°C (figs. 1 and 16)

Experiment	Initial Solution					Temperature (°C)	Aging (hours)
	CaO (mg/l)	MgO (mg/l)	CO_2 (mg/l)	Alkaline reserve (meq/l)	pH		
A. Open systems, at 60°C, aerated with atmospheric air							
165[1]	68	136	460	9.4	-	60	2,160
168[2]	40	220	570	11.2	-	60	960
B. Confined systems, at 150°C, in ampules							
74/1	0.6	783	1,610	33.6	7.9	150	14
74/2	1.3	783	1,610	33.6	7.9	150	20
74/3[3]	3.4	783	1,610	34.6	7.9	150	20
74/4	6.3	776	1,620	34.6	7.9	150	20
74/5	15.5	763	1,629	35.6	7.9	150	20
77[4]	52	622	1,358	30.5	7.94	150	90

TABLE 19. Results of analyses of liquid and solid phases in equilibrium in the CaO-MgO-CO_2-H_2O system at 60° and 150°C (figs. 1 and 16) (Concluded)

Experiment	Solution at equilibrium								
	CaO (mg/l)	MgO (mg/l)	CO_2			Alkaline reserve		pH	CO_2:alk. reserve
			(mg/l)	$\sqrt{\ }$	(meq/l)	(meq/l)	$\sqrt{\ }$		
A. Open systems, at 60°C, aerated with atmospheric air									
165[1]	12	98	330	18.16	15.8	5.8	2.41	9.14	2.58
168[2]	-	-	310	17.61	14.1	8.3	2.88	9.38	1.70
B. Confined systems, at 150°C, in ampules									
74/1	-	-	-	-	-	-	-	-	-
74/2	-	-	-	-	-	-	-	-	-
74/3[3]	-	-	-	-	-	-	-	-	-
74/4	-	-	-	-	-	-	-	-	-
74/5	-	-	-	-	-	-	-	-	-
77[4]	28	86	412	20.30	18.7	6.1	2.67	6.66	3.07

[1] $CaCO_3$ and basic magnesium carbonates (artinite type) in bottom phase: N_g = 1.613, N_p = 1.536, and N_g-N_p = 0.077.
[2] $CaCO_3$ and basic magnesium carbonates (artinite type) in bottom phase: N_g = 1.572, N_p = 1.507, and N_g-N_p = 0.065.
[3] Magnesite rhombohedra.
[4] Coarse, rhombohedral dolomite crystals; N_g = 1.677.

solution and in such cases where the CaO concentrations are as much as 20 mg/l or even lower.

The relatively low pH (6.8 to 7.9) of dolomite and magnesite solutions are in full harmony with the increased partial pressures of CO_2 in the systems yielding crystalline dolomite and magnesite, as observed in all experiments with the sedimentation of $MgCO_3$ and $CaMg(CO_3)_2$ at 60° and 150°C.

One of the many problems on the agenda for further experimental work with the synthesis of dolomite and magnesite is the production of synthetic dolomite and magnesite from bottom sediments in a state of equilibrium and at various lower temperatures, under conditions where the partial pressures of carbonic acid in the system would have to be increased. This would necessarily constitute an imitation of the diagenesis in CO_2-producing bottom silts in deep waters and in other similar diagenetic environments.

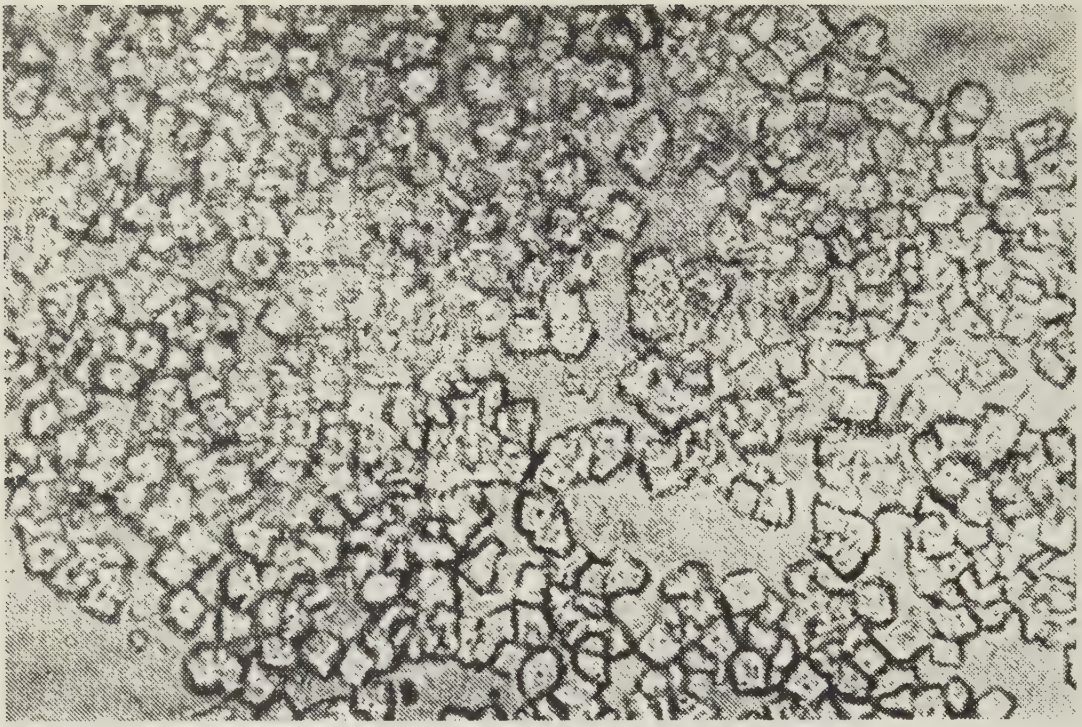

FIGURE 16. Dolomite rhombohedra (experiment 77, X367)

CONDITIONS OF DOLOMITE AND MAGNESITE FORMATION IN SEDIMENTARY ROCK

Comparison of Geochemical Indices in Environments of Dolomite and Magnesite Sedimentation with those of Apatite Precipitated from Sea Water

The following are the characteristic environmental indices for the development of dolomite and magnesite, as determined from our experiments and the analysis of Lake Balkhash waters: 1) concentrations of CaO, MgO, CO_2, and, to some extent, total salinity; 2) the alkaline reserve and pH; and 3) the CO_2:alkaline reserve coefficient, expressing CO_2 in reference to the total alkaline reserve (that is, in reference chiefly to total dissolved Ca and Mg carbonates). These indices are summarized in table 20.

It may be seen clearly from table 21 and figure 17 that the monthly average curve of the alkaline-reserve levels for Lake Elton brines resembles the curves of total salinity and of the percent of Mg which, in turn, replicate the temperature sequence in the brine. The peaks of the alkaline-reserve curve come in the summer months (chiefly August), when the salts of the winter settling pass into solution almost entirely and the highest magnitudes are attained by both solution and evaporation. The minimum levels of the alkaline reserve fall in the winter months when the settling of mirabilite ($Na_2SO_4 \cdot 10H_2O$) and NaCl take place. Thus, the alkaline-reserve curve for the Lake Elton

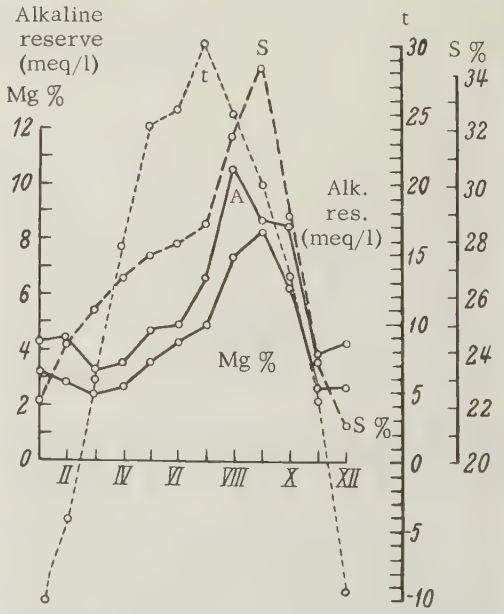

FIGURE 17. Seasonal changes in the hydrochemical regimen of Lake Elton brine (monthly averages for 1934)

TABLE 20. Characteristic geochemical indices for aqueous solutions from which dolomite and magnesite are crystallized (in equilibrium)

Experiment	Equilibrium aqueous phase					
	°C	CaO (mg/l)	MgO (mg/l)	CO_2 (mg/l)	CO_2 (meq/l)	Alkaline reserve (meq/l)
75/5[1]	150	0	126	366	16.6	6.1
75/1[1]	150	0	0	-	-	17.3
77[1]	150	28	86	412	18.7	6.1
165[1]	60	12	98	330	15.8	5.8
167[1]	60	-	-	380	17.3	8.0
Lake Balkhash	43.1	170	-	-	9.6	3 to 4 g/l
Lake Balkhash[2] (Alakal bay)	57.0	296	-	-	12.3	4 g/l
Lake Elton[3]	0 to 240	-	-	-	3 to 10	22 to 34

TABLE 20. Characteristic geochemical indices for aqueous solutions from which dolomite and magnesite are crystallized (in equilibrium) (Concluded)

Experiment	Equilibrium aqueous phase			
	Total salinity	pH	CO_2/alk. res. coefficient	Bottom phases
75/5[1]	-	6.87	2.73	$MgCO_3$ rhombohedra
75/1[1]	-	7.88	-	Magnesite rhombohedra, $CaMg(CO_3)_2$
77[1]	-	6.66	3.07	Dolomite rhombohedra
165[1]	-	9.14	2.58	Sediments near magnesite field
167[1]	-	9.43	2.16	Magnesite rhombohedra
Lake Balkhash	8.6 to 8.9	-	In silts:	
Lake Balkhash[2] (Alakal bay)	8.7 to 9.4	-	Dolomite + $CaCO_3$	
Lake Elton[3]	-	-	Dolomite + $CaCO_3$ Magnesite + $CaCO_3$	

[1]Kazakov, 1948.
[2]Strakhov, 1945: analysis of modern silts containing dolomite and magnesite.
[3]Feigelson and Shlesinger, 1936: analysis of modern silts containing dolomite and magnesite.

TABLE 21. Hydrochemical indices of Lake Elton brine (monthly averages for 1934)

Number of samples	Month	Brine temperature (°C)	Total salinity (%)	Ca (%)	Mg (%)	SO_4 (%)	Cl (%)	Alkaline reserve	
								(mg HCO_3/100 ml)	(meq/l)
4	Jan.	-10	22.2	0.02	3.30	0.88	14.17	26.12	4.28
6[1]	Feb.	- 4.2	24.3	-	2.78	1.50	14.70	22.4	4.40
6	Mar.	5.8	25.4	0.03	2.39	2.00	14.7	19.6	3.21
6	Apr.	15.4	26.6	0.03	2.61	2.25	15.4	21.28	3.50
6	May	24.1	27.4	0.03	3.52	3.00	15.6	29.0	4.75
5	June	25.3	27.8	0.05	4.25	3.66	15.7	29.8	4.89
6	July	30.0	28.6	0.02	4.89	4.14	16.0	40.2	6.60
6	Aug.	25.0	31.8	0.01	7.26	4.21	19.3	64.3	10.54
6[2]	Sept.	20.0	34.2	none	8.33	2.90	22.4	53.0	8.70
6[2]	Oct.	13.3	28.8	none	6.32	3.13	17.8	51.8	8.50
6[3]	Nov.	4.5	23.6	0.02	2.67	1.69	14.1	23.5	3.85
6[3]	Dec.	- 9.3	21.3	0.02	2.72	1.44	13.0	26.3	4.30

[1] $Na_2SO_4 \cdot 10H_2O$
[2] Complete settling of $CaSO_4$ and NaCl
[3] $Na_2SO_4 \cdot 10H_2O$

brine is characterized not as much by chloride (and sulfate) which is dependent primarily on the temperature of the brine and on its concentration. Calcium carbonate does not exist, as no Ca ions occur in the brine at the time of the alkaline-reserve peaks. During the hot summer months, the brine frequently becomes saturated with magnesium sulfate and epsomite.

Accordingly, the customary growth of the alkaline reserve in basins undergoing salinization cannot be referred entirely to the increases in dissolved calcium-magnesium bicarbonate. To regard this phenomenon as a reliable indication of the possibility of settling of dolomite and magnesite, as it is assumed by N. M. Strakhov in his several published articles [7-11], is incorrect. Hydrochemical indices, resembling Lake Elton, are available also for Karabogaz-Gol, the silts of which contain carbonate sediments, including magnesite and calcite.

According to L. S. Selivanov [66], the total salinity of the Karabogaz-Gol brine is 21.0 percent (similar to that of the Lake Elton brines); Ca, 0.0459 percent; Mg, 1.427 percent; SO_4, 2.905 percent; and alkaline reserve 9.89 to 12.79 meq/l. The parallel relationship between increasing alkaline reserve and total CO_2 and salinization of the basin is clearly visible in the magnesium- and chloride-bearing Lake Sakskoye silts in which dolomite was detected. Thus, according to the data of P. G. Danilchenko and M. I. Ravich, the following hydrochemical indicators represented in table 22 correspond to different degrees of salinity of the lake's brine.

TABLE 22. Hydrochemical indices of Lake Sakskoye brine for different degrees of salinity (evaporation)

Specific gravity	CO_2 (mg/l)	CO_2 (meq/l)	Alkaline reserve (meq/l)	CO_2: alkaline reserve
1.0789	100	5	2.86	1.75
1.2527	232.1	10.55	18.89	0.558
1.3031	317.24	14.42	36.84	0.392

High alkalinity was found also in salinized bays of Caspian sea. Thus, M. A. Glazovskaya, in 1938, had established that the alkaline reserve of water in Kaidak bay fluctuates between 5.1 and 19.1 meq/l. The bottom silts of this bay also contain dolomite.

The controlling environmental factors in the settling of magnesite are as follows:

1. A relatively high concentration of magnesium bicarbonate, that is, a high alkaline reserve. The lower limit of the alkaline reserve at 60°C was 6 to 8 meq/l in our experiments; this limit should be raised for 20°C.

2. A relatively high CO_2-tension; the CO_2: alkaline reserve coefficient 2.2.

3. A low calcium content in water (residual concentration approximately 50 mg CaO).

The same conditions remain in force for the settling of dolomite but the CaO concentration should be 50 mg/l.

Settling Environment for Apatite in Natural Basins

As was shown by Kazakov in a number of published articles [1, 69, 70] and confirmed by the entire practice of the exploration for phosphorites, the genesis of the latter is controlled by certain conditions selected for the purposes of the present work:

1. The primary dispersed-colloidal phosphate substance is formed and settled under definite hydrogeologic and hydrochemical conditions from the body of water in marine basins of ordinary salinity. During the early diagenesis, this phosphatic gel is differentiated into concretions and layers of phosphate, depending on its mass and concentration. Phosphorites are not found in halogenic sediments of relict basins or in the sediments of even the early salinization stage.

2. Paleogeographically and hydrochemically, phosphatic basins must have necessarily a direct connection with the ocean (by current), with the principal source of mobile reserves of dissolved phosphates.

3. Sedimentary phosphoritic interlayers are not encountered in sediments of fresh-water basins.

The hydrochemical indices for a number of typical marine and fresh waters are presented in table 23. It is clearly evident from table 23 that:

1. The ordinary concentration of magnesium bicarbonate in oceans and seas of normal salinity and in fresh-water basins is insignificant (the alkaline reserve is 0.8 to 2.5) and is far below the minimum required for the settling of magnesite and dolomite (the alkaline reserve should be 8).

2. Analogous situation is observed with respect to carbonic acid (CO_2) the content of which, in oceanic and marine water, is commonly about 80 to 110 mg - significantly below the minimum required for the settling of magnesite and dolomite (CO_2 - 380 mg).

3. The coefficients of carbonic-acid tensions in oceans, seas, and fresh-water basins are low (CO_2: alkaline reserve = 1.0 to 2.0); coefficients at the time of settling of magnesite and dolomite are 2.2 to 3.0.

TABLE 23. Hydrochemical indices for marine waters of ordinary salinity and for fresh waters

Basin	CO_2 (mg/l)	CO_2 (meq/l)	Alkaline reserve (meq/l)	pH	CO_2:alkaline reserve	References
Fresh-water basins	-	-	0.8 to 1.2	6.4 to 7.4	-	-
Volga river at Kalinin (annual averages, 1931-34)	112.9	5.13	2.47	8.0	2.08	[57]
Ocean (open)						
Surface	90	-	2.2	8.35	1.8	-
Bottom	110		2.5	7.75	2.0	-
Bering sea (summers, 1932-33						
Surface	-	1.85	1.55	8.2 to 8.4	1.20	G. Ratmanov
25 meters	81 to 94	1.95	1.78	-	1.10	-
25 to 100 meters	-	2.15	1.92	-	1.12	-
Bottom	-	-	-	7.5 to 8.3	-	-
Black sea						
Surface	-	-	3.1	8.43	-	-
Bottom	-	-	4.2	7.56	-	-
Caspian sea						
Surface	-	-	3.5	8.48	-	-
800 meters	-	-	3.5	7.69	-	-

CONCLUSIONS

The wide distribution of dolomitic sediments in the Paleozoic and their absence in the Jurassic and the Cretaceous of the Russian platform, the occurrence of dolomites with phosphorites in geosynclinal areas of U. S. S. R., and the absence of dolomite formation in modern marine sediments has been tempting the interest of geologists for a long time. Geologists particularly interested in phosphorites have been trying to determine whether dolomites are formed simultaneously and jointly with phosphorites within identical or, at least very similar hydrochemical environments in marine basins. They have also tried to determine the worth of dolomitized sediments as prospecting indications.

Analysis of magnesitic and dolomitic systems, $MgO-CO_2-H_2O$ and $CaO-MgO-CO_2-H_2O$, respectively, at the 20°C isotherm and, in part, at the 60° and 150°C isotherm is offered in the experimental part of this report. The fields of crystallization and stability of the principal mineral phases are defined for the following systems:

Nesquehonite:	$MgCO_3 \cdot 3H_2O$
Magnesite:	$MgCO_3$
Dolomite:	$CaMg(CO_3)_2$
Basic magnesium carbonates (artinite & hydromagnesite)	$MgCO_3 \cdot Mg(OH)_2 \cdot 2H_2O$, $4MgCO_3 \cdot Mg(OH)_2 \cdot 4H_2O$
Brucite:	$Mg(OH)_2$

For nesquehonite, the roentgenogram and the thermogram characterized by its "explosive" exothermal effect are here presented for the first time. It developed as a consequence of these studies that the chief equilibrium parameters of sedimentation and stability of dolomite and magnesite are markedly different from the parameters of fluorapatite - of which the phosphate bulk of our phosphorite is made - which were also studied by us, earlier, and placed on record for the first time.

The possibility of a simultaneous (synchronous) development of phosphorites and dolomites (magnesites) is excluded entirely, on the basis of our findings, for the hydrochemical regimens of their development are clearly different and mutually incompatible. Dolomites are invariably younger (secondary) formations with respect to phosphorites in dolomitized phosphate-bearing sediments, as it may be seen easily also from the microstructural analysis (in thin sections).

Facts of the not uncommon presence of dolomites together with phosphorites (Karatau, Seleuk) need be explained accordingly by subsequent impositions of diagenetic and epigenetic dolomites on the previously settled phosphate.

From this point of view, secondary (diagenetic) dolomites cannot be regarded as negative prospecting signs (counter-in-dictions) in reference to phosphorites.

On the other hand, in several localities, we

encounter thick primary beds of gypsum-anhydrite-dolomite in halogenic basins (Donets basin, Kungur, the Sterlitamak-Ishimbayevsk Urals foothills). Phosphorites cannot be formed within the primary dolomites of this type, in halogenic basins and, accordingly, such primary dolomites should be interpreted as negative prospecting indications in reference to phosphorites.

Our report presents also a plausible mechanism of the development (accretion) of the alkaline reserve itself (chiefly magnesium bicarbonate) in natural basins, as the fundamental factor in the settling of dolomite and magnesite.

REFERENCES

Geology, Lithology, Genesis

1. Kazakov, A. V., FOSFATNYYE FATSII. 1. PROISKHOZHDENIYE FOSFORITOV I GEOLOGICHESKIYE FAKTORY FORMIROVANIYA MESTOROZHDENY [THE PHOSPHATE FACIES. 1. ORIGIN OF PHOSPHORITES AND GEOLOGIC FACTORS IN THE DEVELOPMENT OF THEIR DEPOSITS]: Nauchn. Inst. po Udobr. i Insektofung. im. Ya. V. Samoylova, 1939, no. 145, p. 1-108.

2. Kovda, V. A., PROTSESSY SOVREMENNOGO SOLENAKOPLENIYA (GALOGENEZA) V POCHVAKH I VODAKH [THE PROCESSES OF MODERN SALT ACCUMULATION (HALOGENESIS) IN SOILS]: Pochvovedeniye, 1947, no. 11.

3. Krotov, V. P., DOLOMITY, IKH OBRAZOVANIYE, USLOVIYA USTOYCHIVOSTI [DOLOMITES, THEIR DEVELOPMENT AND PREREQUISITES OF STABILITY]: Kazansk. Univ., Obshch. Estestvoisp., Trudy, v. 50, no. 6, 1925.

4. _____, O NEOBKHODIMOSTI FIZIKO-KHIMICHESKOGO IZUCHENIYA REAKTSII $2(CaCO_3)+MgSO_4 \rightleftharpoons CaCO_3 \cdot MgCO_3+CaSO_4$ [CONCERNING THE NECESSITY OF PHYSICO-CHEMICAL STUDIES OF THE REACTION $2CaCO_3+MgSO_4 \rightleftharpoons CaCO_3 \cdot MgCO_3+CaSO_4$]: Akademiya Nauk SSSR, Inst. Fiz.-Khim. Analiza, Izvestiya, v. 3, no. 2, p. 662-782, 1927.

5. Pustovalov, L. V., A. N. Lyamina, and others, DOLOMIT [DOLOMITE]: In: Nemetallicheskiye Iskopayemyye SSSR, Akademiya Nauk SSSR, Izvestiya, v. 5, p. 306-403, 1941.

6. Sapozhnikov, D. G., IZVESTKOVO-DOLOMITOVYY IL OZERA BALSKASH [THE LIMESTONE-DOLOMITE SILTS OF LAKE BALKHASH]: Akademiya Nauk SSSR, Doklady, v. 36, nos. 4-5, 1942.

7. Strakhov, N. M., DOLOMITOVYYE OSADKI OZERA BALKHASH I IKH ZNACHENIYE YE DLYA POZNANIYA PROTSESSA DOLOMITOOBRAZOVANIYA [DOLOMITIC SEDIMENTS OF LAKE BALKHASH AND THEIR SIGNIFICANCE IN DOLOMITIZATION STUDIES]: Sovetskaya Geologiya, 1945, no. 4.

8. _____, O ZNACHENII SOVREMENNYKH OZERNYKH I LAGUNNYKH VODOYEMOV DLYA POZNANIYA PROTSESSOV OSADKOOBRAZOVANIYA [IN REFERENCE TO THE SIGNIFICANCE OF MODERN LACUSTRINE AND LAGOONAL BASINS IN UNDERSTANDING OF SEDIMENTATION PROCESSES]: Akademiya Nauk SSSR, Izvestiya, Seriya Geologicheskaya, 1945, no. 1, p. 61-78.

9. _____, KARBONATY V SOVREMENNYKH LAGUNNYKH VODOYEMAKH I IKH ZNACHENIYE DLYA PROBLEMY DOLOMITOOBRAZOVANIYA [CARBONATES IN MODERN LAGOONAL BASINS AND THEIR SIGNIFICANCE IN THE PROBLEM OF DOLOMITIZATION]: Mosk. Obshch. Ispyt. Prirody, Byull., Otd. Geol., v. 22, no. 4, 1947.

10. Strakhov, N. M., and A. I. Tsvetkov, O MAGNEZITE I YEGO GENEZISE V OSADOCHNYKH PORODAKH [IN REFERENCE TO MAGNESITE AND ITS ORIGIN IN SEDIMENTARY ROCK]: Zap. Vseross. Min. Obshch., v. 73, no. 4, 1944.

11. _____, O PARAGENEZISE KARBONATNYKH MINERALOV V OTLOZHENIYAKH SOLENYKH LAGUN I IKH VODOYEMOV [IN REFERENCE TO THE PARAGENESIS OF CARBONATE MINERALS IN SEDIMENTS OF SALINE LAGOONS AND THEIR BASINS]: Zap. Mosk. Obshch. Ispyt. Prirody, Materialy k Poznan. Geolog. Stroyen. SSSR, Noviya Seriya, 1946, no. 3, p. 57-87.

12. Tatarsky, V. B., K VOPROSU O PROISKHOZHDENII DOLOMITA [ON THE PROBLEM OF THE ORIGIN OF DOLOMITE]: Zap. Vseross. Mineralog. Obshch., v. 66, no. 4, p. 677-684, 1937.

13. Tatarsky, V. G., LITOLOGIYA NEFTENOSNYKH KARBONATNYKH POROD SREDNEY AZII I PROISKHOZHDENIYE NEFTENOSNYKH DOLOMITOV [LITHOLOGY OF OIL-BEARING CARBONATE ROCKS OF CENTRAL ASIA AND THE OIL-BEARING DOLOMITES]: Neft. Geol.-Razv. Inst., Ser. A, 1939, no. 112.

14. Teodorovich, G. I., DOLOMITIZATSIYA RIFOVYKH OBRAZOVANY ISHIMBAYEVSKOGO NEFTENOSNOGO RAYONA [DOLOMITIZATION OF REEDS IN ISHIMBAYEVSK PETROLEUM DISTRICT]: Akademiya Nauk SSSR, Doklady, v. 34, no. 6, 1942.

15. _____, KARTINA DOLOMITOOBRAZOVANIYA NA VOSTOCHNOM MASSIVE ISHIMBAYEVSKOGO NEFTYANOGO RAYONA [THE PICTURE OF DOLOMITIZATION IN THE EASTERN MASSIVE OF THE ISHIMBAYEVSK PETROLEUM DISTRICT]: Akademiya Nauk SSSR, Doklady, v. 34, no. 7, 1942.

16. _____, DOLOMITOZAMESHCHENIYA V VERKHNEM PALEOZOYE URALO-BOLZHSKOY OBLASTI [DOLOMITIZATION IN THE UPPER PALEOZOIC, VOLGA-URALS REGION]: Mosk. Obshch. Ispytat. Prirody, Byull., Otd. Geol., Noviya Seriya, v. 20, nos. 3-4, 1945.

17. Yarzhemsky, Ya. Ya., K LITOLOGII SREDNEGO KEMBRIYA PRIANGARYA [IN REFERENCE TO LITHOLOGY OF MIDDLE CAMBRIAN SEDIMENTS OF THE ANGARA RIVER BASIN]: Vost.-Sib. Geol.-Razv. Tresta, Trudy, 1936, no. 16.

18. Dale, T. N., THE LINE BELT OF MASSACHUSETTS AND PART OF EASTERN NEW YORK AND WESTERN CONNECTICUT: U. S. Geol. Survey, Bull. 744, p. 51-56, 1923.

19. Daly, R. A., THE LIMELESS OCEAN OF PRECAMBRIAN TIME: American Journal of Science, v. 23, no. 134, p. 93-115, 1907.

20. Irving, L., THE PRECIPITATION OF CALCIUM AND MAGNESIUM FROM SEA WATER: Marine Biological Association of the United Kingdom, Jour., v. 14, p. 144, 1925.

21. Johnston, J., DIE BESTIMMUNG GEBUNDENER UND FREIER KOHLENSAURE IN LOSUNGEN, INSBESONDERE IN NATURLICHEN WASSERN [THE DETERMINATION OF BOUND AND FREE CARBONATES IN SOLUTION, PARTICULARLY IN NATURAL WATERS]: American Chemical Society, Jour., v. 38, p. 947-975, 1916.

22. Klahn, H., DIE ENTSTEHUNG DER KALKE IN SUSSWASSERN UND MEEREN [THE FORMATION OF LIME IN FRESH AND MARINE WATERS]: Zeit. Deutsche Geol. Ges., 1925, p. 77.

23. Linck, G., DOLOMITISATION [DOLOMITIZATION]: Neues Jahrbuch Min., 1921, p. 545.

24. Murray, J., and R. Irvine, ON THE CHEMICAL CHANGES WHICH TAKE PLACE IN THE COMPOSITION OF SEA WATER ASSOCIATED WITH BLUE MUDS OF THE FLOOR OF THE OCEAN: Royal Soc. Edinburgh, Tr., v. 37, p. 490, 1895.

25. Pfaff, F. W., BEITRAGE ZUR ERKLARUNG UBER DIE ENTSTEHUNG DES MAGNESITS UND DOLOMITS [CONTRIBUTION TO STUDY OF THE FORMATION OF MAGNESITE AND DOLOMITE]: Neues Jahrbuch Mineralogie, 1894, p. 485-507.

26. _____, UEBER DOLOMIT UND SEINE ENTSTEHUNG [ON DOLOMITE AND ITS FORMATION]: Neues Jahrbuch Mineralogie, v. 23, no. 3, p. 569-580, 1894.

27. Philippi, E., UEBER DOLOMITBILDUNG UND CHEMISCHE AUSSCHEIDUNG VON KALK IN HEUTIGEN MEEREN [ON THE DEVELOPMENT OF DOLOMITE AND CHEMICAL PRECIPITATION BY LINE IN MODERN SEAS]: Neues Jahrbuch Mineralogie, 1907, Festband., p. 397-445.

28. Steidtmann, B., EVOLUTION OF LIMESTONE AND DOLOMITE: Journal of Geology, v. 19, p. 323-345, 1911.

29. Van-Tuyl, F. M., THE ORIGIN OF DOLOMITE: Iowa, Geol. Survey, v. 25, p. 241-242, 266-270, 318-324, 1914.

30. _____, THE PRESENT STATUS OF THE DOLOMITE PROBLEMS: Science, v. 44, p. 688-690, 1916.

Mineralogy

31. Kurnakov, N. S., and V. V. Chernykh, FIZIKO-KHIMICHESKOYE ISSLEDOVANIYE BRUSITA I NEMALITA [PHYSICO-CHEMICAL STUDIES OF BRUCITE AND NEMALITE]: Min. Syrye i Yego Pererabotka, 1926, no. 5, p. 367; see also selected papers by N. S. Kurnakov in Akademiya Nauk SSSR, Izvestiya, v. 1, p. 441-451, 1938.

32. Lyamina, A. N., RENTGENOGRAFICHESKOYE IZUCHENIYA DOLOMITOV [ROENTGENOGRAPHIC STUDY OF DOLOMITES]: V. Kh.: Nementalli-

cheskiye Iskopayemyye SSSR, Akademiya Nauk SSSR, Izvestiya, v. 5, p. 307-310, 1941.

33. Serdyuchenko, D. P., O GIDROMAGNEZITE [ON HYDROMAGNESITE]: Akademiya Nauk SSSR, Doklady, v. 68, no. 3, p. 581-584, 1949.

34. Beck, C. W., DIFFERENTIAL THERMAL ANALYSIS CURVES OF CARBONATE MINERALS: American Mineralogist, 1950, nos. 11-12, p. 985-1013.

35. Bruet, E., DOLOMITE UND DOLOMITISCHE KALKSTEINE [DOLOMITE AND DOLOMITIC LIMESTONES]: Naturaliste Canad., v. 66, no. 3 (10), p. 17-26, 1939.

36. Cesaro, G., FORME CRISTALLINE ET COMPOSITION DU CARBONATE MAGNESIQUE HYDRATE PREPARE PAR M. MORESSE. SA RELATION AVEC LA LANSFORDITE [THE CRYSTALLINE FORM AND COMPOSITION OF HYDRATED CARBONATE MAGNESITE PREPARED BY M. MORESSE. ITS RELATIONSHIP WITH LANSFORDITE]: Acad. Roy. de Belg., Bull. de la Glasse de Sciences, 1910, no. 4, p. 234-235.

37. Davis, W. A., STUDY OF BASIC CARBONATES: Indiana, Chem. Soc., Jour., v. 25, p. 788, 1906.

38. Ford, V. E., STUDIES OF THE CALCITE GROUP: Connecticut Academy of Sciences, Tr., v. 22, p. 211-248, 1917.

39. Fovte, H. V., and V. M. Bradley, THE ISOMORPHISM BETWEEN CALCITE AND DOLOMITE: American Journal of Science, v. 37, p. 339, 1914.

40. Genth, F. A., LANSFORDIT, EIN NEUES MINERAL [LANSFORDITE, A NEW MINERAL]: Zeits. Kryst., v. 14, p. 255-256, 1888.

41. Genth, F. A., and S. L. Penfield, UBER LANSFORDIT, NESQUEHONIT UND PSEUDOMORPHOSEN VON NESQUEHONIT NACH LANSFORDIT [ON LANSFORDITE, NESQUEHONITE, AND A PSEUDOMORPHS BY NESQUEHONITE ON LANSFORDITE]: Zeits. Kryst., v. 17, p. 561, 1890.

42. Handelt, J. D., N. W. Frimm, and L. K. Fremel, in: Ind. Eng. Chem., Jour., Anal. ed., v. 10, no. 9, p. 457, 1938.

43. Keller, W. D., and G. E. Moore, STAINING DRILL CUTTING FOR CALCITE-DOLOMITE DIFFERENTIATION: American Association of Petroleum Geologists, Bull., v. 21, p. 949-951. 1937.

44. Knorre, G. V., UBER DAS MAGNESIUM-CARBONAT UND EINIGE DOPPELVERBINGUNGEN DERSELBER [ON THE MAGNESIUM CARBONATES AND THEIR DOUBLE-BONDING]: Zeits. Anorg. Chem., v. 34, p. 260-285, 1903.

45. Larsen, E. S., and H. Berman, THE MICROSCOPIC DETERMINATION OF THE NONAPAQUE MINERALS: U. S. Geological Survey, Bull. 848, 2d ed., 1934.

46. Leitmeier, H., NESQUEHONIT [NESQUEHONITE]: In: Doelter G. Handbuch d. Mineralchemie, v. 1, p. 262-264, 1912.

47. Meixner, H., ARTINIT, PYROAURIT UND HYDROMAGNESIT AUS SUDSERBIEN [ARTINITE, PYROAURITE, AND HYDROMAGNESITE FROM SOUTHERN SERBIA]: Cbl. Min., Ser. A., 1937, no. 1, p. 363.

48. Poitevin, E., A NEW OCCURRENCE OF LANSFORDITE FROM ATLIN: American Mineralogist, v. 9, no. 11, p. 225-228, 1924.

49. Splichal, J., St. Skranovsky, and A. Goll, THERMISCHE ZERSETZUNG VON BERGBAUWICHTIGEN CARBONATEN [THERMAL DECOMPOSITION BY CARBONATES OF MINING POTENTIAL]: Chem. Obzor., Prager Karls., Univ. u. Pribram Berg-akademie, 1937, no. 12, p. 181-183, 203-206, 224-230, 252-257.

50. Steidtmann, E., ORIGIN OF DOLOMITE AS DISCLOSED BY STAINS AND OTHER METHODS: Geological Society of America, Bull., v. 25, p. 431-450, 1917.

51. Vyckoff, R. V., and H. E. Merwin, THE CRYSTAL STRUCTURE OF DOLOMITE: American Journal of Science, v. 8, p. 448-461, 1924.

52. Young, G. A., SUMMARY REPORT OF THE GEOLOGICAL SURVEY DEPARTMENT OF MINES, 1915, p. 50-61.

Hydrochemistry

53. Bruyevich, S. V., and Ye. G. Vinogradova,

KHIMICHESKY SOSTAV GRUNTOVYKH RASTVOROV KASPYSKOGO MORYA. 1. SEVERNYY KASPY (PO MATERIALAM 1939) [CHEMICAL COMPOSITION OF GROUND-WATER SOLUTIONS OF THE CASPIAN SEA. 1. THE NORTHERN CASPIAN (FROM 1939 DATA)]: Gidrokhim. Mat., v. 13, 1947.

54. Bruyevich, S. V., and Ye. G. Vinogradova, KHIMICHESKY SOSTAV GRUNTOVYKH RASTVOROV KASPYSKOGO MORYA. 2. SEVERNYY, SREDNY I YUZHNYY KASPY (PO MATERIALAM 1935, 1936, I 1944 GG.) [CHEMICAL COMPOSITION OF GROUND-WATER SOLUTIONS OF THE CASPIAN SEA. 2. THE NORTHERN, CENTRAL, AND SOUTHERN CASPIAN (FROM 1935, 1936, AND 1944 DATA)]: Gidrokhim. Mat., v. 13, 1947.

55. Butyrin, P. N., POLEVOY KOLICHESTVENNYY KHIMICHESKY GIDROANALIZ PROBIROCHNOKAPELNYM METODOM [THE FIELD QUANTITATIVE CHEMICAL HYDROANALYSIS BY THE TESTTUBE-DROP METHOD]: Gos. Nauchno-Tekhn., Izd., 1931.

56. Danilchenko, P. G., and M. I. Ravich, O SHCHELOCHNOSTI PRIRODNYKH RASSOLOV MORSKOGO PROISKHOZHDENIYA [NOTES CONCERNING THE ALKALINITY OF NATURAL BRINES OF MARINE ORIGIN]: Krymsk. Nauchno-Issl. Inst., Trudy, v. 1, no. 2, p. 12-23, 1927.

57. Drachev, S., and B. Skopintsev, GIDROKHIMICHESKAYA KHARAKTERISTIKA R. VOLGI NA UCHASTKE OT R. KALININA DO USTYA R. DUBNY PO DANNYM ISSLEDOVANY 1931-1934 GG. [HYDROCHEMICAL CHARACTERISTICS OF THE VOLGA RIVER FROM THE KALININ RIVER TO THE MOUTH OF THE DUBNA RIVER BY 1931-1934 DATA]: Gidrokhim. Mat., v. 12, 1941.

58. Kovda, V. A., BIOLOGICHESKIYE TSIKLY DVIZHENIYA I NAKOPLENIYA SOLEY [BIOLOGIC CYCLES IN ACCUMULATION AND MOVEMENT OF SALTS]: Pochvovedeniya, 1944, nos. 4-5, p. 146-157.

59. Kurnakov, N. S., SOLYANYYE OZERA KRYMA [THE SALT LAKES OF THE CRIMEA]: Akademiya Nauk SSSR, Izd., 1936.

60. Kurnakov, N. S., and S. F. Zhemchuzhnyy, MAGNIYEVYYE OZERA PEREKOPSKOY GRUPPY [MAGNESIUM LAKES OF THE PEREKOPSK GROUP]: Akademiya Nauk, Izvestiya, 1917, no. 2, p. 137-162.

61. Kurnakov, N. S., and S. F. Zhemchuzhnyy, O METAMORFIZATSII SOLYANYKH RASSOLOV [ON THE METAMORPHISM OF SALINE BRINES]: In: Otchety o Deyatelnosti Kom. po Izuch. Proizv. sil Rossii Akademii Nauk, 1917, no. 9, p. 216-218.

62. Makarov, S. Z., and D. R. Yenikeyev, PREDVARITELNYYE ITOGI FIZIKO-KHIMICHESKOGO ISSLEDOVANIYA SEVERO-VOSTOCHNYKH ZALIVOV KASPYSKOGO MORYA KOMSOMOLETS (MERTVYY KULTUK) I KAYDAK PO MATERIALAM EKSPEDITSII AKADEMII NAUK SSSR 1934 G [A PRELIMINARY SUMMARY OF PHYSICO-CHEMICAL INVESTIGATIONS OF NORTHEASTERN BAYS OF THE CASPIAN SEA, KOMSOMOLETS (MERTVYY KULTUK) AND KAYDAK, ACCORDING TO DATA OBTAINED BY THE 1934 ACADEMY OF SCIENCES OF THE U. S. S. R. EXPEDITION]: Kom. po Kompleksn. Izuch. Kasp. Morya, Trudy, 1937, no. 1, ch. 1, p. 83.

63. Nikolsky, B., and V. Gortikov, ZHACHENIYE pH DLYA ANALIZA PRIRODNYKH VOD [SIGNIFICANCE OF pH IN THE ANALYSIS OF NATURAL WATERS]: In: Sovremennyye Fiziko-Khimicheskiye Metody Khimicheskogo Analiza, 2d ed., 1935, p. 184-279.

64. Ravich, M. I., NEKOTORYYE DANNYYE O VLIYANII GRUNTA NA SOSTAV RAPY SOLYANYKH OZER [SOME DATA ON GROUND EFFECTS ON COMPOSITION OF BRINE IN SALINE LAKES]: Krymsk. Nauchno-Issl. Inst., Trudy, v. 1, no. 2, p. 31, 1927.

65. Rubenchik, L. I., SULFATREDUTSIRUYUSHCHIYE BAKTERII [THE SULFATE-REDUCING BACTERIA]: Akademiya Nauk SSSR, Izd., 1947.

66. Selivanov, L. S., O SOSTAVE MUTI KARABUGAZSKOGO ZALIVA [CONCERNING THE COMPOSITION OF TURBIDITY IN KARA-BUGAZSK BAY]: Akademiya Nauk SSSR, Doklady, v. 16, no. 9, 1937.

67. Shukarev, S. A., SAKI- KURORT [THE SAKI RESORT]: Kurortn. Delo, 1926-1927.

68. Shukarev, S. A., and T. A. Tolmacheva, VOSSTANOVLENIYE SERNOKISLYKH SOLEY BIOKHIMICHESKIM PUTEM I

METAMORFIZATSIYA RAPY [THE BIOCHEMICAL REDUCTION OF SULFATES AND THE METAMORPHISM OF BRINE]: Akademiya Nauk SSSR, Inst. Fiz.-Khim. Analiza, Izvestiya, v. 4, no. 2, p. 488, 1930.

Equilibrium Systems: Synthesis

69. Kazakov, A. V., KHIMICHESKAYA PRIRODA FOSFATNOGO VESHCHESTVA FOSFORITOV I IKH GENEZIS. 1. SISTEMA $CaO-P_2O_5-H_2O$ V POLYAKH NIZKIKH KONTSENTRATSY (SINTEZ TREKHKALTSIYEVOGO FOSFATA I GIDROKSILAPATITA) [CHEMICAL NATURE OF PHOSPHATE SUBSTANCES IN PHOSPHORITES AND THEIR GENESIS. 1. THE $CaO-P_2O_5-H_2O$ SYSTEM IN THE FIELDS OF LOW CONCENTRATIONS]: Nauchn. Inst. po Udobr. i Insektofung. im. Ya. V. Samoylova, Trudy, 1937, no. 139, p. 1-74.

70. _____, FTORAPATITOVAYA SISTEMA RAVNOVESY V USLOVIYAKH OBRAZOVANIYA OSADOCHNYKH PORODOV [THE FLUORAPATITE SYSTEM OF EQUILIBRIA UNDER CONDITIONS OF DEVELOPMENT OF SEDIMENTARY ROCK]: Akademiya Nauk SSSR, Inst. Geol. Nauk, Trudy, 1950, no. 114, Seriya Geologicheskaya (no. 40), p. 1-21.

71. Kurnakov, N. S., and V. I. Nikolayev, SOLYANYYE RAVNOVESIYA PRI ISPARENII MORSKOY VODY [THE SOLAR EVAPORATION OF SEA WATER AND LAKE BRINES]: Akademiya Nauk SSSR, Inst. Fiz.-Khim. Analiza, Izvestiya, v. 4, no. 2, p. 389, 1930.

72. _____, SOLNECHNOYE ISPARENIYE MORSKOY VODY I OZERNYKH RASSOLOV [SALT EQUILIBRIA DURING EVAPORATION OF SEA WATER]: Akademiya Nauk SSSR, Inst. Fiz.-Khim. Analiza, Izvestiya, v. 10, p. 333-366, 1938.

73. Rykovskov, A. Ye., and N. M. Neshchadimova-Neklyavz, ISSLEDOVANIYE REAKTSII GAYDINGERA [STUDIES OF THE GEIDINGER REACTION]: In: Trudy Soveshchaniya Khimikov Glavnogo Geologo-Razvedochnogo Upravleniya, 1931, p. 153-160.

74. Shelyagin, V. V., and L. A. Lukoshkina, RASTVORIMOST MgO V VODE, NASYSHCHENNOY UGLEKISLOTOY [SOLUBILITY OF MgO IN WATER SATURATED WITH CARBONIC ACID]: Min. Syre, 1932, nos. 2-4.

75. D'Ans, J., and G. Gloss, ÜBER DAS $MgCO_3 \cdot 3H_2O$, UBER BASISCHE CARBONATE, NEUE DOPPELVERBINDUNGEN DES MAGNESIUMCARBONATS UND UBER BASISCHE MAGNESIUMSULFATE [ON $MgCO_3 \cdot 3H_2O$, ON BASIC CARBONATES, NEW DOUBLE-BINDING OF MAGNESIUM CARBONATES, AND ON BASIC MAGNESIUM SULFATE]: Kali, Verwandte Salze, Erdol u. Teer, v. 32, no. 15, p. 155-158, 1938; also: Chem. Cbl., v. 2, p. 3523, 1938.

76. D'Ans, J., and W. Katz, MAGNESIUM HYGROXYDLOSLICHKEITEN, pH ZAHLEN UND PUFFERUNG IN SYSTEM $H_2O \cdot MgCl_2$-$Mg(OH)_2$ [SOLUBILITY OF HYDROUS MAGNESIUM OXIDES, pH CALCULATIONS AND BUFFERING IN THE SYSTEM $H_2O \cdot MgCl_2$-$Mg(OH)_2$]: Kali, 1941, no. 3.

77. Cameron, F., and J. Bell, THE SOLUBILITY OF GYPSUM IN MAGNESIUM SULFATE SOLUTIONS: Journal of Physical Chemistry, v. 10, p. 210, 1906.

78. Cameron, F., and J. F. Breazeale, CALCIUM SULFATE IN AQUEOUS SOLUTIONS OF POTASSIUM AND SODIUM SULFATE: Journal of Physical Chemistry, v. 8, p. 335, 1904.

79. Cameron, F., and A. Seidell, SOLUBILITY OF CALCIUM CARBONATE IN AQUEOUS SOLUTIONS OF CERTAIN ELECTROLYTES IN EQUILIBRIUM WITH ATMOSPHERIC AIR: Journal of Physical Chemistry, v. 6, p. 50, 1904.

80. _____, THE SOLUBILITY OF MAGNESIUM CARBONATE IN AQUEOUS SOLUTIONS OF CERTAIN ELECTROLYTES: Journal of Physical Chemistry, v. 7, p. 578-588, 1903.

81. Frear, P. L., and J. Johnston. DIE LOSLICHKEIT VON CALCIUMCARBONAT (CALCIT) IN GEWISSEN WASSRIGEN LOSUNGEN BEI 25° [THE SOLUBILITY OF CALCIUM CARBONATE (CALCITE) IN CERTAIN WATER SOLUTIONS AT 25°]: American Chemical Society, Journal, v. 51, p. 2082-2093, 1929.

82. Gloss, G., UEBER MAGNESIUMCARBONATE UND WASSERIGE SALZSYSTEME MIT MAGNESIUMCARBONATEN [ON MAGNESIUM CARBONATE AND WATER SALT SYSTEM WITH MAGNESIUM CARBONATE]: Diss., Berlin, 1937.

83. Halla, F., UEBER EINIGE VERSUCHE

ZUR DOLOMITSYNTHESE DURCH DOPPELTE UMLAGERUNG [ON ONE EXPERIMENT ON DOLOMITE SYNTHESIS BY MEANS OF DOUBLE REARRANGEMENT]: Cbl. Min., Ser. A, 1937, no. 1, p. 9-12; also: Chemical Abstracts, v. 31, 1945.

4. Irving, L., THE PRECIPITATION OF CALCIUM AND MAGNESIUM FROM SEA WATER: Marine Biological Association of the United Kingdom, Jour., v. 14, p. 441, 1925.

5. Johnston, J., and E. Williamson, DIE VOLLSTANDIGE LOSLICHKEITSKURVE DAS CALCIUMCARBONAT [THE INTEGRAL SOLUBILITY CURVE FOR CALCIUM CARBONATE]: American Chemical Society, Jour., v. 38, p. 975-983, 1916.

6. Kegel, J., DAS MAGNESIA-KOHLENSAURE-GLEICHGEWICHT IN WASSER [THE MAGNESIA-CARBON DIOXIDE EQUILIBRIUM IN WATER]: Korrosion u. Metallschutz, 1943, no. 8, p. 201-203.

7. Kline, W. D., THE SOLUBILITY OF MAGNESIUM CARBONATE (NESQUEHONITE) IN WATER AT 25° AND PRESSURES OF CARBON DIOXIDE UP TO ONE ATMOSPHERE: American Chemical Society, Jour., v. 51, no. 7, p. 2093-2097, 1929.

88. Leitmeier, H., ZUR KENNTNISS DER KARBONATE [INFORMATION ON CARBONATES]: Neues Jahrbuch Mineralogie, BB, v. 15, 1916.

89. Mitchell, A. E., STUDIES ON THE DOLOMITE SYSTEM: Chemical Society of London, Jour., v. 123, p. 1052-1069, 1087-1094, 1887-1945, 1923.

90. Tillmans, J., and O. Heublein, UEBER DIE KOHLENSAUREN KALK ANGREIFENDE KOHLENSAURE DER NATURLICHEN WASSER [ON THE CARBONIC ACID IN LIME AFFECTING CARBONIC ACID IN NATURAL WATER]: Chem. Zentralbl., v. 2, no. 16, p. 1395-1396, 1912 (ref.).

91. Wells, R. C., THE SOLUBILITY OF MAGNESIUM CARBONATE IN NATURAL WATERS: American Chemical Society, Jour., v. 37, p. 1704-1707, 1915.

VOLCANIC ACTIVITY ON THE MOON[1]

by

N. A. Kozyrev[2]

• *translated by Edgar Huston* •

ABSTRACT

On November 3, 1958, the author observed ejection of volcanic ash and gases from the central peak of Alphonsus crater. Spectrographic analysis of gas fluorescence induced by hard solar radiation, proved that gases were escaping from the crater floor. It appears that tectonic activity is taking place on the moon. Lack of atmosphere and consequent porosity (caused by rapidly escaping gas) of surface layers have resulted in reduced heat emission; these factors all contributing to the moon's ability to retain internal energy sufficient to initiate tectonic activity. Fissures and dark spots on crater floors indicate endogenic development of the moon's basic surface relief, as opposed to relief development by meteoric impact. --D. D. Fisher.

Study of surface morphology shows convincingly that the relief of the moon developed gradually as a result of repeated uplift and subsidence of its crust. Inclined and semisubmerged craters on the borders of the "seas" show that segments of the crust subsided accompanied by fissure formation and subsequent extrusion of molten material. The famous valley in the lunar Alps is approximately 10 to 15 kilometers (km) wide and more than 100 km long, its sides are steep and similar to one another. This rift furnishes an example of crustal uplift accompanied by considerable stretching; undoubtedly, such tectonic processes are connected with volcanic activity.

Let us visualize the extrusion of molten matter from the inner parts of the moon to its surface. Gases present in this lava in the absence of atmosphere, necessarily would have escaped in a vigorous manner creating a foamy structure. Rocks composing the outer layers of the moon must have become extremely porous, resulting in their extremely low thermal-conductivity coefficient. This probably explains why the thermal-conductivity coefficient for external layers of the moon equals only one-hundredth or one-thousandth of that for external layers of the earth. If extrusion of molten material occurred during different periods on individual sectors of the lunar surface, gases liberated in each of these extrusions could not have created any noticeable atmosphere on the moon. Constant bombardment of the moon surface by solar-corpuscles, micrometeorites, and hard solar radiation must have communicated velocities exceeding the parabolic (approximately 2. 4 km/second) to atmospheric particles; that is, these particles must have blown away and thus have been prevented from accumulating. In the instance of a planet with an extensive atmosphere, the effect of particle penetration into its atmosphere would have been analogous to an explosion at depth. The energy would be communicated to large masses, and low velocities to individual gas particles; this could not lead to dissipation of a planetary atmosphere. Hence, if the moon did not have enough of an atmosphere during this period, it could not have accumulated an atmosphere gradually.

At present, causes of tectonic processes and internal energy within cosmic bodies are not known. It is clear, however, assuming that thermal-conductivity coefficients remain the same, that the capacity of a large body to accumulate and conserve internal energy is greater than of a smaller body. These considerations appear to contradict the possibility that the moon could conserve the necessary capacity to undergo tectonic processes. If we bear in mind, however, the extremely low thermal conductivity of the moon's surface layers, the moon surpasses the earth in the ability to accumulate and conserve internal energy. Accordingly, orogenic processes may be taking place on the moon even more intensively than on the earth, at the present time. To present an interesting and somewhat paradoxical conclusion: the absence of atmosphere, which gives rise to a foamy surface structure, sharply reduces heat emission and implements accumulation of internal energy and development of orogenic processes.

Lunar topography has been carefully studied over a period of 200 years; yet up to the present time we have been unable to verify a single example of change in lunar relief. This does not contradict the conclusion as to possibility, even at the present time, of intensive tectonic activity on the moon. As a matter of fact, aside from planetary processes involved in the activity of water, air, and life, it would be very difficult for an observer on the moon to ascertain reliably the presence of orogenic processes on the earth. Since ancient times, many observers have pointed to possible changes occurring in certain lunar craters. Particularly interesting is a report of occlusion by haze of crater-bottom

---

[1]Translated from Vulkanicheskaya deyatelnost na lune: Priroda, 1959, no. 3, p. 84-88.

[2]Doctor of Physical and Mathematical Sciences, Glavny Astronomical Observatory, Academy of Sciences, U.S.S.R.

features. Unfortunately, these observations were visual and therefore not convincing; visibility of details on the lunar surface depends to a great extent on the aspect of solar illumination. Other factors, such as atmospheric conditions and quality of photography, may influence the value of an observation.

In October 1956, the first serious and objective basis for a possible haze occlusion of detail on the moon's surface was obtained by the astronomer Dinsmore Olter. Using the 60-inch reflector at the Mt. Wilson Observatory in California, he obtained a series of photographs in blue and infrared light, of Ptolemaeus, Alphonsus, and Arzachel craters. Because earth's atmosphere disperses light, photographs taken in blue light showed much less contrast than those taken in infrared light. Details of the bottom of Alphonsus crater, however, appeared to be very much faded; the investigation published by Olter convinced the author that this effect merited serious attention and, that gas may be escaping from the floor of Alphonsus crater.

The group of three craters mentioned, of which Alphonsus is the central one (fig. 1), occur on its floor. The crater is approximately 120 km in diameter and its steep central peak is 1,400 meters above the crater floor. Ptolemaeus crater, located north of Alphonsus crater, is a typical large cirque having no central peak. Structure of the bottoms and walls of this crater group confirms a high degree of tectonic activity in this sector of the lunar surface.

Let us consider how the faded effect may have been produced by liberation of gases: The faded effect cannot be produced by the light dispersion in these gases; if this were the case, it would be necessary to have a gas column of about 10^{25} molecules per square centimeter (cm^2) of surface; that is, similar to earth's atmosphere. Or, if the gases in question fluoresce when exposed to hard solar radiation, a veil could be created by a gas column capable of absorbing all hard solar radition. The absorption coefficient of hard solar radiation, that is corpuscular, X-ray, and extreme ultraviolet radiation, would have to be very large. We may suppose then, that even a column of gas about 10^{15} molecules, or approximately 10^{-10} of the earth's atmosphere, would create perceptible fluorescence. Development of local atmosphere could be readily possible from the

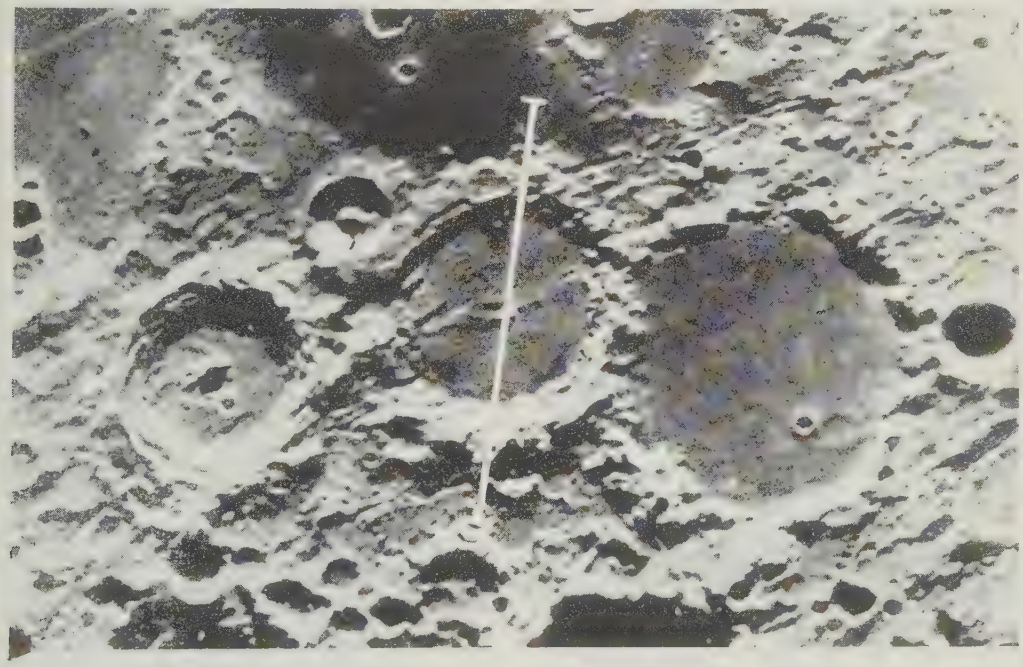

FIGURE 1. Alphonsus (center), Ptolemaeus and Arzachel craters.
The white line through the central peak indicates the position of the aperture of the spectrograph.

is located on a meridian and almost in the center of the lunar disc. The group is of ancient origin; meridional fractures, developed after crater formation, cross the sector in which they occur. An interesting fracture bisects Alphonsus crater; also fissures and dark spots

escape of gases in lunar craters. The only question remaining is whether or not the intensity of hard solar radiation is sufficient to create fluorescent radiation in the visible range of the spectrum, perceptible on the solar spectrum background usually reflected by the moon. It should

be noted that fluorescence of this type can be produced not only by gases, but by minerals present on the lunar surface as well.

In 1955, the author used the spectral method to compare the Fraunhofer-line contours of solar and reflected-lunar spectra; direct proof of fluorescence in the ray system of Aristarchus crater, was obtained. The maximum intensity of fluorescence in the violet band reached approximately 15 percent of the light usually reflected by the moon. This result indicated the possibility of proving the existence of gas escape at the lunar crater floors by means of spectrum analysis of gas fluorescence.

In October and November 1958, V. I. Yezerky an astronomer at the Kharkov observartory, and the author undertook spectrographic investigation on Mars, using a 50-inch reflector at the U. S. S. R. Academy of Sciences' Crimean observatory. At the same time, the author decided to obtain systematically spectrograms, photometrically standardized, of certain lunar details; particularly those of Alphonsus crater. This was done to investigate further the question of gas escape. During observations, the spectrograph aperture was always placed on a direct ascent. On the photographs, linear dispersion amounted to 23 angstroms (A) per millimeter (mm) close to $H\gamma$, with a scale of detail, about 10 seconds per mm. Normal exposure of Kodak 103 AF plates was from 10 to 30 minutes.

No special features were noted on the Alphonsus spectrogram until the night of November 2-3. On the morning of November 3, we obtained three spectrograms of Alphonsus crater; the spectrograph aperture traversed the crater along its diameter passing through its central peak (fig. 1). In obtaining the first spectrogram (at 0400 hours, Moscow time), the author was surprised, during a traverse of the area under examination, to see in the aperture the highly faded and unusually reddish hue of the central peak. Afterward, in accordance with the program, it was necessary to resume spectrographic investigation of Mars.

The second spectrogram of Alphonsus crater was obtained after an interval from 0600 to 0630 hours. As soon as the central peak of the crater appeared in the aperture, the author noted its unusual brilliance and whiteness. During this traverse, the author did not take his eyes from the telescopic sight, and noticed the sudden drop in the peak's brilliance to normal intensity. The exposure was stopped immediately and started again at 0630 hours, and was continued until 0640 with the aperture in the same position. The author did not attach much importance to visual impression; it was thought that all these special features were connected with changes in the quality of the image. In a somewhat unexpected manner, according to the spectrogram, all changes previously noted in visual observations were verified; they actually had occurred on the central peak of Alphonsus crater.

On the first spectrogram, the central peak was perceptibly weaker by violet illumination, compared to adjacent topographic details of the crater; this sort of thing is not usually observed on a spectrogram. Measurement of the print showed absorption to vary inversely with λ and the calculated total absorption obtained was equal to 15 to 20 percent in the visible spectrum. On the second spectrogram this absorption was not perceptible. Our attention, however, was attracted to the gas emission spectrum, which consists of several wide bands imposed on the normal spectrum of the central peak (fig. 2a). On the third spectrogram, the central peak appeared in its normal state (fig. 2 b). Therefore, gas liberation lasted not more than 2.5, and not less than 0.5 hours.

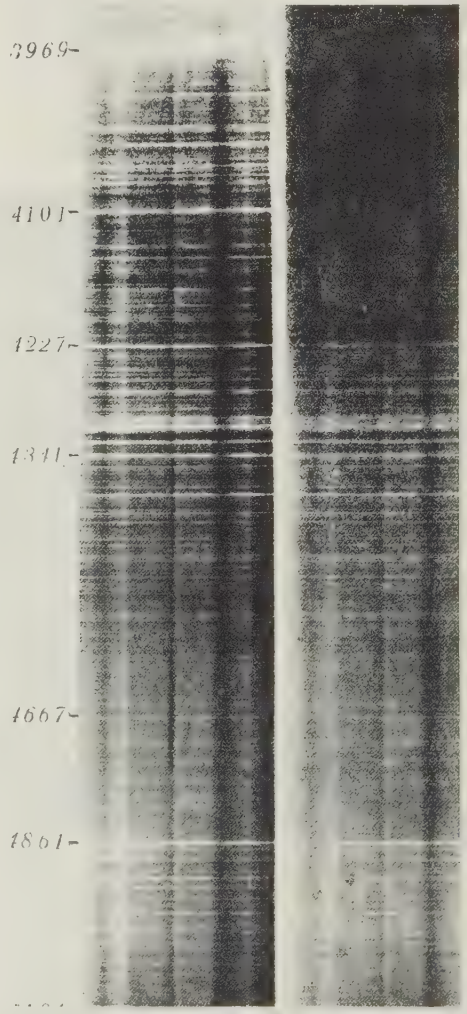

FIGURE 2. Spectrogram of Alphonsus crater left) 0600 to 0630 hours, November 3, 1958; right) 0630 to 0640 hours, November 3, 1958.

On the following night, November 3-4, we obtained two additional spectrograms of Alphonsus crater; the appearance of the crater was normal. By the evening of November 4, the last quarter of the moon had approached, rendering Alphonsus inaccessible to further observation. On the morning of November 3, 1958, Alphonsus crater, specifically the central peak, was the scene of volcanic activity. At first, some dust (volcanic ash) was ejected; then, as usual, gases were liberated. The gases probably escaped from magma rising to the surface; this magma must have contained gases absorbed at depth under high pressure.

The most characteristic feature noted in the emission spectrum of the central peak in Alphonsus, is the group of bands beginning at 4, 754 A and defined comparatively sharply toward the longer wave length region (fig. 2a). The brightness of these bands amounts to 40 percent of the normal brightness of the peak in the corresponding long wavelengths. It is noted that the imposed emission is shifted slightly toward the sun; the shift amounts to approximately 0.7 seconds, or about 1.5 kilometer (km) on the lunar surface. The shift is probably explainable in that hard solar radiation, causing the luminosity, could penetrate only an area of the gaseous column that was emitted from the center of the peak, and on the side exposed to the sun. We must suppose the processes causing gas luminosity to be similar to those of comets. Solar radiation evidently caused dissociation of complex parent molecules into optically active molecular residues (radicals) which created the observed spectrum. It is interesting to compare the surface brightness of the liberated gases to that of comets.

Near the time of full-moon phase, when the incidence of solar radiation is steep, reflectivity of the central Alphonsus peak is 0.13; that is, almost twice the average reflectivity of the lunar surface. At the moment of observation, the altitude of the sun over the horizon of Alphonsus crater was only 18°. According to data collected by the Kharkov astronomer V. A. Fedorets, the reflectivity of the central peak at this solar altitude, is one-tenth that of the full moon. If we assume brightness of supplementary gas luminosity, taking an average over all wavelengths, to have amounted to 10 percent of the peak's brightness, then surface brightness of the observed gas luminosity is equal to one-fiftieth of the average surface brightness of a full moon. The brightness of the full moon is 5.5 stellar magnitudes per square minute; that of the luminous gases is approximately 1 stellar magnitude per square minute; for a comet, however, this amounts to approximately 1/9 stellar magnitude per/sq/min.

The observed luminosity of the gases was 10,000 times more intense than that of a comet. This indicates that the quantity of gases liberated was more than sufficient for the absorption of all hard solar radiation. Luminosity of the gases in spite of their brightness, is barely perceptible near full moon when the sun is at a relatively high altitude; illumination would continue to be barely perceptible even if reflecting power of the moon were greater. We should remember that luminosity of volcanic gases may occur only when lunar detail is lit by the sun; therefore, this phenomenon could not be observed at twilight.

To obtain a clear idea of the emission spectrum, one must subtract systematically the brightness of the central peak and the adjacent sectors of the crater floor over the entire spectrum. Measurements of this type require great accuracy and are yet incomplete; nevertheless, certain conclusions can be drawn at this time.

In the bright group of bands beginning at 4,754 A and gradually weakening towards the violet side of the spectrum the Swan band, of the carbon molecule C_2, stands out as the main component. The distinct maximum on wavelength 4, 737 A corresponds to the beginning of the system of vibrating zones for this molecule. The existence of C_2 is confirmed by the presence of other, much weaker groups of the Swan band with maximums of 5,165 and 5,636 A. On this basis, the existence of the C_2 band in the liberated gases can be established. In the areas from $H\delta$ to the line HCa^{+} a system of weak bands belonging to the linear molecule C_3, are observed, analogous to those of the Swan band in a spectrum of a comet head. Characteristically different from comet spectra is the complete absence of the ultraviolet band CN 3883 A in spectra of escaping gases. Comparatively bright bands occur in the spectrum at wavelengths from 4, 600 to 4, 250 A; and at other wavelengths, a large number of weak bands. It has not yet been possible to determine the molecule which these bands describe. We should note that all bands of this spectrum are very diffused. The Swan band should be very sharp toward the longer wavelengths, but even these bands were diffused by approximately 5 A. It is most probable that this phenomenon is related to a process of the predissociation type; in general, the bands were observed only at the moment of development of the optically active molecular radicals from the complex parent molecules.

The observed phenomena, as a whole, indicate actual volcanic discharges to have occurred in the central peak of Alphonsus crater. It could not have been a weak gas escape from surface fissures, which was probably the phenomenon observed by Olter. Evidently, this conclusion is confirmed by a communication from the English observers P. Wilkins and F. Brion, that deals with the appearance of a small reddish spot around the south side of the Alphonsus central peak. These spots were

observed on November 19, 1958; it was affirmed that they did not exist prior to November 1958.

It is possible that the phenomena described here may not be observed again for a long time; they indicate nevertheless, that the moon still has the internal energy necessary to undergo orogenic processes. The coincidence of the phenomena observed and the position of the central peak cannot be a matter of chance; these indicate the development of basic relief on the moon's surface to be endogenic, not due to meteoric impact.

CHRYSOLITES OF YAKUTIA'S KIMBERLITE PIPES AS PRECIOUS STONES FOR THE JEWELRY INDUSTRY[1]

by

I. V. Ilin, N. A. Kuryleva, L. A. Popugayeva and Ya.B. Sigal

• *prepared by the United States Joint Publications Research Service*[2] •

ABSTRACT

Until recently, economically significant occurrences of chrysolite were not known to exist in the Soviet Union. Geologic investigation of the Udachnaya kimberlite pipe by the TsNILKS has established the presence of gem-quality chrysolite in Yakutia. The crystals are varying shades of light green; the depth of coloration dependent on iron, manganese and, probably, chromium content. So far, 4,300 grams of chrysolite have been recovered from 25 cubic meters of concentrate; the crystals ranged in diameter from 5 to 15 millimeters. The value of the occurrence is enhanced by the association of diamonds, pyrope, and picroilmenite. --G. E. Denegar.

Olivine is an essential component of Yakutian Kimberlites, but is very unstable in the surface-erosion zone; it seldom occurs there in an unweathered state. In some pipes formed of fresh kimberlite of basaltlike appearance, however, olivine is encountered in association with such minerals as diamond, pyrope, and picroilmenite. So far, the best preserved olivines have been noted only in kimberlites of the Udachnaya and Dalnaya pipes.

At present, the diamond-bearing kimberlite of Udachnaya, occurring in carboniferous limestones and dolomites on the right bank of the Daldyn river, is the best-studied occurrence. Kimberlite filling the Udachnaya pipe is characterized by nonhomogeneous structure. The western, most expanded part of the pipe is formed by disintegrated kimberlite breccia, peculiar in its high percentage of extraneous fragmental material. The eastern part of the pipe is formed by less-disintegrated kimberlite of basaltlike appearance, in which olivine occurs.

The basaltic kimberlite is a relatively unfractured rock of a dark greenish-gray color. It has porphyritic structure with some brecciated elements (also, it contains some xenoliths of the countryrock). The magmatic character of the cementing substance is a distinctive peculiarity of basaltic kimberlite.

The rock consists of 25 to 30 percent olivine, fresh but locally weathered phenocrysts and xenocrysts; 5 to 6 percent phlogopite; 10 to 15 percent countryrock fragments; 3 to 5 percent of ore minerals, angular grains; and 45 to 50 percent basic rock, decomposed.

The olivine crystals generally range in size from 0.5 to 8 millimeters (mm); rare crystals are as much as 15 mm in diameter. Most crystals are irregularly shaped; their outlines are smoothed or angular (fig. 1). A careful study

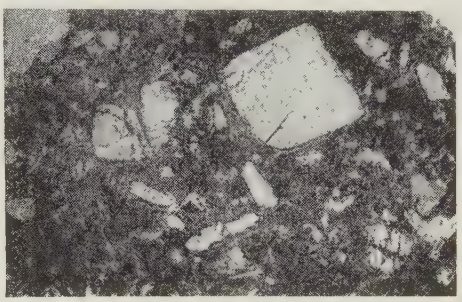

FIGURE 1. Basaltic kimberlite containing a chrysolite crystal (X 4.75)

of the olivines has shown their color to vary in light-green shades: olivine green, pistachio, and wine yellow. Some crystals contain very small, dark inclusions; or as a result of serpentine substitution for olivine, they may be banded. Perfectly pure, transparent chrysolites, suitable for the jewelry industry, are frequently encountered.

A polished thin section of chrysolite, cut along (010), was examined optically. The following measurements made were: N_g = 1.682, N_m = 1.663, N_p = 1.642, N_g-N_p = 0.038 [sic] and 2V = 80 to 83°.

Chemical analyses of chrysolites of various shades show their composition to differ for each shade. The depth of color in the chrysolite crystals depends upon their iron and magnesium content (in percent); and probably, upon their chromium content (table 1).

A technical investigation of chrysolites, carried out by an exploration team of TsNILKS [Central Scientific-Research Laboratory of Gems], and preparation of cut stones from samples collected, confirmed fully the value of chrysolites from Yakutia. It should be noted here that genuine, gem chrysolite occurs infrequently. For example, crystals of quality

---

[1] Translated from Khrisolity kimberlitovykh trubok Yakutii kak dragotsennyye kamni dlya yuvelirnoy promyshlennosti: Razvedka i Okhrana Nedr, 1958, no. 2, p. 8-9.

[2] JPRS/DC-L-1178.

having pretty green and yellowish-green coloration, are imported from placer deposits in upper Egypt (east of Esne), India, Anatolia, and Brazil.

TABLE 1. Chemical analyses of chrysolites of various shades

Major constituents	Light-green chrysolite from Udachnaya pipe	More deeply colored chrysolite from Udachnaya pipe	Average chemical composition of chrysolite (after P. N. Chirvinsky)
SiO_2	41.45	41.62	40.04
TiO_2	-	-	0.38
Al_2O_3	-	-	0.81
Cr_2O_3	0.01	0.01	0.08
Fe_2O_3	-	-	0.47
FeO	7.64	9.60	11.33
MnO	0.01	0.01	0.23
CaO	-	-	0.19
MgO	50.22	49.02	45.64
K_2O	-	-	0.06
Na_2O	-	-	-
H_2O	-	-	0.42
Insoluble residue	-	-	0.12
Total	99.33	99.66	99.77

No commercial occurrences of chrysolite were known in the Soviet Union until recently. The so-called "chrysolites," both in the jewelry industry of old Russia and the U. S. S. R., are Ural adamantine minerals of the garnet group; used in imitation of genuine chrysolite. During a special geologic investigation of the Udachnaya pipe, it was established that chrysolites of commercial importance do occur in the Soviet Union.

The commercial importance of chrysolite from the Udachnaya pipe was determined on the basis of spot sampling of both rock and concentrate tailings. Approximately 4,300 grams (g) of chrysolite were handpicked from 25 cubic meters of concentrate. The average chrysolite content amounted to 19 grams per square meter of rock. The crystal diameters ranged from 5 to 15 mm; crystals 5 to 7 mm in diameter predominated.

Chrysolite-bearing basaltic kimberlites occur extensively within the limits of the pipe, especially at depth. Chrysolite quality (transparency, purity, size) improves with depth. The value of the occurrence is augmented by the presence, and ease of recovery, of diamonds. Thus, the exposure of a chrysolite deposit in Yakutia is of considerable interest.

ON CENOZOIC VERTEBRATES IN KOREA[1]

by

Fuyuji Takai

• *translated by the author* •

ABSTRACT

Cenozoic fossil mammals, relatively rare in Korea, were first discovered there in 1915 by K. Jimbo and identified as possibly Pleistocene horse and rhinoceros remains. Subsequently, seven mammalian species of Eocene Carnivora and Perissodactyla were found in the Pongsan coal fields. Miocene fossils discovered include 4 vertebrate species; the most extensive occurrences are represented by the Pleistocene. Of 19 mammalian species, 15 were taken from a single terrace deposit. Correlation with other far-eastern fossil localities is attempted where sufficient data was available. Tentative identifications are made of an elephantine tooth and a sabre-toothed tiger, both Pleistocene. Specimens from Tungryong-gul limestone cave are probably too recent to be properly designated fossils. --D. D. Fisher.

Cenozoic fossil vertebrates of Korea are much inferior to those of China and even inferior to those, considered to be rather poor, of Japan. To summarize present knowledge of these fossils may be of significance in future studies on Korean Cenozoic formations; their specific names, the fossil-bearing formations, and their localities are stated below according to their geologic succession. Paleontological descriptions are omitted, but reference works concerning these fossils, including their original descriptions, are listed at the end of this article.

EOCENE

Seven mammalian species, following, occur in coal seams of the Pongsan and Sariwon coal mines of the Pongsan coal field in Pongsan-gun, Hwanghae-do; by their relationship with the Shara Murun and Irdin Manha formations of Mongolia, age of the fossils is presumed to be upper Eocene.

Carnivora	Harpagolestes koreanicus Shikama
Perissodactyla	Cristidentinus sp.
	Desmatotherium grangeri Tokunaga
	Lophialetes tokunagai Takai
	Colodon hodosimai Takai
	Caenolophus makii Takai
	Protitanotherium koreanicum Takai

Occurrence of mammalian remains in the Pongsan coal field was first reported by Shigeyasu Tokunaga [25] and from insufficient specimens he considered them to be of Miocene age, as did Tamezō Mori [9] and Tokunaga [27] later on. Tokunaga [29, 30, 32] concluded finally, from the occurrence of late Eocene species related to those of Mongolia (collected by the Asiatic Expedition of the American Museum of Natural History), that they were late Eocene. Results of research on fresh-water molluscan and plant remains by Susumu Matsushita, Takefumi Onoyama, and Shunrō Maejima [7] also confirmed their age to be late Eocene. Further study by the author [16, 17, 20] and Tokio Shikama [14] revealed that the Pongsan (Hōzan) mammalian fauna consisted of the above-mentioned seven species.

According to its mammalian faunal assemblage, the author [21] concluded that the Pongsan (Hōzan) formation can be correlated safely with the Ube coal-bearing formation and the Sōshu sandstone, (in a previous report, the following: "The Gonosawa sandstone member, the lower part of the Tachibetsu formation," was used erroneously; the author, accordingly, corrected it to: "The Sōshu sandstone member, the upper part of the Tachibetsu formation.") in the upper part of the Tachibetsu formatin in Japan. Other corresponding beds assigned to upper Eocene

[1]Translated from Geology and Mineral Resources of the Far East, Korea, pt. III-13, Stratigraphy: published under the auspices of the Compilation Committee of Geology and Mineral Resources of the Far East, 1951; translation prepared for the Office of the Engineer, Headquarters, United States Army, Japan; edited by Carol Broline, U. S. Geological Survey.

Place names, as far as possible, correspond to those approved by the U. S. Board on Geographic Names. Geologic names in parentheses are Japanese.

are: the Kuanchuang series of Shansi province; the lower Yüanch'ü series of Shansi and Honan provinces; the Lushih series and the Fanchuang series of Honan province; the Lunan series of Yunnan province, China; the Irdin Manha formation and the Shara Murum formation, Inner Mongolia; the Pondaun formation, Burma; and the Melawa group, Borneo.

MIOCENE

Miocene series occur in several limited areas; but comparatively prominent among them are: in North Korea, the Myŏngch'ŏn and Kilchu districts of north Hamgyŏng-do and the Yŏngil, Changgi, and Yŏngil districts of north Kyŏngsang-do in the south. The Myŏngch'ŏn (Meisen) series in the north is divided into the lower P'yŏngnyuk (Heiroku) and upper Hamjin (Kanchin) stages. The latter contains several molluscan remains characteristic of the Miocene; the former four vertebrates. The remains indicate that geologic age of these stages may be middle Miocene.

Pisces	Teleostei	Clupea sp.
Mammalia	Cetacea	Cetacea gen. and sp. indet.
	Proboscidea	Bunolophodon annectens (Matsumoto)
	Perissodactyla	Rhinoceros sp.

From the Yŏnil (Ennichi) series of the south, a shark of the species Carcharodon megalodon Agassiz, several bones and scales of indeterminable bony fishes were collected together with mollusca, other fossils, plants and animals. Their age, and extending from middle to late Miocene, is considered to be somewhat later than the Kanchin stage.

Among fossil fishes, occurrences of Clupea sp. and other bones and scales were reported for the first time by Iwao Tateiwa [21, 22]; Kinji Kanehara [2] later added the occurrence of Carcharodon megalodon Agassiz. Precise paleontologic studies of these fossils have never been undertaken.

Among three mammalian remains the first fragments, undeterminable cetacean bones, were reported by Mori [8, 9], but have not been studied paleontologically. The second, a mastodon, was first reported by Jirō Makiyama [3, 4] under the name Trilophodon cfr. angustidens (Cuvier), but later [5, 6] he described it under the new specific name Bunolophodon yokotii Makiyama. The author [16, 18, 19], however, considered that it might be identical to the Japanese mastodon, Bunolophodon annectens (Matsumoto). The third, a rhinoceros, was also reported by Mori [9] with no elaboration, but by its occurrence, the author [16, 18] supposed it to be related to the Japanese Miocene rhinoceros, Chilotherium pugnator (Matsumoto).

PLEISTOCENE

Development of the mammaliferous Pleistocene series also is extremely slight. Remains were found at several localities, such as Kaesong-bu, Kyonggi-do; Changyon-gun, Hwangju-gun, and Kumch'on-gun, Hwanghae-do; Songch'on-gun, south P'yongan-do; and Kilchu-gun and Chongsong-gun, north Hamgyong-do. Some of these remains were taken from fissure-filling or terrace deposits, but the original localities of others are unknown. From the above-mentioned localities, several investigators found the following 19 mammalian species. Judging from species contained in the terrace deposits at Chongsong-gun, north Hamgyong-do (marked by an asterisk (*)), geologic age of the deposit is clearly upper Pleistocene; all other remains are, possibly, late Pleistocene.

Rodentia	*Citellus tomanensis Tokunaga and Mori
	*Myospalax cfr. epsilanus Thomas
	*Microtus maekawai Tokunaga and Mori
	*Ochotona sp.
Carnivora	*Hyaena ultima dokantinensis Tokunaga and Mori
	Megantereon nihowanensis (Teilhard and Piveteau)
Proboscidea	Palaeoloxodon naumanni Makiyama
	*Mammonteus primigenius Blumenbach
Perissodactyla	*Equus przewalskii Poliakoff
	E. caballus fossilis Linnaeus
	*Rhinoceros antiquitatis Blumenbach
	R. shindoi Tokunaga
Artiodactyla	*Capreolus cfr. pygargus ochracea Barclay
	*Cervus elaphus elaphus Linnaeus
	*C. elaphus canadensis Erxleben
	*Megaceros sp.
	*Ovis cf. ammon Linnaeus

Artiodactyla (concluded)

*Bos primidenius Bojanus

*Bison exguus Matsumoto

Of the 19 species listed, 15 (marked by an asterisk (*)), were excavated by Mori [12], and by Tokunaga and Mori [33] from the terrace deposit at Tonggwan-jin, Changgwan-myŏn, Chongsŏng-gun, north Hamgyŏng-do; they resemble closely fossils being excavated at Ho-chia-kou, Ku-hsiang-tung near the city of Harbin, Manchuria, but appear to be younger than the Manchurian specimens. The author considers them to be upper Pleistocene.

A saber-toothed tiger, collected from the residual clay at the Hwan-san limestone quarry at Kyŏmip'ŏ-up, Hwangju-gun, Hwandhae-do, was identified by Shikama [13] as Machairodus cf. cultridens (Curvier); he concluded its geologic age to be Pliocene. The author [16] had some doubt concerning Shikama's conclusion and supposed its age to be late Pleistocene. Later, P. Teilhard de Chardin and P. Leroy [24] identified this specimen with the Villafranchian species Megantereon nihowanensis (Teilhard and Piveteau), originally described from the Nihowan formation at Ni-ho-wan, Hopeh province in northern China, and presumed it to be early Pleistocene. Therefore, the early Pleistocene mammalian fauna are expected to be confirmed eventually in Korea.

Mori [9] reported the occurrence of an elephantine tooth, related to the Indian species Palaeoloxodon namadicus (Falconer ad Cautley), near Kilchu-ŭp, Kilchu-gun, north Hamgyŏng-do, without information concerning its precise locality, formation, or other data. The author boldly identified it with the Japanese Pleistocene species Palaeoloxodon naumanni Makiyama because of its resemblance to the Indian fossil Palaeoloxodon. This may be the northernmost occurrence of Palaeoloxodon in Japan, Korea, or China. Another occurrence of this species was reported by Takai [15, 16] from the sea floor near the island of Paengnyŏng, Changyŏn-gun, Hwanghae-do; it is the only confirmed specimen from Korea. As Palaeoloxodon naumanni Makiyama flourished in Japan during the Pleistocene, it may occur also in late Pleistocene formations of Korea.

Kotora Jimbo [1] reported the first occurrences of mammalian remains found in a limestone cave near Kyejŏng, Kodong-myŏn, Kŭmch'ŏn-gun, Hwanghae-do. Afterwards Tokunaga [26, 27, 28] specified them to be horse and rhinoceros remains; in addition he [32] corrected the name of the locality, previously mentioned, to Kyŏnggi-do. On the other hand, Mori [9] gave account of fossil horses and rhinoceroses from a limestone cave near Chesok-san, Kaesŏng-gun, Kyŏnggi-do. The proximity of these localities indicates that these fossils separately reported by Tokunaga and Mori, probably occurred in the same locality and possibly belong to the same species. The horses were named Equus caballus fossilis Linnaeus; Tokunaga [27, 28] without any description or illustrations, gave the new specific name, Rhinoceros koreanicus Tokunaga, to the rhinoceroses. Takai [16] questionably considered that the latter specimen might be identified with the Japanese Pleistocene species Rhinoceros shindoi Tokunaga. The geologic age of these two fossils may be Pleistocene; a more specific age determination is now impossible.

Tokunaga [26] and Mori [9] each reported, but did not describe, a red deer from the limestone cave at Majŏn-ni, Sŏngsh'ŏn-myon, Sŏngsh'ŏn-gun, south P'yŏngan-do; its geologic age may be Pleistocene.

HOLOCENE

Mori [10, 11] reported a Korean bear Ursus ussuricus Heude, and a Korean boar Sus coreanus Heude, from Tungryong-gul, a famous limestone cave, at Unhakch'am, Yongsan-myŏn, Yŏnghyŏn-gun, north P'yŏngan-do. Their occurrence of both specimens is unknown so it is impossible to determine whether they are Pleistocene or Recent species which entered the cave to hibernate; for this reason, neither specimen properly may be designated a fossil.

REFERENCES

1. Jimbo, K., MAMMALIAN REMAINS IN A LIMESTONE CAVE IN CHOSEN (KOREA): Geol. Soc. Tokyo, Jour., v. 22, no. 266, p. 425-426, 1915 (in Japanese).

2. Kanehara, K., GEOLOGY OF THE NORTHERN PART OF YŎNGIL (GEIZITU) DISTRICT, NORTH KYŎNGSANG-DO (KEISHŌDŌ), KOREA: Geol. Soc. Japan, Jour., v. 43, no. 509, p. 73-103, 1936 (in Japanese).*

3. Makiyama, J., THE MYŎNGCH'ŎN (MEISEN) SERIES, A MIOCENE STRATA, IN NORTH KOREA: Chikyū, v. 24, no. 1, p. 1-9, 1935 (in Japanese).

4. _____, THE MYŎNGCH'ŎN (MEISEN) MIOCENE OF NORTH KOREA: Kyoto Imp. Univ., Coll. Sci., Mem., ser. B., v. 11, no. 4, p. 193-228, 1936.*

5. _____, FOSSIL PROBOSCIDEA: Kagaku, v. 6, no. 11, p. 481-482, 1936 (in Japanese).

6. _____, JAPONIC PROBOSCIDEA: Kyoto Imp. Univ., Coll. Sci., Mem., ser. B., v. 14, no. 1, p. 1-59, 1938.*

7. Matsushita, S., T. Onoyama, and S. Maejima, GEOLOGY OF THE PONGSAN (HOZAN) COAL FIELD, HWANGHAE-DO (KOKAI-DO), KOREA: Chikyū, v. 23, no. 6, p. 403-420, 1935 (in Japanese).*

8. Mori, T., CETACEA FROM KILCHU (KISSHU), KOREA (CHŌSEN): Geol. Soc. Tokyo, Jour., v. 33, no. 398, p. 473, 1926 (in Japanese).

9. _____, CATALOGUE OF MAMMALIAN FOSSILS OF KOREA (CHOSEN): Chōsen Nat. Hist. Soc., Jour., 1929, no. 8, p. 25-26 (in Japanese).

10. _____, A LARGE LIMESTONE CAVE AND ANIMAL BONES FOUND IN THE CAVE: Chōsen Nat. Hist. Soc., Jour., 1929, no. 9, p. 41-42 (in Japanese).

11. _____, GRAND SIGHT OF TUNGRYŎNGGUL, A LARGE LIMESTONE CAVE: Chōsen (Korea), 1930, no. 177, p. 63-78 (in Japanese).*

12. _____, PLEISTOCENE ANIMAL REMAINS AND HUMAN ARTIFACTS EXCAVATED ALONG THE BANK OF THE TUMEN (TOMAN) RIVER, KOREA: Geol. Soc. Tokyo, Jour., v. 42, no. 501, p. 364-365, 1935 (in Japanese).

13. Shikama, T., NOTE ON AN OCCURRENCE OF MACHAIRODUS IN KOREA: Imp. Acad., Tokyo, Proc., v. 10, no. 8, p. 490-493, 1934.*

14. _____, A NEW EOCENE CREODONT FROM THE PONGSAN (HŌZAN) COAL MINE, KOREA (CHŌSEN): Biogeogr. Soc. Japan, Bull., v. 13, no. 2, p. 7-11, 1943.*

15. Takai, F., AN ELEPHANT TOOTH FROM THE SEA FLOOR NEAR THE ISLAND OF PAENGNYONG (HAKUREI), HWANGHAE-DO (KOKAIDŌ), KOREA: Geol. Soc. Japan, Jour., v. 44, no. 523, p. 304-305, 1937 (in Japanese).*

16. _____, CENOZOIC MAMMALIAN FAUNA OF THE JAPANESE EMPIRE (A PRELIMINARY NOTE); Geol. Soc. Japan, Jour., v. 45, no. 541, p. 745-763, 1938 (in Japanese).

17. _____, EOCENE MAMMALS FOUND FROM THE PONGSAN (HŌZAN) COAL FIELD, KOREA (CHŌSEN): Imp. Univ. Tokyo, Fac. Sci., Jour., sec. 2, v. 5, pt. 6, p. 199-217, 1939.*

18. _____, THE MAMMALIAN FAUNA OF THE HIRAMAKIAN AND TOGARIAN STAGES OF THE JAPANESE MIOCENE: Jub. Publ. Commem. Prof. H. Yabe, v. 1, p. 189-203, 1939.*

19. _____, ON SOME CENOZOIC MAMMALS FROM JAPAN (PART I): Geol. Soc. Japan, Jour., v. 46, no. 552, p. 481-489, 1939 (in Japanese with English resume).

20. _____, EOCENE MAMMALS FROM THE UBE AND PONGSAN (HŌZAN) COAL FIELDS IN NIPPON: Imp. Acad., Tokyo, Proc., v. 20, no. 10, p. 736-741, 1945.*

21. _____, AMYNODON WATANABEI FROM THE LATEST EOCENE OF JAPAN WITH A BRIEF SUMMARY OF THE LATEST EOCENE MAMMALIAN FAUNULE IN EASTERN ASIA: Geol. Surv. Japan, Rept., 1950, no. 131, p. 1-14.

22. Tateiwa, I., GEOLOGICAL ATLAS OF CHŌSEN (KOREA); no. 2, Yŏnil (Ennichi), Kuryongp'o (Kyuryuho), and Choyang (Choyo) sheets, 1924.

23. _____, GEOLOGICAL ATLAS OF CHŌSEN (KOREA): no. 4, Kŭk-tong (Kyokudo), Myŏngch'ŏn (Meisen), Ch'il-bo-san (Shichi-hosan), and Koch'am-dong (Kotendo) sheets, 1925.

24. Teilhard de Chardin, P., and P. Leroy, LES FELIDES DE CHINE [THE FELIDAE OF CHINA]: Inst. Géobiol., Pékin, 1945, no. 11, p. 1-58.*

25. Tokunaga, S., FOSSILS OF RHINOCEROTIDAE FOUND IN JAPAN: Imp. Acad., Tokyo, Proc., v. 2, no. 6, p. 289-291, 1926.

26. _____, MAMMALIAN FOSSILS FOUND IN LIMESTONE CAVES IN KOREA: Imp. Acad., Tokyo, Proc., v. 5, no. 3, p. 139-141, 1929.

27. _____, ANCIENT RHINOCEROSES WHICH LIVED ON THE MAIN ISLANDS OF JAPAN, CHŌSEN (KOREA), AND MANCHURIA: Dōbutsugaku Zasshi (Zool. Mag.), v. 41, nos. 490-491, p. 377-378, 1929 (in Japanese).

28. _____, PLEISTOCENE CAVE-DWELLING MAMMALS IN HONSHU, KYUSHU, AND CHŌSEN (KOREA): Japan, Assoc. Advanc. Sci., Trans., v. 6, p. 175-178, 1930 (in Japanese).

29. _____, COAL-BEARING FORMATIONS OF JAPAN: 5th Pan-Pacific Sci. Congr., Proc., p. 1483-1489, 1932.

30. _____, ON THE GEOLOGICAL AGE OF PONGSAN (HŌZAN) COAL FIELD,

KOREA (CHŌSEN): Geol. Soc. Tokyo, Jour., v. 40, no. 475, p. 179-182, 1933 (in Japanese).*

31. _____, ON FOSSIL MAMMALS IN JAPAN: Dōbutsugaku Zasshi (Zool. Mag.), v. 45, no. 535, p. 253-254, 1933 (in Japanese).

32. _____, A LIST OF THE FOSSIL LAND MAMMALS OF JAPAN AND KOREA WITH DESCRIPTIONS OF NEW EOCENE FORMS FROM KOREA: Amer. Mus. Novitates, 1933, no. 627, p. 1-7.*

33. Tokunaga, S., and T. Mori, REPORT ON DIGGINGS AT TONGGWAN-JIN (DOKAN-TIN), THE BANK OF THE TUMEN (TOMAN) RIVER, KOREA: 1st Sci. Exp. Manchoukuo, Rept., 1939, sec. 2, pt. 4, p. 1-43 (in Japanese with English resume).*

*Designated references contain illustrations of fossil species described in the foregoing paper.

THE MANGANESE ORES[1]

by

Paul Ramdohr[2]

• *translated by W. O. J. Groeneveld Meijer* •

ABSTRACT

Twenty-two major manganese minerals are described in manual form. Crystallographic and optical properties are outlined and compared. Where variations in mineral characteristics are outstanding or similarities among various minerals hinder identification, a description of diagnostic features is more fully developed. Mode of occurrence is briefly, and quite generally, given. Text is supplemented by X-ray powder patterns and data, as well as by photomicrographs. --G. E. Denegar.

Minerals which contain manganese as major constituent are quite numerous. The number of minerals which can or do contain manganese in diadochic substitution for another element runs in the hundreds. All of the first named cannot be regarded as possible manganese ores. The latter, although of great importance as sources for deposits of manganese formed by secondary processes, cannot be treated because of space requirements.

Which manganese minerals can occur in exploitable amounts, while having at the same time tenors of commercial value, is a problem that cannot be answered unequivocally. Time and again it happens that minerals considered as being very rare or unusual become "ore." Thereby it is often decisive whether the accessories are useful, even valuable or hindersome or possibly even detrimental. Larger deposits of manganese-rich ankerite (kutnohorite) could very well be of interest; even for Germany, the siderite of Siegerland, containing only 5 to 10 percent manganese, is the most important source of our element. In contrast, fresh rhodonite ($MnSiO_3$) is useless and even the largest accumulation of alabandite (MnS) would not be a manganese "ore." However, the products of weathering of both these could of course form quite important deposits.

By far of greatest importance among the oxide compounds are those which chemically more or less resemble MnO_2 ($\pm H_2O$) and which largely are formed either by direct weathering or by solution and redeposition, but, at any rate, supergenetically by the action of atmospheric oxygen. Only most recently has one realized how multiform this group of minerals is, how most "Braunstein" (brownstone) ores represent complex mixtures, how variable even with uniform samples the characteristics can be and so come to coincide with those of others, and finally how properties, previously considered diagnostic (for example, many etch reactions) may presently be completely meaningless and even misleading. A determination in polished section is positive only with more or less coarse-grained material and good sections; a determination by X-ray powder data is only positive with homogeneous or at least uncomplicated aggregates. The extremely fine state of subdivision of the often colloidally precipitated minerals and the coincidence of one or two dimensions of their unit cells complicates for many members the interpretation of the diagrams so much, that even today many uncertainties persist. The manganese oxides of the "Braunstein group" will thus occupy the larger part of this paper. It has been attempted here to allow as certain a diagnosis as possible by including clear powder-pattern data. However it must be mentioned that the composition of an ore specimen can change completely in a short time - without being able to notice anything in the absence of polished section or powder pattern.

It is not always easy to obtain good powder patterns. Some samples may be too small, even of colloidal size, so that it is impossible to obtain sharply measurable lines. Also, a very strong background blackening generally occurs with Cu, Co, or Ni radiation so that very diffuse patterns result where the weaker lines are almost lost. This may be avoided with Mn-filtered $Fe_{K\alpha}$-radiation which has been used for all patterns shown.

Using the diagram easiest by matching a halved copy of the film to be compared (the user will not like to cut up the originals) with the prints shown, some difficulties will be met because of the small deformation which cannot be avoided during the drying of the film but particularly those which arise through reproduction in print. We have tried to limit as well as possible a further source of error by transposing the negatives to a positive in making the copy on diapositive plates.

Very slight changes in the d-values should not be considered a tragedy; neither should small changes in intensities which might be caused by a diadochic, sometimes insignificant

---

[1] Translated from Die Manganerze: Symposium sobre yacimientos de manganeso, XX Congreso Geologico Internacional, Mexico, v. 1, p. 19-73, 1956.

[2] Professor of Mineralogy, Heidelberg, Germany.

substitution (for instance Ba for K).

The experimental configuration of the so-called Guinier camera yields considerably sharper and line-richer patterns. Nevertheless we disregarded its use here as the obtained data should be reproducible even with a small amount of experimentation.

The "rod thickness" was standardized at about 0.3 millimeters (mm). Fine powder was filled into Li-borate glass. However clearer lines are obtained for large d-values (0.1 mm) by sticking powder on the finest of glass bristles; those with small d-values are less sharp or are not shown at all.

Here the following selection shall be treated. It is somewhat haphazard with respect to the rarer minerals and with regard to frequently abbreviated or unsubstantiated chemical formulae:

Hausmannite group
- Hausmannite - Mn_3O_4
- Hydrohausmannite - $(Mn^{2+}, Mn^{3+})_{3-x}(O, OH)_4$
- Hetairolite - $ZnMn_2^{3+}O_4$
- Hydrohetairolite - $ZnMn_{5/3}^{3+}O_3(OH)$

Jacobsite - $MnFe_2O_4$
- Vredenburgite - $(Mn, Fe)_3O_4$

Franklinite - $(Zn, Mn)(Fe^{3+}, Mn^{3+})_2O_4$
Bixbyite - Mn_2O_3
Braunite - Mn_7SiO_{12}
Manganite - $MnO(OH)$
Groutite - $HMnO_2$
Polianite - MnO_2
Pyrolusite - MnO_2
Ramsdellite - MnO_2
Psilomelane - $H_4Mn_2^{2+}Mn_8^{4+}O_{20}$
Cryptomelane - $KMn^{2+}Mn_8^{4+}O_{16} \cdot 2H_2O$
Hollandite $\approx BaMn^{2+}Mn_8^{4+}O_{16} \cdot 2H_2O$
Coronadite $\approx PbMn^{2+}Mn_8^{4+}O_{16} \cdot 2H_2O$
Lithiophorite (??)
- $Li_2Mn_2^{2+}Al_8Mn_{10}^{4+}O_{35} \cdot 14H_2O$

Chalcophanite $\approx Mn^{2+}Mn_2^{4+}O_5 \cdot 2H_2O$
Todorokite - $(Mn^{2+}, Ca)_2Mn_5^{4+}O_{12} \cdot 4H_2O$
Woodruffite - $(Zn, Mn^{2+})_2Mn_5^{4+}O_{12} \cdot 4H_2O$

Not as manganese ore are considered: manganosite - MnO, pyrochroite - $Mn(OH)_2$, crednerite - $CuMn_2O_4$, cesarolite - $H_2PbMn_3O_8$, because of their rarity; alabandite - MnS, hauerite MnS_2, because of sulfur content; and many others from the silicate (and phosphate) group because of large Si or P contents, respectively.

Many colleagues aided us with kind references or with materials which in part were very difficult to obtain: M. Fleischer, Washington; C. Frondel, Harvard; J. W. Gruner, Minneapolis; E. Hellner, Marburg; A. Schroder, Hamburg.

HAUSMANNITE GROUP

At least four minerals, as recently has been found, give a powder pattern very similar to hausmannite which might be overlooked with less precise work: hausmannite, Mn_3O_4; hydrohausmannite, $(Mn^{2+}, Mn^{3+})_{3-4}(O, OH)_4$; hetairolite, $ZnMn_2^{3+}O_4$; and hydrohetairolite, $ZnMn_{5/3}^{3+}O_3(OH)$. The outward appearance can vary considerably; the paragenesis can be completely different. Isomorphically, variable substitution is conceivable, small amounts of iron often belong in the lattice. This is a tetragonally deformed spinel lattice with a_o = 5.75, c_o = 9.0-9.5 (for zinc-bearing members the smaller value), and Z = 4. The cleavage parallel to (001) is distinct; hardness, density, index of refraction, and transmittancy vary considerably and not always in the manner as expected from the formula. However, the polish is always good but very characteristic is the frequent occurrence of old polish scratches which have been polished closed throughout with a moirelike gackground under crossed nicols, particularly with oil immersion (fig. 1).

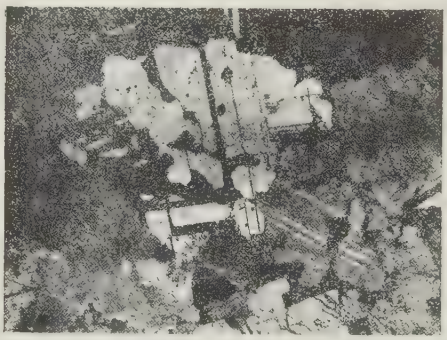

FIGURE 1. Hausmannite. Manganese mine Boz Nam, Ardishan, central Persia. Lammellar twining, grain intergrowth, and old scratches are easily discernible. (Note: In ordinary light the luster is faultless; oil immersion, crossed nicols, x 140.5).

Aside from the, by far, most important hausmannite, the other members of the group must also be briefly characterized.

Hausmannite

Crystallography. Octahedrallike crystals and isometric grains: a_o = 5.75, c_o = 9.42 A (angstroms)

Optical Properties. Only transparent in the thin splinters (dark red-brown): n_{OLi} = 2.45, n_{ELi} = 2.15, H = 5, D = 4.8.

Occurrence. Large range of formation.

Rarely of distinct superficial formation (suspect hydrohausmannite and hydrohetairolite), generally of epi- to mesometamorphic nature; formed from preexisting manganese ores of different heritage, or hydrothermally.

Reflection behavior. Color dark gray; slight reflectivity, strongly suppressed in oil (ϕ yellow 16.5, 6 percent respectively) - color, however, is not markedly changed. Bireflection distinct, strong in oil. Anisotropic effects are high (less than hydrohetairolite), particularly in oil. Internal reflections of blood-red color are frequent in oil, particularly parallel (001).

Etch reactions. Somewhat characteristic: concentrated HNO_3 and HCl, very little reaction. $SnCl_2$ and $H_2O_2 + H_2SO_4$, dark.

Structures. Lamellar twinning parallel (101), visible with crossed nicols, is almost always present (not with the other minerals of the hausmannite group!); lamellae remain of same width and are generally similar among each other (fig. 1). Frequently idiomorphic, often coarse, mosaic structure (crossed nicols!). Almost always incipient supergene formation of pyrolusite or psilomelane; hypogene, it replaces bixbyite, braunite, and others; also replaced by braunite.

Diagnosis. In polished section, easy and certain (internal reflections, twinning lamellae, moire sheen). The similar manganite is rarely twinned, generally columnar (caution with hydrohetairolite!), and replacement by pyrolusite is generally oriented. Jacobsite is isotropic; braunite is much less anisotropic and more brownish in oil and also without internal reflections.

Powder pattern. Quite characteristic. Strong lines: 4.92 (s/m), 3.08 (st), 2.75 (st), 2.48 (sst), 2.36 (m), 2.03 (m), 1.79 (m), 1.57 (st), 1.54 (sst), 1.44 (st), 1.28 (m), 1.12 (m). (See powder pattern 1 and accompanying table.)

Hydrohausmannite (Bäckströmite)

Crystallography. Often lobed, skeletal growth, however, uniform coarse crystallinity. Lattice dimensions hardly different from hausmannite: a_o = 5.79, c_o = 9.49 A.

Optical. More transparent than hausmannite, hetairolite, and hydrohetairolite; n_{oLi} = 2.055, n_{ELi} = 1.95. Absorption E>0, H<5, D hardly determinable [9].

Reflection behavior. Dark gray, less reflectivity than in hausmannite, bireflection is strong in oil but less than that of hausmannite. Anisotropism is strong but quite masked, particularly in oil, by internal reflections. Internal reflections are much more numerous than with hausmannite, hetairolite, and hydrohetairolite; their color is brown red to brown yellow.

Structures. No twinning has been noticed! In the examined specimen, strange structures were observed but no details can be given on their extent. The relict cleavage of pyrochroite is visible.

Diagnosis. Twinning lamellae are absent in contrast to that of hausmannite; the internal reflections, however, are much more frequent and much brighter, so that they are similar to those of goethite. Samples from Franklin and Långban were examined.

Powder pattern. With the exception of the strongest line, d = 4.61 A, completely absent from the hausmannite pattern, the pattern is almost identical with that of hausmannite. Strong lines of hydrohausmannite: 4.61 (sst), 3.14 (m), 2.74 (m), 2.47 (st), 2.35 (s/m), 2.03 (m), 1.92 (st/m), 1.57 (m), 1.53 (st), 1.44 (m), 1.11 (m). Characteristic in comparison to hausmannite is the very strong line at d = 4.61. Strong lines of pyrochroite: 4.65 (sst), 2.85 (s/m), 2.43 (st), 1.81 (st), 1.65 (m/s), 1.56 (m/s), 1.38 (m), 1.22 (s/m), 1.06 (m). (See hausmannite powder pattern and accompanying tables for hydrohausmannite and pyrochroite.)

Hetairolite

Crystallography. Single crystals and polygonal aggregates: a_o = 4.74, c_o = 9.15 A, H = 6, D = 5.18.

Optical. Brown red powder; n_o = 2.34, n_E = 2.12; black, semimetallic in hand specimen.

Occurrence. Insofar as known, restricted to Franklin; however, it should be expected to occur in outcrops of $MnCO_3$-rich ore veins. Only as a product of weathering.

Reflection behavior. Similar to hausmannite. In oil the reflection is strongly decreased and the bireflection ($R_O > R_E$) is increased. Reflection power (R_O = 17.7, R_E = 13 percent) and anisotropism are less than with hydrohetairolite. Anisotropic effects are quite striking in oil but hindered by internal reflections. Ubiquitous brown red internal reflections.

Structures. Polygonal aggregates; towards cavities crystal development. In one instance, the finest of lamellations, similar to alteration lamellation, was observed; it looks quite different from hausmannite lamellae.

Diagnosis. Almost no twin lamellae (in contrast to hausmannite) also, the internal reflections are brown red and more numerous. To the present, hydrohetairolite has only been observed in radial aggregates.

Powder pattern. The difference in regard to

Hausmannite, Ilfeld, Harz, Germany

d (A)	I	d (A)	I	d (A)	I	d (A)	I
4.92	s/m	1.82	ss	1.38	ss	1.10	ss
3.08	st	1.79	m	1.34	ss	1.08	m
2.87	ss	1.70	ss	1.28	m	1.06	ss
2.75	st	1.64	ss	1.23	s	1.03	m
2.48	sst	1.57	st	1.19	ss	1.02	m
2.36	m	1.54	sst	1.18	ss	0.985	m
2.03	m	1.44	st	1.12	m		

Hydrohausmannite, "Bäckströmite", Långban, Sweden

d (A)	I	d (A)	I	d (A)	I	d (A)	I
4.61	sst	2.03	m	1.44	m	1.11	m
3.14	m	1.92*	st/m	1.36	ss	1.10	ss
2.88	s	1.84	ss	1.35	ss	1.08	s
2.74	m	1.78	s	1.27	s	1.06	ss
2.47	st	1.69	ss	1.25	s	1.05	s
2.35	s/m	1.64	s	1.23	ss/s	1.03	ss
2.17	ss	1.57	m	1.19	ss	1.02	ss
		1.53	st	1.18	ss		

* This relatively strong line is not mentioned among the d-values given by Frondel [9].

Pyrochroite, Nordmarkem, Sweden

d (A)	I	d (A)	I	d (A)	I	d (A)	I
4.91	s	2.43	st	1.56	m/s	1.14	s/ss
4.65	sst	2.36	ss	1.38	m	1.09	s
4.52	ss	1.81	st	1.22	s/m	1.06	m
2.85	s/m	1.65	m/s	1.18	s	0.984	s

Hetairolite, Franklin, New Jersey

d (A)	I	d (A)	I	d (A)	I	d (A)	I
3.00	m	1.75	m	1.32	s	1.089	m
2.82	ss	1.68	m	1.29	ss	1.070	st
2.79	ss	1.61	m	1.28	ss	1.062	ss
2.68	st	1.56	m	1.26	m	1.054	m
2.57	ss	1.51	st	1.23	ss	1.041	m
2.44	sst	1.47	s	1.21	ss	1.014	st
2.29	ss	1.43	m	1.17	st	1.010	s
2.01	ss	1.40	ss	1.15	m	1.003	ss
1.90	ss	1.37	s	1.12	m	0.984	s
1.79	s/ss	1.35	s	1.11	st/m		

hausmannite can somewhat be noticed when the d-values are carefully measured. Also some intensities, particularly those of lines with small d-values, are quite different. Hydrohetairolite is quite similar: 1.56 and 1.51 are stronger, 1.17 is much weaker. (See hetairolite powder pattern and accompanying table.)

Hydrohetairolite

Crystallography. Fine fibrous aggregates in crusts: $a_O = 5.71$, $c_O = 9.04$ A. The literature value of D = 4.65 is too low.

Optical. Dark-brown powder, more opaque than hetairolite, $n_O = 2.26$, $n_E = 2.18$ (as the reflection is larger than that of hetairolite, these values are likely to be somewhat too low); Δ_n is thus noticeably smaller than with hetairolite. Metallic, pitch black in hand specimen. Often breaks out in splinters and fibers while polishing.

Occurrence. To the present known from Franklin and Leadville. The author could identify it abundantly in the Namib II field of the Km 24 deposit in southwest Africa. Probably occurs more frequently in outcrops of manganese-rich zinc deposits.

Reflection behavior. The reflective power is, regardless of the refractive indices, distinctly higher than that of hausmannite, also higher than that of hetairolite. The bireflection in air is weak, and very much increased in oil; anisotropic effects are quite striking in oil but only in tones of gray. Internal reflections are much rarer than with hausmannite, hydrohausmannite, and hetairolite. At any rate, there is no possibility here that they mask the effects of anisotropism.

Structures. Fine fibrous aggregates in crusts, the thin ends of the fibers are often terminated with crystal planes. The fiber direction is not defined crystallographically and it varies. The notation of Frondel and Heinrich [10], that the fiber axis is the (110) zone and that the cleavage (001) is parallel to it is at any rate not generally true. Twinning lamellae, as in hausmannite, is completely absent. Both examined specimens are altered slightly, sometimes distinctly at the margins and parallel to the fibers, to psilomelane.

Diagnosis. In polished section, the mineral may be easily confused with manganite particularly as the cleavage in hydrohetairolite can also be parallel to the long axis. The oriented formation of pyrolusite is almost always slightly visible in manganite; internal reflections are more frequent; and the powder pattern is completely different.

Powder pattern. Compare with hetairolite. Samples were examined from the Wolfton mine, Leadville, and from the Km 24 deposit near Swakopmund. The patterns were almost identical. (See hydrohetairolite powder pattern and accompanying table.)

JACOBSITE

Chemical. $(Fe, Mn)_3O_4$ (with some Mg and Mn^{3+}; unlimited solid-solution series with magnetite; with hausmannite solid solution proceeds via α - vredenburgite which, with more than 54 percent Mn_3O_4 is limited by the breaking up of vredenburgite.

Crystallography. Spinel-type structure: $a_O = 8.49$ A, D = 4.75.

Optical. Not completely opaque, deep black, strongly magnetic.

Polish. Good, better than magnetite.

Occurrence. Very rare, apparently only with high-grade metamorphism or possibly contact metamorphism.

Reflection behavior. Reflective power is low, color is gray to olive (particularly in comparison with magnetite). Reflective power is strongly diminished in oil (17 and 7 percent, respectively). Isotropic. Deep-red internal reflections, particularly with oil immersion, are frequently seen.

Etching. All usual etch media are negative.

Structures. Mosaic of rounded grains. In vredenburgite, jacobsite forms the groundmass, hausmannite the lamellae.

Diagnosis. Only observed in few deposits. Often a characteristic secondary formation of pyrolusite and psilomelane. The similar braunite almost never has internal reflections (brown) and in oil it is distinctly anisotropic.

Powder pattern. Is given of the very rarely pure jacobsite only because of the much more widespread vredenburgite. Strong lines: 2.94 (st), 2.52 (sst), 1.61 (st), 1.48 (sst), 1.09 (st), 1.05 (st). (See jacobsite powder pattern and accompanying table.)

Vredenburgite

Under certain rare conditions, as mentioned under jacobsite, a solid solution remains even above 54 percent Mn_3O_4 between Fe_3O_4 and Mn_3O_4. This is the tetragonal α-vredenburgite. Generally, however, this separates into hausmannite and jacobsite, the usual vredenburgite. In the resulting netlike pattern, hausmannite forms the meshes and jacobsite the filling. As hausmannite is strongly anisotropic, the structures can be readily recognized even without etching (with HF). Naturally, the structure is

Hydrohetairolite, Wolfton Mines, Leadville, Colorado

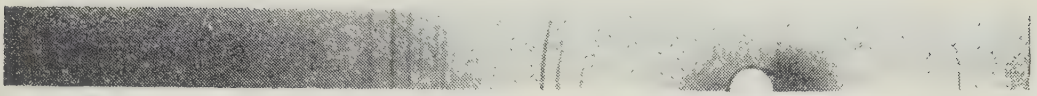

d (A)	I	d (A)	I	d (A)	I	d (A)	I
2.97	m	1.61	s	1.26	m	1.10	s/m
2.83	s	1.56	st	1.23	ss	1.09	s
2.63	st	1.50	sst	1.21	ss	1.07	m/st
2.44	sst	1.43	st	1.16	s	1.06	m
2.23	s	1.42	ss	1.15	s	1.05	ss
2.01	m	1.31	ss	1.13	ss	1.014	st
1.76	s	1.29	ss	1.12	s	1.005	ss
1.71	m	1.28	ss	1.11	s	1.001	m
1.67	m						

Jacobsite, Jacobsberg, Sweden

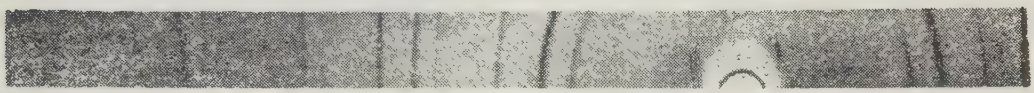

d (A)	I	d (A)	I	d (A)	I	d (A)	I
4.81	ss	2.09	m	1.32	s	1.12	m
2.94	st	1.71	m	1.28	m	1.09	st
2.78	ss	1.61	st	1.26	ss	1.05	st
2.52	sst	1.48	sst	1.21	s	0.990	m

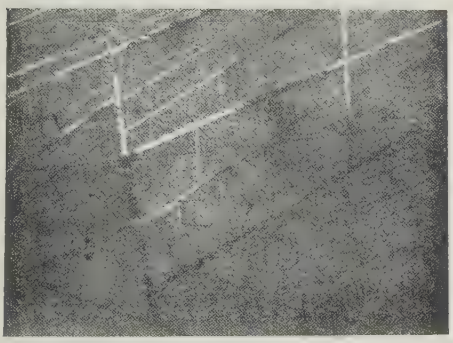

FIGURE 2. Vredenburgite. Manganese mine Kodur, Vizagapatan, India. "Vredenburgite" composed of Jacobsite (principal constituent) with minute lamellae of Hausmannite. In this portion of the preparation Hausmannite, secondary to the considerably brighter Pysolusite, is nearly hidden. (Oil immersion, x 84.3).

of different coarseness from case to case, but insofar as observed it is always easily seen under the microscope. Vredenburgite forms aggregates of single grains, in part in braunite crystals. Under conditions of weathering, the hausmannite lamellae are much more rapidly transformed to pyrolusite than the filling (jacobsite) (fig. 2). The powder pattern is of course that of a hausmannite-jacobsite mixture.

FRANKLINITE

Chemical. $(Zn, Mn^{2+})(Fe, Mn)_2O_4$, also complex substitutions; delineation with jacobsite is not sharp (note powder patterns).

Crystallography. Spinel-type structure: $a_o \approx 8.46$ A.

Optical. Deep red and isotropic in the finest of powder, $n_{Li} \approx 2.36$. Cleavage is parallel (111), of variable quality.

Polish. Easy to get a tolerable section. Some samples are strongly magnetic; most are not.

Occurrence. Presently only known from the Franklin-Sterling Hill deposit but there are tremendous masses.

Reflective behavior. Gray white, reflective power is not high (ϕ = 14 1/2 or 5 1/2 percent), isotropic. Internal reflections may be seen when care is taken.

Etching. Ordinary etch reagents are generally negative.

Structures. In the type locality, exsolutions in older generations of franklinite are very wide-

spread in occurrence; however, in part they are extremely fine in grain size; the product appears to be a zinc spinel; the coarser grained material appears to be pyrophanite, $MnTiO_3$, and certainly there are other exsolution products. Aggregates of round grains, single crystals are also strongly rounded.

Diagnosis. A wrong diagnosis will hardly be made because of the limitation in occurrence to one single deposit, in spite of the slightly variable properties. Transitions occur towards jacobsite, but the latter is devoid of zinc.

Powder pattern. Strong lines: 2.99 (st), 2.55 (sst), 1.62 (st), 1.49 (st), 1.10 (st), 1.06 (m). (See franklinite powder pattern and accompanying table.)

BIXBYITE (SITAPARITE)

Chemical. $(Mn, Fe)_2O_3$, possibly some Ca for Mn^{3+}

Crystallography. Cubic (T_h^5), a_o = 9.37 A; cleavage parallel to (111), only in larger pieces. H = 6, D = 5.0.

Optical. Opaque, semimetallic with a slightly bronze hue.

Polish. Good.

Occurrence. Variable! The deposits of economic importance are generally metamorphosed and formed from preexisting sedimentary manganese ores. Often it is formed from braunite and hematite which are products of metamorphism. Primary bixbyite occurs as volcanic exhalations. The mineral occurs much more widely than generally believed.

Reflection behavior. Light gray, quite similar to braunite; in oil the reflective power decreases. (yellow, 20 to 9 1/2 percent, respectively). In oil it has a distinctly olive-yellow hue in comparison with braunite; it is also lighter in color. Often isotropic, however, also often anisotropic (in oil), that is, it is only pseudocubic. No internal reflections.

Etching. Normal etch reagents are negative. Structural etch with HF in 1 minute.

Structures. Many deposits show again and again the very pretty, complicated parquetlike twinning (fig. 3). Zonal structure is distinct in single crystals. Occurs as idioblastic crystals and aggregates of same.

Diagnosis. In its properties it resembles both braunite and jacobsite. The latter is, as bixbyite, somewhat yellow in direct comparison with braunite; however, it is always isotropic and it occasionally has internal reflections. Braunite is anisotropic but without mimetic lamellation. D is low, but noticeably larger that of braunite and jacobsite.

Powder pattern. Strong lines: 3.84 (m), 2.71 (sst), 2.35 (m), 2.00 (m), 1.85 (m), 1.66 (sst), 1.45 (m), 1.42 (st), 1.08 (st), 1.05 (m). (See bixbyite powder pattern and accompanying table.)

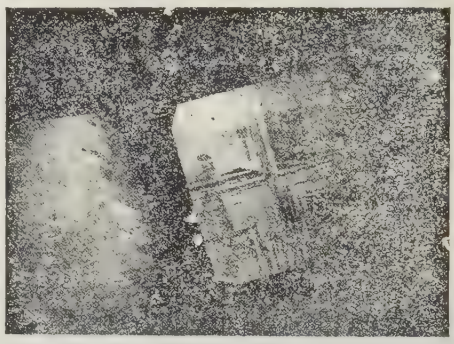

FIGURE 3. Bixbyite (Sitaparite). Postmasburg, Bechuanaland, South Africa. Idiomorphic crystals with characteristic lammellar twinning (after cubic), simultaneous zonal growth. (Oil immersion, crossed nicols, x 28.5).

BRAUNITE

Chemical. Mn_7SiO_{12}, in part with Fe^{3+}.

Crystallography. Tetragonal, pseudocubic as $c_o \cdot 1/2\sqrt{2}$, a_o = 13.44, c_o = 18.93 A. Cleavage parallel to (112), rarely visible. H>6, D = 4.8, Gray-black color.

Polish. Good.

Occurrence. Very variable. Occurs with very low-temperatured hydrothermal activity, generally however, of higher temperature hydrothermal formation and often as a product of metamorphism. Also of very high temperature of formation (possibly even directly crystallized from hybrid magmas).

Reflection behavior. Gray, slightly brownish, reflective power not high (16 1/2 and 8 percent, respectively). Bireflection can only be noticed with difficulty in oil at grain boundaries. Anisotropic effects are also weak with crossed nicols; however, with oil immersion, they hardly can be overlooked. Internal reflections are hardly ever visible.

Etching. Ordinary etch reagents are negative. Structural etch with concentrated HF.

Structures. Not characteristic for single grains. Aggregates are polygonally grained (fig. 4) and towards voids, and calcite for

Franklinite, Franklin, New Jersey

d (A)	I	d (A)	I	d (A)	I	d (A)	I
4.91	s	2.11	m	1.33	s	1.13	m
2.99	st	1.72	m	1.29	m	1.10	st
2.80	ss	1.62	st	1.27	ss	1.06	m
2.55	sst	1.49	st	1.22	s	0.996	m
2.44	ss						

Bixbyite, Postmasburg, South Africa

d (A)	I	d (A)	I	d (A)	I	d (A)	I
3.84	m	1.61	ss	1.30	ss	1.11	ss
2.71	sst	1.57	ss	1.28	s	1.09	ss
2.51	ss	1.53	s	1.26	ss	1.08	st
2.35	m	1.48	ss	1.19	ss	1.05	m
2.00	m	1.45	m	1.18	s	1.04	ss
1.85	m	1.42	st	1.16	s	1.025	ss
1.72	ss	1.39	s	1.14	ss	1.014	m
1.66	sst	1.36	s	1.12	ss		

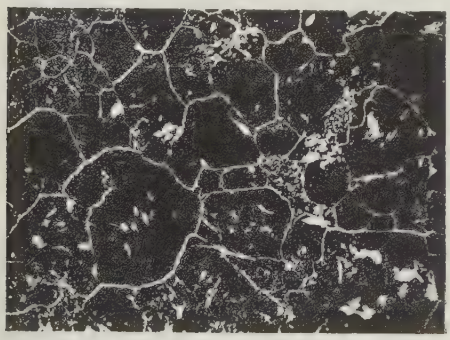

FIGURE 4. Braunite. "Unterer Lindenbergweg" near Darmstadt, Germany. Homogeneous granular aggregate (bireflection is very weakly perceptible!) with a pyrolusite intergrowth (white) formed owing to incipient disintegration. The tiny needles in the Braunite grains also are composed of pyrolusite. (Oil immersion, x 140.5).

instance, grains are rounded idiomorphic. Replacement by pyrolusite from grain boundaries inwards or from the interior outwards.

Diagnosis. The similarity with hausmannite, manganite, jacobsite, magnetite, and not to speak of minerals of other parageneses, can be dangerous, however, particularly the similarity with bixbyite. The three first-named generally have slightly visible internal reflections; the two first-named are much more anisotropic. Magnetite (in oil) is almost always distinctly brown red in color. Bixbyite is more yellowish in color.

Powder pattern. Strong lines: 2.72(sst), 2.36 (m), 2.15 (st), 1.66 (sst), 1.42 (st), 1.36 (m), 1.08 (st), 1.054 (m). (See braunite powder pattern and accompanying tables.)

MANGANITE

Chemical. MnO(OH).

Crystallography. Monoclinic but very distinctly pseudorhombohedral: a_o = 8.86, b_o = 5.24, c_o = 5.70 A, $\beta = 90^o$; cleavage perfect parallel (010). H = 4, D = 4.3.

Optical. Gray black; not wholly opaque, thinnest of splinters are red. n_x = 2.25, n_y = 2.25, n_z = 2.53 (all for Li-light).

Polish. Good, with fresh material.

Occurrence. Formed at low temperatures in thermal veins and as replacements, or sedimentary (for instance, as oölites); is frequently rapidly transformed into pyrolusite. However, considerably more frequent in occurrence than

occasionally thought to be.

Reflection behavior. Color gray to brownish, reflective power is low and strongly decreased in oil (ϕ 16 and 5 percent respectively), with little change in color. Bireflection is distinct and quite different depending on the section. Anisotropic effects are strong, colors are lively. Blood-red internal reflections are frequent, particularly in sections close to the cleavage.

Etching. The effect of all usual etch reagents is almost negative.

Structures. In single grains, a peculiar parquet-like structure is sometimes visible. Twinning is rare however. Long and short columnar crystals and aggregates of same. Actually always inclined to idiomorphic development. Virtually always transformation to pyrolusite in all states of development (fig. 5) which progresses in part from the edges and in part from the interior.

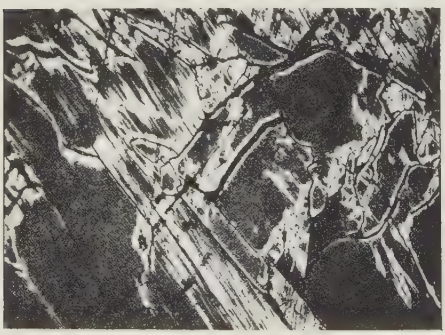

FIGURE 5. Manganite. Ilmenau, Thüringen, Germany. Coarse aggregate of diversely oriented grains; those marginally oriented change into Pyrolusite (white). The minute cavities in the background are characteristic. (Oil immersion, x 140.5).

Powder pattern. Strong lines: 3.41 (sst), 1.77 (st), 1.66 (st), 1.13 (st). (See manganite powder pattern and accompanying table.)

GROUTITE

Chemical. $HMnO_2$, possibly with some Fe.

Crystallography. Orthohombic crystals, somewhat lenticular parallel to (001). a_o = 4.56, b_o = 10.70, c_o = 2.85 A, thus about the same as ramsdellite [5]. Cleavage excellent, parallel to (010), very good parallel to (100), and also parallel to (Okl). H≈4, D = 4.14.

Optical. Similar to manganite, metallic black, finest powder is dark brown red; extremely pleochroic.

Polish. Excellent.

Occurrence. Proven at few deposits. Particularly at Cayuna Range, Minnesota. However, quite likely extensive in occurrence. Accessories: geothite, hematite, and quartz.

Reflection behavior. Bireflection is always quite marked in section parallel to (010), parallel to (001) is the lightest position, parallel to (010) is the darkest position, also quite distinct parallel (010); it is considerably increased in oil. Maximum reflective power is somewhat similar to magnetite. Anisotropic effects are strong but no vivid colors occur. Internal reflections are only frequent (with immersion!) in sections parallel to (010), otherwise they are of rare occurrence; they are dark brown red in color. On the whole they are much less striking than in manganite.

Structures. Little known. The classic occurrences of the Cayuna Range are well crystallized. An occurrence in the Schwarzwald (Germany) forms firm, fine-grained aggregates.

Diagnosis. In spite of equal c_o dimensions as in manganite, pyrolusite, cryptomelane, all of which are columnar or acicular, groutite is tabular or lenticular. Thus, when lenticular crystals are present, an important clue is given by a peculiarity in bireflection; the bright position is perpendicular, not parallel to the long axis. Otherwise it is quite similar to manganite.

Powder pattern. Material was investigated from Sagamore mine, Cayuna Range, and Hammereisenbach, Schwarzwald; the latter is somewhat different. Strong lines: 4.17 (sst), 2.79 (st), 2.66 (st), 2.36 (st), 2.29 (st), 2.20 (m), 1.69 (st), 1.60 (st), 1.51 (m), 1.150 (m), 1.131 (m), 1.065 (m), 1.001 (st). (See groutite powder pattern and accompanying table.)

POLIANITE AND PYROLUSITE

Polianite and pyrolusite are names of the same mineral which can be completely different in its mode of occurrence. Pyrolusite has priority; polianite is nevertheless frequently preferred in the literature. The author suggested to use polianite-pyrolusite as coupled designation and otherwise pyrolusite proper (for the much more frequent pseudomorphic and replacement material), and polianite proper (for the primary, independently grown, crystals). Herewith, the differences in genesis and characteristic properties are rather clearly defined although transitions are frequent. No differences exist in the crystal structure; and the powder diagrams of both forms are thus identical.

Polianite Proper

Chemical. MnO_2, tetragonal, generally badly

Braunite, Tifernine, Morocco

d (A)	I	d (A)	I	d (A)	I	d (A)	I
3.50	s	1.82	ss	1.47	ss	1.15	ss
2.72	sst	1.74	ss	1.42	st	1.08	st
2.36	m	1.66	sst	1.36	m	1.054	m
2.15	st	1.54	s	1.18	ss	1.046	ss
1.88	ss	1.50	ss	1.17	s		

Manganite, Ilfeld, Harz, Germany

d (A)	I	d (A)	I	d (A)	I	d (A)	I
3.41	sst	1.70	st	1.28	ss	1.11	m/s
2.64	m	1.66	s	1.26	ss	1.10	m/s
2.52	s	1.63	st	1.24	ss	1.08	m/s
2.41	m	1.50	m	1.21	ss	1.03	m
2.26	m	1.43	m	1.18	m	1.01	m
2.18	m	1.32	m	1.16	m	0.990	m
1.77	m	1.29	ss	1.13	st		

Groutite, Cuyuna Range, Minnesota

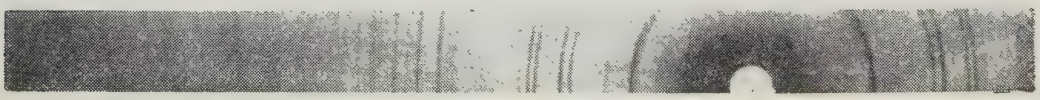

d (A)	I	d (A)	I	d (A)	I	d (A)	I
5.31	s	1.92	s	1.39	s	1.117	ss
4.17	sst	1.79	ss	1.36	s	1.105	s
3.45	s	1.75	s	1.34	s	1.083	s/ss
2.79	st	1.73	s	1.30	ss	1.075	ss
2.66	st	1.69	st	1.28	s	1.070	ss
2.52	s	1.60	st	1.26	s	1.065	m
2.36	st	1.55	s	1.253	s	1.053	s
2.29	st	1.51	m	1.217	s/ss	1.024	m/s
2.20	m	1.47	ss	1.208	s/ss	1.019	m/s
2.00	s	1.45	s	1.196	s	1.014	s/ss
1.95	ss	1.44	s	1.150	m	1.001	st
		1.43	s	1.131	m		

developed crystals and twins; often on skeletal remains of partially dissolved manganite.

Crystallography. Rutile type: a_o = 4.58, c_o = 2.95 A. Cleavage hardly discernable. H>6, D ≈ 5.0.

Optical. White to cream, resembles more a sulfide than an oxide.

Polish. Very difficult but good with the Vanderwilt machine.

Reflection behavior. Only in very good sections are polianite proper and pyrolusite proper similar or even indistinguishable. Color white, somewhat creamy. Reflection power is very high, certainly in the ideal case about 55 percent with hardly any change in oil. Bireflection is distinct, particularly with oil immersion. E is brighter. Anisotropic effects are bright. No internal reflections.

FIGURE 6. Pyrolusite. Abu Ramad, near Halaib, Red Sea. White crystals (varying brightness owing to bireflection) originated through pseudomorphism of manganite in a ground mass of fine-grained psilomelane. An unusually good preparation! (Oil immersion, x 140.5).

Etching. All standard etch reagents are negative.

Structures, diagnosis and powder pattern. Same as pyrolusite proper.

Pyrolusite Proper

Chemical. MnO_2, but frequently with adsorbed water and various metal oxides.

Crystallography. Always pseudomorphic; very frequently after manganite but not so universally as often believed. With the transformation of the manganite (and with other minerals also) a_o and c_o remain about the same, while b_o decreases markedly (from 5.24 to 4.38 A). This is exhibited in fairly large to submicroscopic cracks parallel to (010). The cracks give rise to the adsorption of H_2O, and also to the optically, often distinctly rhombohedral, character of many pseudomorphic pyrolusites. They also lead to large apparent changes in hardness and cause the bad polish when primitive polishing techniques are applied. Pseudocleavage is frequently very distinct, hardness and density are quite variable.

Optical. Metallic luster varying from white to dull gray. Often colors the fingers as does graphite.

Polish. Extremely bad when using ordinary methods and particularly with large masses which are pseudomorphic after manganite. Somewhat better for material of different genesis. Very good with careful application of mechanical polishing (fig. 6).

Occurrence. Next to cryptomelane and psilomelane, pyrolusite is the most frequent ore mineral among manganese minerals in the zone of oxidation. However, it is wholly unknown why and where these members occur alone or, as is more usual, in certain combinations or why they are replaced in rare cases by ramsdellite. It also occurs as a product of oölitic marine sedimentation and as a residual product of weathering.

Reflection behavior. Quite variable with the quality of the polished section; under ideal conditions exactly as polianite. The reflectivity is not particularly decreased with oil immersion; in bad sections it even appears to be higher. The bireflection is always distinct and the distinction between the a and b axes of the replaced manganite ore can be easily made. Sections parallel to (001) are darkest. Anisotropic effects are strong, and very strong in oil. No internal reflections are visible; however, they may be simulated by the refraction of light on cracks parallel to (010) (fig. 7).

Etching. In comparison with polianite proper,

FIGURE 7. Pyrolusite. Kremelsberg, near Triberg, in Schwarzwald (Black Forest), Germany. White, with characteristic shrinkage fissures parallel to (010) of the altered manganite, gray. Only rarely is the manganite-pyrolusite relationship so easily perceptible. (x 84.3).

etch reactions are frequently more distinct because of the fine grain size. HCl, KCN, and $FeCl_3$ may yield good positive reactions.

Structures. As pyrolusite replaces many manganese minerals, the structures may be quite different in appearance (fig. 6 through 8, inclusive). Particularly distinctive are pseudomorphic developments after manganite. Fine-grained rhythmic curved layers may occur in botryoidal masses of psilomelane and geothite. A pseudomorphic zonal structure may be distinct. The cracks, caused by the formation from manganite, may be open or filled with limonite which then increases the strength of the aggregate and the apparent hardness. Only few examples can be described here from the multitude of manners of occurrence.

Diagnosis. In a typical case, the reflective power is much higher than with all other manganese ores. In its bright position, chalcophanite can be similar but its bireflection [Tr.: high] excludes any mistake. Submicroscopic intergrowths will of course make a diagnosis impossible, except by using the powder pattern.

Powder pattern. Is the same for all varieties, different as they might appear outwardly. Strong lines: 3.13 (sst), 2.41 (st), 2.12 (m), 1.97 (m), 1.62 (sst), 1.56 (st), 1.31 (st), 1.05 (m). (See pyrolusite and polianite powder patterns and accompanying table for pyrolusite.)

RAMSDELLITE

Chemical. MnO_2.

Crystallography. Orthorhombic: $a_o = 4.533$, $b_o = 9.27$, $c_o = 2.866$ A, Z = 4. The structure is analogous to that of diaspore. Cleavage is after three pinacoidal directions and one prismatic direction. H = 3, D = 4.7. The color is iron black but with reddish percussion marks and a reddish streak. (The black streak, reported in the literature, is incorrect.)

Occurrence. Little is known about the occurrence but it certainly must be quite widespread and often mistaken for pyrolusite. Part of the "weakly reflecting variety of pyrolusite," noted in many deposits, is probably ramsdellite.

Pyrolusite, Niedertiefenbach, Nassau, Germany

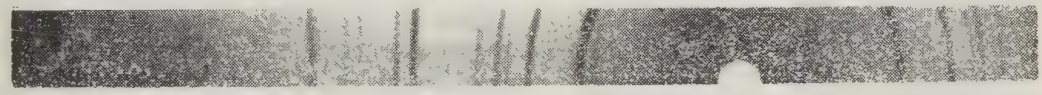

d (A)	I	d (A)	I	d (A)	I	d (A)	I
3.43	s	1.97	m	1.31	st	1.10	ss
3.13	sst	1.62	sst	1.25	ss	1.05	m
2.41	st	1.56	st	1.20	ss	1.04	s
2.20	s	1.44	s	1.16	ss	1.00	s
2.12	m	1.39	s	1.12	ss		

Polianite, Platten, Germany

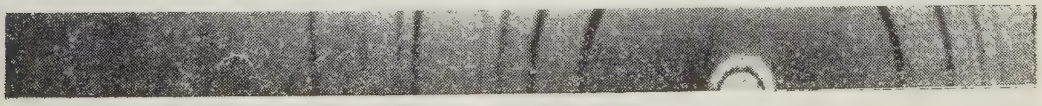

Ramsdellite, Lake Valley, New Mexico
(pattern contains pyrolusite lines (X))

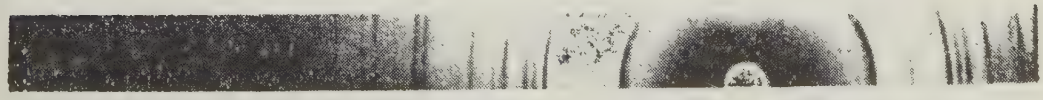

d (A)	I	d (A)	I	d (A)	I	d (A)	I
4.03	sst	2.05	s	1.35	sst	1.08	ss
3.20	ss	1.89	m	1.32[X]	s	1.07	sst
3.09[X]	s	1.82	s	1.30	ss	1.05[X]	ss
2.61	ss	1.70	ss	1.27	m	1.04	ss
2.53	st	1.65	st	1.25	m	1.03	s
2.41[Xz. T.]	m	1.61[Xz. T.]	st	1.17	ss	1.01	ss
2.32	m	1.54	s	1.16	s	1.00	ss
2.24	ss	1.46	st	1.12	m	0.995	m
2.13	m	1.43	m	1.10	ss	0.984	ss

Reflection behavior. Relatively weak reflectivity which somewhat resembles that of pyrolusite. Pleochroism of reflection is distinct and strong in oil. The brightest position is yellowish white; the other positions are grayer. It appears that [001] > [010] > [100] but this is not certain as the excellence of the three pinacoidal cleavages hinders the distinction. Dark purplish-red internal reflections are abundant with oil immersion, particularly at such locations in the section where needles have been torn out in polishing.

Structure. Not much material available for comparison! Coarse platy aggregates which at the edges have a somewhat skeletal appearance. Marginally, and in irregular cracks it is replaced by pyrolusite (this replacement is in part oriented, in part unoriented with respect to the ramsdellite crystal).

FIGURE 8. Ramsdellite, Lake Valley, New Mexico, U.S.A. Gray white, with inclined, pitted fibrous cleavage impregnated with a fissure filling of pyrolusite, white; the latter is, in part, oriented intergrowth with Ramsdellite. (Oil immersion, x 140.5).

Diagnosis. At first impression, the resemblance with pyrolusite is quite strong in polished section (fig. 8). There, where a direct comparison is possible - and this is often the case - the brightest position of pyrolusite is much brighter than that of ramsdellite. Very distinctive are locations where needles have been torn out of the section due to cleavage after (110) and (010).

Powder pattern. Material was examined from Lake Valley, New Mexico [1], and Gozoren, Eregli, Anatolia [15]. Strong lines: not present in pyrolusite are: 4.03 (sst), 2.53 (st), 1.65 (st), 1.46 (st), 1.35 (sst), 1.07 (sst). (See ramsdellite powder pattern and accompanying table.)

PSILOMELANE GROUP

In mineral collections and in technology, the term "psilomelane" is used for hard, high-grade manganese ores that have a grapelike, concretionary appearance and which seem to have been precipitated as gels. The properties and the chemical composition are quite variable. In particular, they are included often in the element group K, Ba, Cu, Co, Ca, Ag, W, and others. Formerly these latter elements in part were erroneously considered to be "adsorbed in gels."

The microscopic examination and in part only the powder pattern showed that many of these "psilomelanelike" mixtures were mixtures of various combinations, for instance of pyrolusite, limonite, and quartz, but that many samples were at least somewhat uniform in composition. These latter may be separated into a group of four minerals which are very similar in properties: psilomelane "proper," cryptomelane, hollandite, and coronadite [3, 11, 16]; although the former is a particular case, the latter are closely related structurally and chemically although they do not appear to form extensive series of solid solutions with the very low temperatures at which they are generally formed. What happens with products that are formed at higher temperatures, such as part of the hollandite, is not very well known. In the ore microscope, the distinction generally cannot be made; in spite of pulverization in solid carbon dioxide, powder patterns are of bad quality because of background blackening. However, the distinction can be made on slightly coarser grained material. The distinctive d-spacings of the patterns are given here, although they are similar; however, it must be pointed out that mistakes in identification can occur because of the bad quality of the obtained powder patterns.

Relative strong lines which in part are not absent from other members but then occur with much weaker intensities are:

Psilomelane	—	—	—	2.38	2.16	1.42	—
Cryptomelane	6.84	4.85	3.09	2.38	2.14	—	—
Hollandite	—	—	3.07	2.38	(2.13)	1.53	1.07
Coronadite	—	—	3.11	2.39	(2.15)	1.54	—

Psilomelane Proper

Chemical. $BaMn^{2+}Mn_6^{4+}O_{16}(OH)_4$.

Crystallography. Orthorhombic: a_o = 9.1, b_o = 13.7, c_o = 2.86 A [20].

Optical. Black, often conchoidally breaking masses. H = 5 to 6, D = 4.7; both frequently appear to be lower.

Occurrence. Not yet clearly distinguishable from that of cryptomelane or coronadite.

Reflection behavior. As cryptomelane. The expected anisotropism has not yet been detected because of the fine grain size.

Structures. As cryptomelane, often very neatly

rhythmical. Even the finest of single crystals have yet to be seen (fig. 9).

FIGURE 9. "Psilomelane." Euel Mine, Nassau, Germany. Gray white in varying shades, alternating with needle ore, dark gray; pronounced fracturing. It was not certain whether Psilomelane, strictly, or Cryptomelane was present. (x 4.3).

Diagnosis. The distinction of psilomelane with respect to the slightly wider occurring cryptomelane is only possible by powder pattern.

Powder pattern. Strong lines: 2.38 (m), 2.16 (m), 1.42 (m). (See psilomelane powder pattern and accompanying table.)

Cryptomelane - (Romanechite)

Chemical. Approximately $K_2 (Mn^{2+}, Fe, Cu) Mn_7^{4+}O_{16}$ whereby water, which belongs in the structure, has been omitted for simplification.

Crystallography. Pseudotetragonal: a_o = 9.82, c_o = 2.86 A. The crystal structure gives rise to the very strong tendency for a very fine acicular development parallel to the c-axis. Always rhythmical, grapelike botryoidal aggregates consisting of the finest of needles which are frequently perpendicular to the concretionary development. D = 4.3, frequently in practice hardly determinable. Hardness is high (5-6), but variable. Black to brownish color often showing a fine conchoidal fracture with a dull pitchlike luster.

Polish. Good; polishing hardness is frequently quite variable in different layers of the concretionary aggregate.

Occurrence. Apparently always formed close to the surface. It is formed by weathering and by solution and redeposition of various minerals, which in part might be very poor in manganese. Almost always accompanied by pyrolusite and very frequently associated with a chalcophanite-like mineral.

Psilomelane , Schneeberg, Saxony, Germany

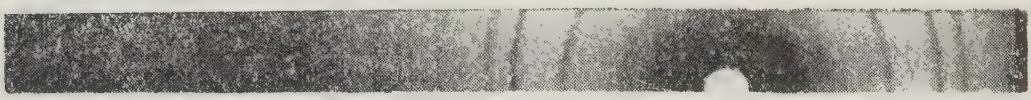

d (A)	I	d (A)	I
2.38	m	1.55	s
2.16	m	1.42	m
1.81	s	1.39	s/ss
1.71	ss		

Cryptomelane, Hollerter Zug, Siegen, Germany

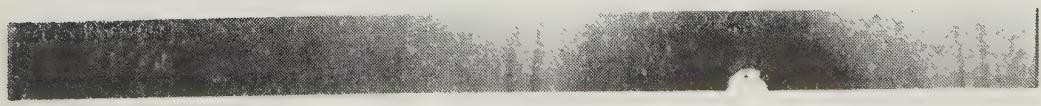

d (A)	I	d (A)	I	d (A)	I	d (A)	I
6.84	m	3.09	st	1.82	m	1.35	s
5.83	ss	2.38	sst	1.63	s	1.29	s
4.85	m	2.14	st	1.53	m	1.24	ss
4.02	ss	1.99	ss	1.42	m	1.15	ss
3.47	ss	1.91	ss	1.39	ss	1.08	ss

Reflection behavior. Quite variable due to grain size and particularly porosity and also because of the finest of intergrowths with pyrolusite. The most compact masses have a reflectivity of up to 25 percent. Only the "most coarse-grained" masses, which are still extremely fine in grain size, show a strong pleochroism. (Parallel to E = c-axis: much brighter; parallel to O: darker, about "dull gray"), and anisotropic effects are then visible.

Etching. Quite uncharacteristic.

Structures. Distinction of cryptomelane from hollandite and psilomelane can only be made by means of X-rays; however, hollandite is generally much coarser grained. Coronadite is on the average brighter and it has a distinctly higher density; otherwise it is quite similar. Pyrolusite is much brighter even though the brightest position of cryptomelane is about equal to the darkest position of pyrolusite.

Powder pattern. The best results of many trials with material from Hollerter Zug, Siegen, were obtained from a specimen that was pulverized in solid carbon dioxide. Strong lines: 6.84 (m), 4.85 (m), 3.09 (st), 2.38 (sst), 2.14 (st), 1.82 (m), 1.53 (m), 1.42 (m). (See cryptomelane powder pattern and accompanying table.)

Hollandite

Chemical. Approximately $Ba(Mn^{2+}, Fe^{2+})Mn_7^{4+}O_{16}$ (thus, about the same as psilomelane originally was).

Crystallography. Pseudotetragonal: a_o = 9.82, c_o = 2.86 A [3]. Generally much coarser grained than cryptomelane, similar to boulangerite aggregates; single crystals up to 30 centimeters in length. Here also a distinct cleavage parallel to (110). D = 4.95 (more easily determined than with its so variably porous cousin). Color, gray black; luster, semimetallic, similar to manganite.

Polish. It is frequently difficult to achieve a good section due to the breaking out of needles parallel to the c-axis.

Occurrence. In contrast to related minerals it is often a product of formation at high temperature and it occurs as a product of regional as well as contact metamorphism. Many other modes of occurrence are possible as the distinction from psilomelane proper has been made only rarely.

Reflection behavior. Almost exactly like well-polished cryptomelane; possibly a bit brighter.

Texture. Twinning along a steep pyramidal face; frequently finely lamellar. Occasionally the finest of polysynthetic twinning after a different law.

Diagnosis. The otherwise dangerous similarity with pyrolusite is of no concern with a good polish. The radial development is typical in contrast to other minerals. Manganite often has internal reflections.

Powder pattern. Specimens from Sitapar and Ultevis. Strong lines: 4.81 (m/s), 3.07 (sst), 2.38 (st), 2.18 (m), 2.13 (m), 1.83 (m), 1.81 (m), 1.64 (m), 1.61 (m), 1.53 (st/m), 1.36 (m), 1.34 (m), 1.08 (m), 1.07 (st). (See hollandite powder pattern and accompanying table.)

CORONADITE

Chemical. Approximately $PbMn^{2+}Mn_7^{4+}O_{16}$.

Crystallography. As cryptomelane, a_o = 9.82, c_o = 2.86 A. In aggregates practically the same as cryptomelane.

Occurrence. Coronadite is the product of the simultaneous weathering of manganese- and lead-bearing minerals. This requirement is often met with. It will always be associated with other manganese oxides. However, in the best known deposit at Bou Tazoult near Imini, Morocco, the source of the lead is somewhat nebulous (fig. 10).

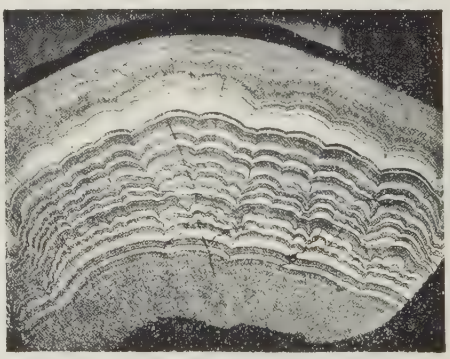

FIGURE 10. Coronadite. Bou Tazoult Mine, Atlas, Morocco. In almost regularly alternating structures; at the same time, the latter are characteristic of the entire "Psilomelane Group." (x 1.7).

Reflection behavior. Similar to cryptomelane, but on the average distinctly brighter. The reflection can be quite different in the rhythmic layers. As with cryptomelane, single crystals (on the average possibly somewhat larger than those of cryptomelane), are strongly anisotropic. A typical texture is shown in figure 10.

Diagnosis. Coronadite often occurs with cryptomelane and it is very similar to it, so that it certainly will be frequently overlooked (for instance, for several decades at Broken Hill). Although the reflectivity and density are on the

Hollandite, Sitapar, India

d (A)	I	d (A)	I	d (A)	I	d (A)	I
6.80	ss	2.13	m	1.43	s	1.11	ss
5.71	ss	1.93	s	1.40	ss	1.10	s
4.81	m/s	1.89	ss	1.36	m	1.08	m
3.44	s	1.83	m	1.34	m	1.07	st
3.07	sst	1.81	m	1.30	s	1.00	s
2.46	s	1.64	m	1.27	ss	0.994	ss
2.38	st	1.61	m	1.19	ss	0.990	ss
2.18	m	1.53	st/m	1.15	s		

average considerably higher, a powder pattern or a qualitative test for lead will often be necessary for distinction.

Powder pattern. Quite similar to that of psilomelane, cryptomelane, and hollandite. The first worthwhile strong reflection is for d = 3.49 [10]. Important is d = 1.63 [7] which has, however, a considerably lower intensity. Specimens were examined from Bou Tazoult and Broken Hill. Strong lines: 3.47 (m), 3.11 (sst), 2.39 (m), 2.19 (m/st), 2.15 (m), 1.83 (m), 1.54 (m/st). (See coronadite powder pattern and accompanying table.)

LITHIOPHORITE

Chemical. The natural occurrences yield analyses showing a considerable variation which certainly is not wholly due to impurities alone. The lithium content can be quite small but it is, nevertheless, considerable and the formula is approximately: $Li_2(Mn, Co, Ni)_2Al_8Mn_{10}^{4+}O_{35} \cdot 14H_2O$, which might also be written as $(Li, Mn, Al)Mn_2O_3 \cdot H_2O$. The product $(Li, Al, Mn)_4Mn_6O_{18} \cdot 4H_2O$ has been synthesized and it is similar to the mineral although it has a considerably larger unit cell.

Crystallography. Hexagonal: a_o = 2.92; c_o = 9.39 A (probably variable). Aggregates of plates, in part crystals with micaceous cleavage; however, generally fine-grained. D≈3.4. Color is black; luster, metallic when coarse grained.

Polish. Frequently good, somewhat leafy in coarse-grained aggregates; the polish is very bad in porous fine-grained aggregates.

Occurrence. Little known, but rather widespread. At least it occurs frequently as a weathering product of triphylite.

Reflection behavior. Strongly dependent on the polish, somewhat like chalcophanite. The bireflection is quite strong but nevertheless less than that of chalcophanite: O = white; E = dark gray (in oil!). Anisotropism is very strong but only in degrees of black and white. The brighter position has a steely-blue hue.

Structures. Quite variable as mentioned above. Also, sheaflike aggregates.

Diagnosis. Not well enough known.

Powder pattern. Although similar in polished section to chalcophanite, lithiophorite has a quite different powder pattern. Samples from White Oak, Tennessee, were examined. Strong lines: 9.45 (m), 4.71 (sst), 2.37 (st), 1.88 (st), 1.57 (m), 1.45 (m), 1.39 (m), 1.23 (m). (See lithiophorite powder pattern and accompanying table.)

CHALCOPHANITE

Chemical. $(Zn, Mn^{2+}, Fe^{2+})Mn_2O_5 \cdot 2H_2O$.

Crystallography. Hexagonal plates: c:a = 3.527. Apparently a very pronounced layered structure with excellent cleavage. Black, shiny and semimetallic; not quite opaque, with a red streak. Indices are not well known: $n_O > 2.72$, $n_E \approx 1.95$.

Polish. Moderate.

Occurrence. In only rare cases, alone, and then relatively coarse-grained with zinc oxide minerals. Much more widespread as an auxiliary component of many "psilomelanes" (together with cryptomelane, psilomelane proper, and pyrolusite), where it frequently occurs, it is very fine-grained. In the latter cases, it is often devoid of zinc; possibly this "variety" is also a more or less independent mineral.

Reflection behavior. Gray white in various shades (uncrossed nicols) (fig. 11). Reflection is much larger for O than for E (30 and 9 percent, respectively). Thus, very strong bireflection and enormous anisotropic effects but without particularly bright colors (important characteristic!). Internal reflections are deep red and are widespread in occurrence with zinc-rich members.

Structures. Little known. Aggregates of coarse tablets, in part as radial leaves or as the finest of scales between layers of "psilomelane."

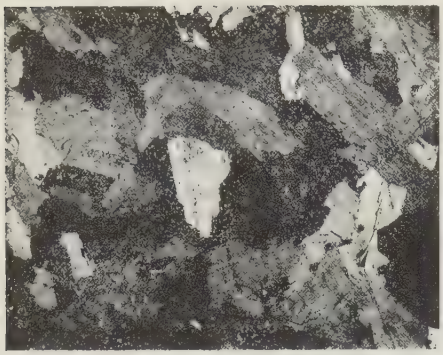

FIGURE 11. Chalcophanite "Km 24 Mine," near Swakopmund, South Africa. Monomineralic aggregate, whose grain boundaries are prominent yet, owing to the bireflection, questionable. Cleavage after (0001) frequently is evident. (Note: only one nicol used. x 84.3).

Diagnosis. Diagnosis and spotting is easy with regard to all other manganese minerals because of the very large bireflection (with the exception of lithiophorite on occasions). Molybdenite and graphite, however, are similar but have quite different parageneses.

Powder pattern. Characteristic lines are: 7.54 (st), 6.75 (sst), 4.03 (st), 3.44 (st), 2.21 (st), 1.58 (sst). The rather strong lines for d = 7.54 is absent from the pattern described by Neumann and Sellevoll [14]. The powder patterns of material from Sterling Hill and the Km 24 deposit were examined; both patterns are almost identical. (See chalcophanite powder pattern and accompanying table.)

TODOROKITE AND WOODRUFFITE

Todorokite and Woodruffite are two recently described minerals which occur as oxidation products. They are only slightly known as yet. Structurally they are certainly closely related. The main difference is the presence or absence of zinc. It is possible, even probable, that these minerals and probably other, as yet unknown, analogies, shall be found more frequently among "wadlike" manganese ores. Crystal structure and habit are not yet certain. Todorokite is described as monoclinic; both are probably, as cryptomelane, pseudotetragonal.

Todorokite

Chemical. $(Mn^{2+}, Ca, Ba)_2Mn_6{}^{3+}Mn_{11}{}^{4+}O_{33} \cdot 8H_2O$. This of course represents a rather arbitrary formula.

Crystallography. Monoclinic(?), finest of needles parallel to the c-axis; perfect cleavage after (100) and (010).

Optical. Color and luster like graphite; color is brown in the finest of splinters; $n > 1.74$. Blackens the human finger. D = 3.67 [23].

Occurrence. Only proven as a product of weathering of the manganiferous zeolite inesite from a gold-quartz vein; it probably is more widespread in occurrence.

Reflection behavior. The tiny available sample was insufficient for the preparation of a section.

Structure. Finest of needles, distinct twinning.

Diagnosis. Not well enough known; the powder pattern, although quite blackened, is somewhat characteristic. Compare with woodruffite.

Powder pattern. Compare with woodruffite. (See todorokite powder pattern and accompanying table.)

Woodruffite

Chemical. $(Zn, Mn^{2+})_2Mn_5{}^{4+}O_{12} \cdot 4H_2O$. The valence of the manganese and thus the formula, are unproven.

Crystallography. As yet unknown. Very fine-grained and loose aggregates similar to "wad" or compact in botryoidal aggregates.

Optical. Coarse powder, black; finest powder, chocolate brown [9].

Occurrence. As yet only as a product of weathering of franklinite together with hemimorphite and chalcophanite at Sterling Hill, New Jersey.

Reflection behavior. Moderate reflection (ϕ = 25 percent in air). Bireflection is distinct with oil immersion; the anisotropism is quite different.

Structures. Little known. Of very fine and uniform grain size. Short acicular (or thick tabular?) tiny grains at random orientation.

Diagnosis. Woodruffite will really only be correctly identified by accident as little is known about it.

Powder pattern. (Sterling Hill material). Strong similarity with todorokite, less with cryptomelane, quite different from chalcophanite. The order of intensities are somewhat characteristic in contrast with todorokite: d = 9.46 (ss), 4.68 (sst) and for todorokite: 9.46 (sst), 4.75 (m), 3.31 (m). For cryptomelane, d = 9.46 is absent and 4.85 is of average (m) intensity. The strongest line of cryptomelane, d = 3.10 (sst), is absent in both todorokite and woodruffite. (See woodruffite powder pattern and accompanying table.)

Coronadite, Bou Tazoult, Morocco

d (A)	I	d (A)	I
3.47	m	1.54	m/st
3.11	sst	1.39	s
2.39	m	1.37	s
2.19	m/st	1.35	s
2.15	m	1.29	ss
1.93	ss	1.23	ss
1.83	m	1.22	ss
1.73	ss	1.15	ss
1.68	ss	1.07	ss
1.63	s	1.05	ss

Psilomelane* Schneeberg, Saxony Germany		Cryptomelane Hollerter Zug, Siegen Germany		Hollandite Sitapar, India		Coronadite Bou Tazoult, Morocco	
d (A)	I	d (A)	I	d (A)	I	d (A)	I
		6.84	m	6.80	ss		
		5.83	ss	5.71	ss		
		4.85	m	4.81	m/s		
		4.02	ss				
		3.47	ss	3.44	s	3.47	m
		3.09	st	3.07	sst	3.11	sst
				2.46	s		
2.38	m	2.38	sst	2.38	st	2.39	m
				2.18	m	2.19	m/st
2.16	m	2.14	st	2.13	m	2.15	m
		1.99	ss				
				1.93	s	1.93	ss
		1.91	ss	1.89	ss		
		1.82	m	1.83	m	1.83	m
1.81	s			1.81	m		
1.71	ss					1.73	ss
						1.68	ss
		1.63	s	1.64	m	1.63	s
				1.61	m		
1.55	s	1.53	m	1.53	st/m	1.54	m/st
1.42	m	1.42	m	1.43	s		
1.39	s/ss	1.39	ss	1.40	ss	1.39	s
		1.35	s	1.36	m	1.37	s
				1.34	m	1.35	s
		1.29	s	1.30	s	1.29	ss
				1.27	ss		
		1.24	ss			1.23	ss
						1.22	ss
				1.19	ss		
		1.15	ss	1.15	s	1.15	ss
				1.11	ss		
				1.10	s		
		1.08	ss	1.08	m		
				1.07	st	1.07	ss
						1.05	ss
				1.00	s		
				0.994	ss		
				0.990	ss		

* More extensive data are to be found in [6] and [11].

Lithiophorite, White Oak, Tennessee

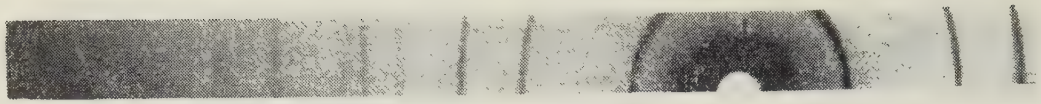

d (A)	I	d (A)	I	d (A)	I	d (A)	I
9.45	m	2.37	st	1.88	st	1.23	m
4.71	sst	2.28	ss	1.57	m	1.18	s
3.14	s	2.13	ss	1.45	m	1.15	s
2.49	s	2.05	ss	1.39	m	1.07	ss

Chalcophanite, Sterling Hill, New Jersey
(possibly with hetairolite lines (X))
(powder pattern of specimen from Ogaensburg,) [Ed.: Probably Ogdensburg, New Jersey.]

d (A)	I	d (A)	I	d (A)	I	d (A)	I
7.54	st	2.44X	m	1.49	m	1.14	ss
6.75	sst	2.38	ss	1.42	st	1.12X	ss
6.15	s	2.21	st	1.39	s	1.11X	s
4.21	ss	2.11	s	1.35	ss	1.10	ss
4.03	st	1.96	ss	1.31	ss	1.07X	ss
3.60	ss	1.88	m	1.30	ss	1.06	s/m
3.44	st	1.83	ss	1.27	st	1.05X	ss
3.29	ss	1.78	m	1.23	ss	1.04X	ss
2.99X	ss	1.70	ss	1.21	ss	1.03	ss
2.75	s	1.65	s	1.20	ss	1.01	ss
2.67	ss	1.58	sst	1.18	ss	1.00	ss
2.53X	m	1.55X	ss	1.17X	ss	0.991	ss
		1.51X	ss	1.15X	ss		

Todorokite, Todoroki Mine, Hokkaido, Japan

d (A)	I	d (A)	I	d (A)	I	d (A)	I
9.46	st	2.44	s	1.97	s	1.53	s
4.75	m	2.37	ss	1.81	s	1.42	s/m
4.33	ss	2.21	ss	1.74	ss	1.37	s
3.31	m	2.11	ss	1.66	ss		

Woodruffite, Sterling Hill, New Jersey

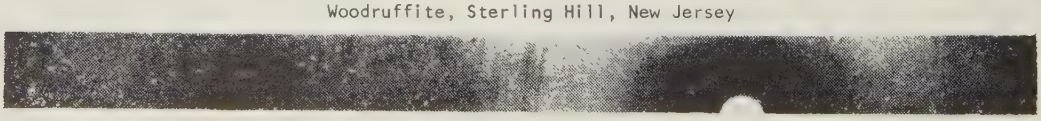

d (A)	I	d (A)	I	d (A)	I	d (A)	I
9.46	ss	2.30	ss	1.72	ss	1.38	ss
4.68	sst	2.20	m	1.66	ss	1.28	s
4.32	ss	2.10	m	1.62	m	1.22	ss
2.96	s	1.97	m	1.52	ss	1.13	ss
2.52	st/m	1.89	ss	1.48	st	1.10	m
2.44	ss	1.78	ss	1.41	st	1.06	ss
2.38	s						

ACCESSORY MINERALS

For comparison, the patterns of the very frequently occurring accessory minerals hematite, geothite, and lepidocrocite are presented.

Hematite, Sieger, Germany

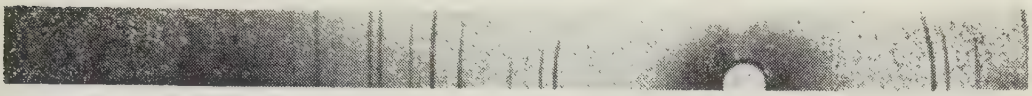

d (A)	I	d (A)	I	d (A)	I	d (A)	I
2.65	s	1.63	ss	1.25	m	1.100	st
2.95	ss	1.59	m	1.22	ss	1.074	ss
2.68	sst/st	1.48	st	1.21	ss	1.054	sst
2.49	st	1.44	st	1.184	m	1.037	m
2.18	m	1.34	ss	1.160	m	0.988	st
1.83	st	1.30	st	1.137	st	0.986	s
1.68	sst						

"Goethite," Winthrop Mine, Ishpeming, Michigan

d (A)	I	d (A)	I	d (A)	I	d (A)	I
5.06	s	2.00	ss	1.39	s	1.096	ss
4.61	s	1.91	s	1.36	s	1.077	ss
4.19	sst	1.80	m	1.32	m	1.067	s
3.38	s	1.72	st	1.29	ss	1.054	s
2.97	ss	1.69	m	1.26	ss	1.044	ss
2.69	sst	1.66	ss	1.24	ss	1.030	s
2.58	m	1.60	s	1.198	s	1.023	m
2.45	sst	1.56	st	1.151	s	1.012	m
2.25	m	1.51	m	1.142	s	1.006	ss
2.18	st	1.45	m	1.126	m	0.997	m
2.09	ss	1.42	s	1.116	ss		

Ruby Mica (Lepidocrocite), Bieber, Hessen, Germany

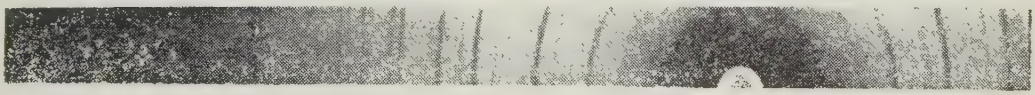

d (A)	I	d (A)	I	d (A)	I	d (A)	I
6.20	st	2.08	m	1.41	ss	1.07	s
4.16	s	1.93	st	1.39	s	1.06	ss
3.63	ss	1.84	s	1.37	m	1.05	ss
3.28	st	1.73	st	1.26	ss	1.04	s
2.70	s	1.56	m	1.23	ss	1.03	ss
2.46	st	1.52	m	1.22	s	1.01	ss
2.35	s	1.48	ss	1.20	s	0.994	s
2.18	ss	1.45	ss	1.19	m	0.991	s
		1.43	m	1.10	s		

REFERENCES

1. Byström, A. M., THE CRYSTAL STRUCTURE OF RAMSDELLITE, AN ORTHORHOMBIC MODIFICATION OF MnO_2: Acta Chem. Scandinavica, 1949, no. 3, p. 163-173.

2. Byström, A., and B. Mason, THE CRYSTAL STRUCTURE OF BRAUNITE - $3Mn_2O_3 \cdot MnSiO_3$: Arkiv Kemi, Mineral. Geol., v. 16B, no. 15, 1943.

3. Byström, A., and A. M. Byström, THE CRYSTAL STRUCTURE OF HOLLANDITE, THE RELATED MANGANESE OXIDE MINERALS, AND α-MnO_2: Acta Crystallog., v. 3, p. 145-154, 1950.

4. Cole, W. F., A. D. Wadsley, and A. Walkley, AN X-RAY DIFFRACTION STUDY OF MANGANESE DIOXIDE: Electrochemical Society, Trans., 1947, no. 92, p. 133-158.

5. Collin, R. L., and W. N. Lipscomb, THE CRYSTAL STRUCTURE OF GROUTITE $HMnO_2$: Acta Crystallog., v. 2, p. 104-106, 1949.

6. Fleischer, M., and W. E. Richmond, THE MANGANESE OXIDE MINERALS: Econ. Geology, v. 38, p. 269-286, 1943.

7. Fleischer, M., MINERALOGY OF THE MANGANESE OXIDES: Applications to problems of dry cell batteries, Maschinenschrift, Symposium sponsored by the U. S. Natl. Bur. of Standards, Washington, D. C., v. 4, no. 7, 1944.

8. Friedrich, O., DIE MIKROSKOPISCHE UNTERSUCHUNG DER ERZE DES EISENS UND DER WICHTIGSTEN STAHLMETALLE [MICROSCOPIC INVESTIGATION OF IRON AND IMPORTANT STEEL-METAL ORES]: Handb. Mikroskopie Technik, v. 2, no. 2, 1954.

9. Frondel, C., and Wm. Henrich, NEW DATA ON HETAIROLITE, HYDROHETAIROLITE, CORONADITE AND HOLLANDITE: Amer. Mineralogist, v. 27, p. 48-52, 1942.

10. Frondel, C., NEW MANGANESE OXIDES: HYDROHAUSMANNITE AND WOODRUFFITE: Amer. Mineralogist, v. 38, p. 761-769, 1953.

11. Gruner, J. W., THE CHEMICAL RELATIONSHIP OF CRYPTOMELANE (PSILOMELANE), HOLLANDITE, AND CORONADITE: Amer. Mineralogist, v. 28, p. 497-506, 1943.

12. _____, GROUTITE, $HMnO_2$, A NEW MINERAL OF THE DIASPORE-GEOTHITE GROUP: Amer. Mineralogist, v. 32, p. 654-659, 1947.

13. Harcourt, G. A., TABLES FOR THE IDENTIFICATION OF ORE-MINERAL BY X-RAY POWDER PATTERNS: Amer. Mineralogist, v. 27, p. 63-113, 1942.

14. Neumann, H., and M. A. Sellevoll, X-RAY POWDER PATTERNS FOR MINERAL IDENTIFICATION (II. OXIDES AND HYDROXIDES): Norske Vid. Akad., Avh. (Math.-N. Kl.), 1955, no. 3.

15. Ramdohr, P., DIE ERZMINERALIEN UND IHRE VERWACHSUNGEN [ORE MINERALS AND THEIR CONCENTRATIONS]: 2nd, ed., Berlin, Akademieverlag, 1955.

16. Ramsdell, L. S., THE UNIT CELL OF CRYPTOMELANE: Amer. Mineralogist, v. 27, p. 611-613, 1942.

17. Schneiderhöhn, H., MINERALBESTAND UND GEFÜGE DER MANGANERZE VON POSTMASBURG, GRIQUALAND-WEST, SÜDAFRIKA [MINERAL CONSTITUENTS AND STRUCTURE OF MANGANESE ORES FROM POSTMASBURG, WEST BECHUANALAND, SOUTH AFRICA]: Neues Jahrb. Mineralogie B. B., v. 64A, p. 701-726, 1931.

18. Schröder, A., DER ELEMENTARKÖRPER UND DIE DICHTE DES RAMSDELLITS, MnO_2: [THE ELEMENTARY COMPOSITION AND DENSITY OF RAMSDELLITE]: Fortschritte Mineralogie, v. 31, no. 11, 1952.

19. Wadsley, A. D., SYNTHESIS OF SOME HYDRATED MANGANESE MINERALS: Amer. Mineralogist, v. 35, p. 485-499, 1950.

20. _____, THE CRYSTAL STRUCTURE OF PSILOMELANE (Ba, H_2O) Mn_5O_{10}: Acta Crystallog., v. 6, p. 433-438, 1953.

21. _____, HYDROHAUSMANNITE AND HYDROHETAIROLITE: Amer. Mineralogist, v. 40, p. 349-353, 1955.

22. Winchell, H., ELEMENTS OF OPTICAL MINERALOGY, PART II. DESCRIPTION OF MINERALS: 4th ed., New York, Wiley and Sons, 1951.

23. Yoshimura, T., "TODOROKITE" A NEW MANGANESE MINERAL FROM THE TODOROKI MINE, HOKKAIDO, JAPAN: Hokkaido Univ., I. Fac. Sci., Ser. 4, v. 2, p. 289, 1934; Amer. Mineralogist, v. 20, p. 678, 1935.

CONTRIBUTION TO THE STUDY OF SEDIMENTARY MANGANESE DEPOSITS[1]

by

H. Marchandise

• *translated by W. O. J. Groeneveld Meijer* •

ABSTRACT

The iron content of rocks is 50 times that of manganese; yet sea water, as is the case for sedimentary manganese oxide deposits, contains iron and manganese in the ratio of 2:1 respectively. Apparently, manganese enrichment occurs in marine environment; under oxidizing conditions, iron precipitates at a relatively low potential (Eh), manganese remaining in solution. It is noted that sedimentary iron deposits contain comparatively little manganese. Manganese precipitation is accompanied by comparatively little iron; this is in agreement with the observed iron content of manganese oxide deposits. Domains of iron and manganese precipitation as carbonates (weakly oxidizing, weakly reducing environments) and sulfides (reducing environments) indicate: the carbonates are similar and can precipitate simultaneously; the sulfide of manganese is not known to occur, and, in agreement with observation, the manganese carbonate precipitates again with the sulfide of iron. --D. D. Fisher.

The large sedimentary concentration of manganese precipitated at the bottom of the seas, give rise to several genetic and geochemical problems.

Derived from continental drainage dissolved manganese ions are transported by large and small rivers to the ocean. It is known that rocks contain on the average, 50 times more iron than manganese; how is it, then, that manganese deposits almost wholly devoid of iron can be formed? The existence of this problem has been generally acknowledged but it does not appear that a rigorous scientific solution has been offered for it.

Average characteristics of marine environments (after Krumbein and Garrels).

1. Open marine environment, with free circulation:
   Tenors: Fe: 0.002 to 0.02 ppm
   Mn: 0.001 to 0.01 ppm
   O_2: at surface: 4.9-9.00 ml/l
   CO_2: at surface: 46 ml/l
   pH at surface - 7.5-8.4, at depth - 7.8
   Eh at surface - 0.2-0.4v, at depth - 0.1-0.3v

2. Semi-closed marine environment - (Euxinic) Metallic ions as in open marine environments:
   Gas: O_2: at surface 6 ml/l, at depth 0
   CO_2: at surface 46 ml/l, at depth 46 ml/l and higher
   H_2S: at surface 0, at depth 9.14 ml/l
   pH at surface - 0.8, at depth 7.0
   Eh at surface - 0.1v, at depth -0.3v

3. Closed marine environment, with high evaporation:
   Gas: O_2: 1-2 ml/l
   CO_2: 5-10 ml/l
   H_2S: 0
   pH: 8 - 9
   Eh: 0.0 - + 0.1v

Study of Conditions Conducive to Manganese Precipitation in Marine Environment

Precipitation of manganese is regulated by the ionic concentration of Mn^{2+}, pH, and Eh. It may be influenced also, by other ions in the sea water, but we shall disregard these for the moment. The form in which manganese precipitates is dependent solely on pH and Eh; theoretically, manganese may precipitate as oxide, carbonate, or sulfide. In the following we shall try to outline the domains in which these three compounds are formed. In calculation we shall use the same values as activities of CO_3^{2-} and $SO_4^{2-} + S^{2-}$, as those chosen by Krumbein and Garrels for sea water. (The given figures are activities but to simplify the notations we shall represent them as elementary molar concentrations).

pH	(CO_3^{2-})*	$(SO_4^{2-} + S^{2-})$
6	3×10^{-8}	7×10^{-2}
7	2.4×10^{-7}	2.2×10^{-2}
8	4.4×10^{-6}	3×10^{-2}
9	1.4×10^{-5}	7×10^{-2}

*[Tr.: Ions in parentheses signify concentrations of the particular species]

Pyrolusite-Rhodochrosite System

The precipitation of MnO_2 is solely regulated by the Eh. The electrochemical reaction is as follows:

$$MnO_2 + 4H^+ + 2e = Mn^{2+} + 2H_2O \quad (1)$$

[1]Translated from Contribution a l'etude des gisements de manganèse sédimentaires: Symposium sobre yacimientos de manganeso, v.1, p. 107-118, XX Congreso Geológico Internacional, Mexico, 1956.

Relation (1) represents an oxidation-reduction system whose potential is given by:

$$Eh = 1.3 + 0.03 \log \frac{(Mn^{2+})}{(H^+)^4} \qquad (2)$$

Precipitation of the carbonate $MnCO_3$ is regulated by the solubility products:

$$s = (Mn^{2+})\ (CO_3^{2-}) = 8.8 \times 10^{-11} \qquad (3)$$

To determine the boundary between precipitation areas of MnO_2 and $MnCO_3$, it is sufficient to study properties of the system to ascertain equilibrium conditions between the two components MnO_2 and $MnCO_3$. This system is taken at different pH values corresponding Eh values are calculated; in effect, every pH corresponds to a well-defined concentration of CO_3^{2-}. Let us study this system with pH equal to 8. We know that the CO_3^{2-} concentration is 4.4×10^{-6}. Precipitation of $MnCO_3$ starts at the point where $(Mn^{2+})\ (CO_3^{2-}) = s$; that is, when $(Mn^{2+}) = 2 \times 10^{-5}$. Because there is equilibrium, system (1) necessarily is in equilibrium; particularly in the special case where $(Mn^{2+}) = 2 \times 10^{-5}$. Thus one may calculate its Eh:

$$Eh = 1.3 + 0.03 \log \frac{(10^{-8})\ 4^4}{2 \times 10^{-5}}$$

[Ed. : The last term should probably read:

$$0.03 \log \frac{2 \times 10^{-5}}{(10^{-8})^4}\ ]$$

Eh = 0.481 v.

Conclusion: In water, pH = 8, where the activity of (CO_3^{2-}) is 4.4×10^{-6} moles per liter (1), manganese precipitates as MnO_2 if the potential Eh, is larger than 0.481 v, and as $MnCO_3$, if the Eh is less than 0.481 v.

performing the same calculations for other pH values, it is found:

pH	6	7	8	9
Eh (v)	0.656	0.567	0.481	0.376

Curve (a) (fig. 1) is derived from the preceding calculation.

Rhodochrosite-Alabandite System

Seawater contains SO_4^{2-} and S^{2-} ions; both form an oxidation-reduction system, represented by:

$$S^{2-} + 4H_2O = SO_4^{2-} + 8H^+ + 8e \qquad (4)$$

whose potential is given by:

$$Eh = 0.14 + 0.075 \log \frac{(SO_4^{2-})\ (H^+)^8}{(S^{2-})} \qquad (5)$$

On the other hand, the solubility product of MnS is:

$$s = (Mn^{2+})\ (S^{2-}) = 1.4 \times 10^{-15} \qquad (6)$$

It is estimated easily, under equilibrium conditions in the pyrolusite-rhodochrosite system, that no sulfide of manganese can form. This evident a priori, given the potential of this system to be very high, and that the sulfide can form only in reducing media. At pH = 8 we have seen that Eh = 0.48 v; introducing these values in equation (5) one finds:

$$\frac{\log\ (SO_4^{2-})}{(S^{2-})} = 109$$

Accordingly, it is calculated easily that $(S^{2-}) = 3 \times 10^{-111}$. As a result, $(Mn^{2+})\ (S^{2-}) = 6 \times 10^{-116}$; considerably less than the solubility

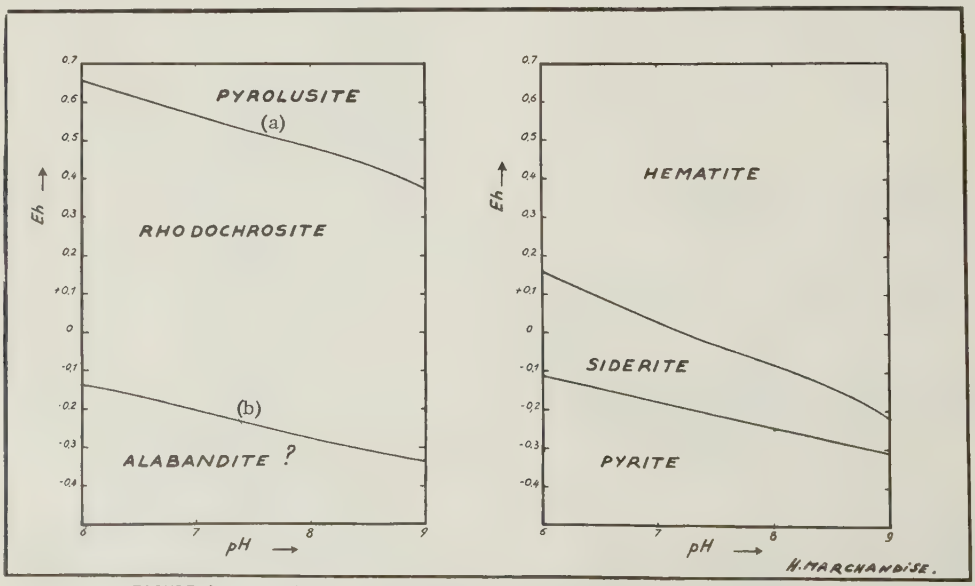

FIGURE 1. Equilibrium diagrams of minerals in marine environment
1) Manganese (calculated) [1]
2) Iron (after Krumbein and Garrels) [2]

product of MnS.

To study equilibrium conditions of the carbonate-sulfide system, the same reasoning is used as for the system previously examined;

$MnCO_3$: $s = (Mn^{2+})(CO_3^{2-}) = 8.8 \times 10^{-11}$

MnS : $s = (Mn^{2+})(S^{2-}) = 1.4 \times 10^{-15}$

At equilibrium state for a sulfide-carbonate solution one has:

$$\frac{(CO_3^{2-})}{(S^{2-})} = 6.3 \times 10^{4}$$

As (CO_3^{2-}) is known; one may calculate easily $(S^{2-}) = 7 \times 10^{-11}$. Also, one knows that at pH = 8: $(SO_4^{2-}) + (S^{2-}) = 3 \times 10^{-2}$, and the ratio $(SO_4^{2-})/(S^{2-})$ can be found easily. Thus, all necessary data are available to calculate Eh by formula (5):

$Eh = 0.14 + 0.0075 \log (4.3 \times 10^{8} \times 10^{-64})$

$Eh = -0.275$ v.

At pH = 6, Eh = -0.136 v; and at pH = 9, Eh = -0.336 v. This relationship is described by curve (b) in Figure 1.

The two curves calculated (fig. 1) describe the domains in which the different manganese compounds form. Thus, sulfide formation is possible; alabanite, however, is not known to occur in sedimentary deposits. Conversely, hauerite (MnS_2) is known to occur, although very rarely, in certain sedimentary formations. Thermodynamic data for MnS_2, a rather unstable sulfide, are insufficient to study the problem of its formation.

Relative Behavior of Manganese and Iron

Oxidizing Environments

In the preceding discussion, we have found sea water to contain on the average, at least twice as much iron as manganese. One should expect the iron content to be 50 times greater than that of manganese; if not, it is because iron content is limited by its solubilities. The problem, to which we have alluded previously, is concomitant to formation of sedimentary manganese deposits; it concerns separation between iron and manganese.

It should be noted that all important sedimentary manganese deposits are composed of manganese oxides, and that the Mn:Fe ratio is of the order of 10 to 20; such considerable enrichment is not due to chance.

Precipitation of hydroxides: In a reducing medium Fe^{2+} precipitates as $Fe(OH)_2$ at a pH of 5.5 (from a 10^{-2} molar (M) solution precipitation begins at this point). The solubility product of $Fe(OH)_2$ is 10^{-19}; this ferrous hydroxide precipitate is very unstable and it rapidly oxidizes to ferric hydroxide. Mn^{2+}, out of contact with oxidizing media, precipitates as $Mn(OH)_2$ at a high pH;(precipitation commences at pH = 8.5 from a 10^{-2} molar solution). The manganese hydroxide precipitate is very unstable and oxidizes rapidly to MnO_2. Ferric iron precipitates as $Fe(OH)_3$ at a relatively low pH (precipitation commences at pH = 2.4 from a 10^{-2} molar solution). The solubility product of ferric hydroxide is $10^{-37.1}$. In oxidizing media MnO_2 precipitates directly; evidently, $Mn(OH)_4$ does not exist.

Electrochemical Study of Oxidation: Let us consider an aqueous solution containing iron and manganese in the presence of atmospheric oxygen; the solution becomes then, an oxidizing environment whose properties are determined by the equilibrium relation:

$$O_2 + 4H^{+} + 4e = 2H_2O$$

The potential of this system depends on the pH and is given by:

$$Eh = 1.23 - 0.06\ pH$$

Manganese and iron in solution oxidize according to the reactions:

$Fe^{3+} + e \rightleftharpoons Fe^{2+}$, $Eh = 0.75 + 0.06 \log \frac{(Fe^{3+})}{(Fe^{2+})}$,

$MnO + 4H^{+} + 2e \rightleftharpoons Mn^{2+} + 2H_2O$

$Eh = 1.3 + 0.03 \log \frac{(Mn^{2+})}{(H^{+})^{4}}$

From a first examination of the normal oxidation-reduction potentials, it follows immediately, under normal conditions, that the oxygen system, very oxidizing for iron, is hardly effective for manganese. In order to make a rigorous study of these phenomena, one must study the respective potentials of the three systems and their variations as a function of their pH values and activities.

Oxygen System

$$O_2 + 4H^{+} + 4e \rightleftharpoons 2H_2O$$

When the partial pressure of oxygen (P_{O_2}) differs from that of the atmosphere, the potential of the system is given by:

$$Eh = 1.23 + \frac{0.06}{4} \log P_{O_2} - 0.06\ pH$$

Under atmospheric conditions, the second term of the formula equals:

$$\frac{0.06}{4} \log P_{O_2} = \frac{0.06}{4} \log 2 \times 10^{-1} =$$

$$-0.7 \left(\frac{0.06}{4}\right) = -0.0105 \text{ v}$$

Accordingly, for atmospheric conditions we use:

$$Eh = 1.22 - 0.06\ pH$$

The variation of Eh as a function of pH is thus calculated simply, giving curve 1 (fig. 2). It is important to remark that values of potential

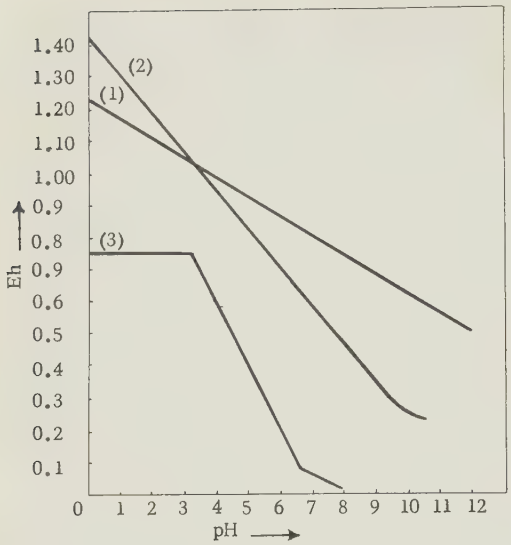

FIGURE 2. Oxygen, manganese and iron systems:
1) $O_2 + 4H^+ + 4e \rightleftharpoons 2\ H_2O$
2) $MnO_2 + 4H^+ + 2e \rightleftharpoons Mn^{2+} + 2H_2O$; ($10^{-4}$ molar solution)
3) $Fe^{3+} + e \rightleftharpoons Fe^{2+}$; ($10^{-4}$ molar solution)

are easily calculated; also in reality, reaction rates are so weak that equilibrium is not established.

MnO_2 - Mn^{2+} System: The potential Eh, is easily calculated by formula (2). If we assume the activity of Mn^{2+} to be 10^{-4}, we find then:

$$Eh = 1.42 + 0.03 \log (H^+)^4$$

Thus, Eh varies as a linear function of pH. At pH = 9, Eh = 0.34 v; beyond this point manganese precipitates as $Mn(OH)_2$; in other words the concentration of the solution having reached a limit:

pH = 10, the maximum content of Mn^{2+} is 10^{-5};
pH = 12, the maximum content of Mn^{2+} is 10^{-9}.

Fe^{3+} - Fe^{2+} System. The iron system is more delicate because solubility of the hydroxide is very weak. Similarly, starting with a 10^{-4} molar iron solution, allowing for separation, the ratio Fe^{3+}:Fe^{2+} is equal to one. At pH = 2, there is no precipitation, thus Eh = 0.75 v; similarly, for pH = 3. At pH = 4, the maximum concentration of Fe^{3+} is $10^{-7.1}$; concentration of Fe^{2+} stays at 5×10^{-5}. Thus:

$$Eh = 0.75 + 0.06 \log \frac{5 \times 10^{-5}}{10^{-7.1}} = 0.582 \text{ v},$$

and so forth, resulting in curve 3 (fig. 2).

Separation of Iron and Manganese. From the preceding discussion, conditions characterizing marine environment are apparent. For example, in water containing iron and manganese, both with an activity of 10^{-4}, let us say that the pH is raised to 8, and the potential to 0.39 v. The Fe^{3+}:Fe^{2+} ratio is calculated easily under these conditions:

$$0.39 = 0.75 + 0.06 \log \frac{(Fe^{3+})}{(Fe^{2+})}$$

from this relation $(Fe^{3+}) = 10^{-6}(Fe^{2+})$

then, pH = 8, $(Fe^{3+}) = 10^{-19.1}$ maximum,

it follows that $(Fe^{2+}) = 10^{-13.1}$;

finally, a solution is obtained containing not more than $10^{-13.1}$ moles per liter.

Manganese concentration remains 10^{-4}; the potential of the environment is too low for MnO_2 formation. Similarly, from a relatively concentrated solution in an oxidizing environment, only pure iron hydroxide precipitate can form; manganese remains in solution. This demonstrates well the process of manganese enrichment in water. Sedimentary iron ore deposits can contain only very little manganese. By contrast, when manganese precipitates as oxide, iron must also precipitate; yet in comparison to manganese, it remains as a relatively minor constitutent.

Inert Environments
(weakly oxidizing and reducing)

The solubilities of the iron and manganese carbonates are very similar; in addition, their carbonates have overlapping stability fields. Under these conditions, there is no reason at all for the two metals to separate. To the contrary, there are good reasons why they should be intimately associated; carbonates of iron and manganese have, in effect, the faculty to crystallize simultaneously.

Reducing Environments

As we have mentioned previously, the sulfide domain calculated from present data, is very hypothetical, and, possibly inexact. Observation shows, in effect, that no sulfide forms. It is logical to assume that manganese carbonate forms again in the lower domain, and as a consequence, the association must consist of rhodochrosite and pyrite. Moreover, this assumption corresponds to observation.

REFERENCES

1. Kirk, R. E., and D. F. Othmer, ENCYCLOPEDIA OF CHEMICAL TECHNOLOGY, v. 8, 2nd printing, New York, Interscience Encyclopedia Corp., 1952-1957.
2. Krumbein, W. C., and R. M. Garrels, ORIGIN AND CLASSIFICATION OF CHEMICAL SEDIMENTS IN TERMS OF pH AND OXIDATION-REDUCTION POTENTIALS: Journal of Geology, v. 60, pp. 1-33, 1952.

3. Charlot, G., MODERN METHOD OF QUANTITATIVE ANALYTICAL CHEMISTRY, 2nd ed., Paris, Masson & Co., 1946 (in French). [Ed.: Verification of this title is as follows: NEW THEORY AND METHOD OF QUANTITATIVE ANALYSIS].

4. Krauskopf, K. B., SEPARATION OF MANGANESE FROM IRON IN SEDIMENTARY PROCESSES: Geochim. et Cosmochim., Acta, v 12, pp. 61-84, 1957.

[Ed.: The reference preceding was included by the translator].

Review Section

Sokolov, V. A., MIGRATION OF GAS AND OIL, Akademiya Nauk SSSR, Moscow, 1956. A Synopsis by Paul A. Witherspoon and W. D. Romey.[1]

ABSTRACT

This work reviews petroleum and natural gas composition and environment. Migration of petroleum hydrocarbons is considered from the standpoints of Darcy-type flow and diffusion. Chemical and biochemical processes which occur during migration are discussed; in addition, petroleum-genesis theories are reviewed. Of importance from the standpoint of petroleum prospecting, is the conclusion that oil and gas pools can be detected at the surface; this is indicated by Soviet experience in the detection of natural-gas microseeps, plus the occurrence in soils of microflora associated only with oxidation of hydrocarbon gases. Microbiological and microgas surveys, used singly or in combination, are reported to provide, therefore, an effective method of petroleum prospecting. Academician Topchiyev, who writes the preface to the book, mentions that some of Sokolov's ideas on petroleum and natural-gas formation are open to discussion. He praises the work, nevertheless, as a step forward in the solution of theoretical and practical problems inherent in petroleum geochemistry and prospecting for oil and gas.

Chapter I: GENERAL CONSIDERATION ON THE COMPOSITION AND OCCURRENCE OF NATURAL GAS AND PETROLEUM

Composition of natural gases from the atmosphere, earth's surface, and of sedimentary and igneous rocks, is discussed. Classification of these gases by their major and minor components is presented in table form. Petroleum composition is analyzed for 14 Soviet crude oils in terms of their paraffin, napthene, and aromatic content. Oxygen, sulfur, and nitrogen compounds of petroleum are examined as are trace elements found in petroleum ash. Bitumen content is given for peat, lignite, sapropel, oil shale, and coal and various sediments.

Physical conditions influencing the gas and oil occurrence in the earth's crust include critical data for various gases; description of structural and stratigraphic traps; and determinations of geothermal gradients from seven Soviet oil fields, ranging from $1^{\circ}C$ per 10 meters (m) up to $1^{\circ}C$ per 86 m.

Chapter II: TYPES OF NATURAL-GAS MIGRATION

Examination of free gas flow, involves application of Darcy's law to gas movement in porous media; gas flow may occur also through fissures, fractures, and faults. Review is given of movement and entrapment of free gas in water-filled, porous media. In considering the problem of gas solubility and sorption, it is observed that gas migrates also as a dissolved phase in oil; solubility curves and tabulated data are included; as are adsorption data for methane, propane, butane, and nitrogen on various rocks.

Discussion of gas diffusion is amplified by a table of diffusion constants for various hydrocarbons and other gases given for both air and water. Diffusion rates of methane and other gases through various water-filled rocks were measured as a function of rock temperature and moisture content. Based on experimental data (Antonov, 1953 and 1954), the following table shows calculated diffusion rates for methane in various water-filled rocks, under a pressure gradient of 1 atmosphere (atm) per 10 m:

Diffusion medium	Depth (m)	Diffusion rate (m^3) per surface area (m^2) per 10^6 years
Water	-	230
Clay	-	19-41
Limestones	various	8-20
Marls	14-20	4.5-15.5
Argillites (Serafimovka)	1,793	3.6
Argillites (Serafimovka)	1,790	20.6
Siltstone (Serafimovka)	1,781	23.7
Sandstone (Serafimovka)	6-15	9-19.8
Sandstone (Serafimovka)	1,757-1,777	3-8.38
Marble	-	2.4

The general nature of gases migration in sedimentary rocks is examined by Sokolov

[1]Minerals Research Laboratory, University of California, Berkeley, California.

from the theoretical viewpoint: gas migration is assumed to occur in homogeneous, stratified, and nonhomogeneous strata; it is noted also that gas composition can change during flow. The magnitude of gas-concentration anomalies at the earth's surface is affected by oil of these factors. Intermittent gas migration involves the effect of stratigraphic variations on vertical migration.

Chapter III: FLOW AND OTHER TYPES OF MIGRATION OF PETROLEUM IN ROCKS

Darcy's law is applied to petroleum flow in porous media. Viscosity-temperature relationships are given for seven Soviet crudes; data from American literature show variation of oil viscosity with gas content and specific gravity. Petroleum flow in the presence of gas and water involved discussion of relative permeabilities (two- and three-phase flow), based on American literature. Oil buoyancy, from the aspect of gravity segregation of oil in water-filled rocks is reviewed along lines of Illing's work (1933-1939).

Oil migration as a result of rock compaction and deformation reviews the work of Athy, Hedberg, Van Tuyl, McCoy, Ross-Keyte, Waldschmidt, and others. In the Soviet Union, Lomatadze has done experimental work, certain of his results are presented here, on water and oil movement owing to compaction of Cambrian shales. Influence of capillarity and sorption on the petroleum migration is reviewed in presentation of surface tension and capillarity concepts: surface-tension measurements were taken on Tuymazin Devonian oil, at pressures up to 300 atm; curves are given in text; Sokolov mentions his experimental migration studies (1948); in addition, observations are made on oil and water distribution in hydrophilic and hydrophobic situations. The study of petroleum diffusion reveals the diffusion rate of liquid hydrocarbons through water-filled sediments to range from 1,000 to 10,000 times less than that of natural gas.

Chapter IV: MOVEMENT OF SUBSURFACE WATERS AND THE SUBSTANCES THEY CONTAIN

Subsurface water composition is described graphically using the mineral content of brines in the upper and central Volga regions, the Caspian depression, and the Kulundin steppes. Formation waters of given age have, in some areas, characteristically different mineral content: For example, formation waters from Silurian limestones in the Leningrad region are high in HCO_3^-, Ca^{2+}, and Mg^{2+} and low in SO_4^{2-} and Cl^-. Certain Cambrian, Devonian, and Permian formation waters are recognizable also by their content; concentration range of various ions is given for oil-field waters.

As bases for the study of subsurface water flow, laminar- and turbulent-flow regimes are discussed in general terms. In underground rocks of the Russian platform, the calculated velocity of water movement is 10^{-4} centimeters (cm) per day, if the average permeability is 10 millidarcies; measured hydraulic gradients range from 0.057 to 0.09 atm per kilometer (km).

Permeability in sedimentary rocks is distributed in, approximately, the following manner (based on 1,000 determinations);

Sedimentary rocks (%)	Permeability in darcies
80	0 to 10^{-6}
13	10^{-6} to 10^{-3}
5	10^{-3} to 1
2	more than 1

Flow of subsurface water can have a marked effect on vertical migration of gases tending to disperse them; also discussed is the transport of oil by moving water. Investigations on diffusion of salts contained in subsurface waters reveal diffusion of NaCl in moist shale to be two or three times greater than that of methane. Concentration of subsurface brines depends on velocity of water movement through the aquifer.

Chapter V: THE EFFECT OF BIOCHEMICAL PROCESSES ON THE MIGRATION OF PETROLEUM

Bacteria distribution is considered with respect to sedimentary rocks and subsurface waters: three types of bacteria found in oils of the Baku, Grozny, and Neftegorsk deposits, according to Ginzburg-Karagicheva, are: sulfate reducing, denitrifying, and cellulose digesting. In non-oil-bearing and dry rocks, these bacteria are either non-existent or found only in very small numbers. Presence of active and varied microflora in reservoir fluids generally is considered unequivocal proof that an oil reservoir exists; this discovery has led to development of microbiological prospecting methods. Presence of bacteria in petroleum is related to their presence in water: oil field waters were found to have bacteria concentrations ranging from 25,000 to 600,000 organisms per milliliter (ml); oils containing only a trace of water content, have much less bacteria than those of 1 percent or greater. In oil-bearing rocks of the second Baku, bacteria concentration ranges from 10 million to 117 million per gram (g) of rock. Seldom encountered in shales, bacteria were found to be absent at great depth.

The effect of biochemical processes on the hydrocarbons of migration at depth involves discussion of the following subjects: biogenic oxidation of diffusing hydrocarbons; influence of biogenic oxidation on flow of hydrocarbon gases; and effects of free oxygen formation by radioactive disintegration of oxide compounds

and water. Factors lowering the intensity of biogenic oxidation of hydrocarbons at great depth are discussed in the text.

An aspect in the discussion of biogenic oxidation of hydrocarbons in surface layers of rock is the decrease of bacteria concentration with depth and variation with soil type. Bacteriological studies revealed that ethane-oxidizing bacteria can oxidize ethane and higher paraffin hydrocarbons only; similarly, propane-oxidizing bacteria can oxidize propane and higher hydrocarbons, and so on. Presence of these particular microflora, consequently, is valuable as a hydrocarbon indicator.

Chapter VI: INFLUENCE OF CHEMICAL REACTIONS ON THE MIGRATING COMPONENTS FROM OIL POOLS

Inquiry into disintegration of hydrocarbons and other natural organic substances presents general discussion on thermal disintegration of various hydrocarbons. It is found that disintegration of organic substances contained in surface layers of rock also may produce hydrocarbons and other substances.

Hydrocarbon interaction with rocks is indicated in various ways: chemical reduction causes rock colors above gas deposits to lighten; red and brown coloration changes to green and blue. Near Kuibyshev, the light-colored zone indicates the location of a dispersion halo of areal extent from three to three and one half times that of the gas deposit. Naphthenic acids in petroleum and petroleum waters can combine with alkali metals (the Na, K group) during migration; but not with the insoluble alkali-earth metals (the Ca, Mg group).

Oxidation of migrating hydrocarbons in surface layers is reviewed: Methane is the most stable hydrocarbon; its reactivity with oxygen increases directly as the hydrocarbon series progresses from ethane to propane, and higher hydrocarbons. Oxidation of petroleum tends to produce asphaltic compounds, similarly, oxidation of naphthenic hydrocarbons produces naphthenic acids and resins.

Influence of radioactive elements in sedimentary formations is indicated, for example, in alpha-particle bombardment of organic substances; a number of gases are produced, including methane, ethane, propane, and butane. Ionization also can cause various chemical changes in hydrocarbon gases. Influence of radioactivity on migrating gases involves discussion of the isotopic composition of hydrocarbons; $C^{12}:C^{13}$ ratios for various carbon-containing rocks are given, as are ratios for petroleum and asphalt.

Reaction with migrating salts (brines) is discussed in the text.

Chapter VII: APPEARANCE OF PETROLEUM AT THE EARTH'S SURFACE

Appearance of oil seeps at the surface is controlled by structures, faults, and lithology, among other factors. Gas seeps under water are easily observed, but dry seeps are more difficult to locate. One procedure for detecting dry gas seeps, in the Apsheron area, is described as follows: A cone having a diameter of 50 cm, was placed on the ground, base downward, and left in position for 30 minutes; air trapped under the cone during that period, was found to contain from 2 to 5 percent hydrocarbon gas. The calculated flow rate of the seep was from 10 to 12 liters per square meter per day. Halos of relatively higher hydrocarbon content are found around all types of seeps.

General considerations and influencing factors on gas microseeps are outlined as follows: Gas exchange between soil and atmosphere may occur as the result of several factors: changes in atmospheric pressure, temperature changes, wind action, free diffusion of gas, and atmospheric precipitation.

An unusual occurrence of soil gas is described in the Saratovsk-Stalingrad area. Heavy hydrocarbon gases (ethane and propane, for example) were found to be highly concentrated; from 60 to 70 percent of total soil gas at depths from 2 to 4 meters below the surface. Below this depth, their content fell off rapidly. Natural gas in the underlying reservoir is essentially methane containing only 2 to 3 percent of the heavier gases. Measurement of gas-microseep intensity indicates overall hydrocarbon-gas concentration as a result of diffusion, in soil atmosphere ranges from 10^{-3} to 10^{-7} percent at a depth of 3 meters.

Gas background is defined as follows: Biochemical and chemical processes may form minute quantities of various gases in soil and subsoil layers, producing a certain constant gas background. Microseeps may be found if their intensity surpasses that of the background. To determine the magnitude of this background, many samples have been taken from areas of the Soviet Union where gas and oil deposits are known not to occur. Measurements in six different areas have shown that methane background varies from 0.0003 to 0.0006 percent and heavy hydrocarbon gases vary from 0.0001 to 0.0003 percent; the latter consists of ethane through butane fractions; but may include cycloparaffins, ethers, and other substances as well. In addition, the average N_2O content in subsoil atmosphere is of the order of 0.001 to 0.0001 percent.

Accumulation of hydrocarbons on silica gel was attempted in order to measure ethane, propane, and butane occurrence in the field. Large volumes of soil gas are drawn through

a tube containing silica gel, to provide sufficient concentration of heavy hydrocarbon gases. Chromatographic methods are used then to separate ethane from propane while heavier components remain on the gel. The author presents a 2-page table summarizing percentage of gases (H_2, CH_4, heavy hydrocarbon fraction, CO_2 plus H_2S, and N_2) produced by bacterial action on a variety of organic compounds. In non-oil-bearing regions, concentration of methane and heavier hydrocarbons lowers rapidly with increasing sample depth, from the surface to 3 m. At the 3 m depth, background in approximate figures is: For methane, 10^{-4} percent; for ethane, 10^{-6} percent; and 10^{-8} percent for propane.

On considering gas and other geochemical anomalies dependent on gas migration; it is found that geologic conditions are very important in determining the character and path of gas migration. Variation in properties and composition of the deposit, as well as geological conditions, cause geochemical anomalies, in turn, to differ.

Use of gas anomalies as indicators, led directly to discovery of petroleum in the Buzovin and Mashtagin areas. Geologic and geochemical evidence indicated an oil deposit in the Buzovin area, was subsequently confirmed by drilling. In the Mashtagin area, geologic evidence was unfavorable; but drilling done on the basis of a positive geochemical anomaly, found oil and gas. Striking surface-gas anomalies (both methane and heavy hydrocarbon) occur above faulted oil fields in the Emba, Turkmen, and Fergana valleys and as well, in several other areas. Surface-gas anomalies also have been discovered above faulted coal fields. Graphical illustrations are included.

Use and value of bacterial anomalies as oil and gas indicators are described. A combination of gas-bacteria and surface-gas surveys showed the same anomaly to exist in two areas of the northern Caucasus. Subsequent drilling confirmed presence of gas in the lower Maikop formation. An oil deposit was found also in the middle Volga region by combining the two methods described; graphic illustrations are included in the text. Bacterial surveys were unsuccessful in dry areas of Azerbaidzhan and Fergana valley; whereas gas survey continued to give good results. Climate, ground water movement, and a large number of other factors complicate gas and bacterial anomalies.

Occurrence of bituminous and Eh anomalies, is discussed, briefly: Bituminous anomalies, as determined by Florovskaya's luminescence method, are "invariably" found above gas and petroleum deposits (along with gas and Eh anomalies). Radiometric anomalies appeared in surface measurements of radioactivity over oil fields, made along the Volga and elsewhere; the well known "halo effect" has been observed.

TABLE 1. Geochemical indicators of petroleum

Geochemical indicator	Characteristic of geochemical indicator in relation to deposit	Natural occurrences and processes producing background interference at 3 m depth
I. Gas Indicators		
Heavy hydrocarbons (C_2-C_4)	Directly related to main oil and gas deposit	-
CH_4	Directly related to main oil and gas deposit	CH_4 present in coal and swamp gases, also present in small quantities in soils and subsoils
H_2S	Product of reducing action by gas and oil on sulfur compounds. Deposition product of sulfurous compounds in petroleum	Can form independently, not requiring presence of petroleum, by other reducing processes
CO_2	Oxidation product of petroleum and of hydrocarbon gases; or, decomposition product of oxygen containing substances in petroleum	Forms independently of oil and gas when coal and various organic substances are oxidized; or also, upon destruction of carbonates and bicarbonates
H_2	Possible decomposition product of petroleum hydrocarbons	Forms also with decomposition of H_2O and various organic substances

TABLE 1. Geochemical indicators of petroleum (Continued)

Geochemical indicator	Characteristic of geochemical indicator in relation to deposit	Natural occurrences and processes producing background interference at 3 m depth
I. Gas Indicators (Concluded)		
N_2O	There is a possible connection with migrating hydrocarbons by biochemical processes; as in the case of other indicators of surface origin, it may influence orientation in relation to structural geologic conditions	Forms in soil and subsoil as a result of chemical and biochemical processes
II. Bacterial Indicators		
Bacteria which oxidize heavy hydrocarbons (C_2-C_4)	Hydrocarbons, C_2-C_4, are related to main part of oil deposit	-
Methane oxidizing bacteria	Methane is related to principal oil and gas deposit	CH_4 is present in coal and swamp gases and forms in small quantities in soils and subsoils. Occurrence of methane forming bacteria allows one to judge the intensity of CH_4 formation in soils and subsoils.
Hydrogen oxidizing bacteria	H_2 is a possible decomposition product of petroleum hydrocarbons	H_2 forms during decomposition of H_2O and various decomposition substances
III. Bituminous Indicators		
Bituminous luminescence indicators, bitumens, determined by extraction with various solvents	Indicates presence of petroleum and products of its oxidation and weathering; presence of bituminous oxidation products and of hydrocarbon gas polymerization. Light oily bitumens invariably associated with oil; higher molecular weight bitumens can have some other origin	Some bituminous substances are found in coal. Transformation of organic substances in soils leads to formation of substances which are bituminous in character. In sedimentary rocks, there is always dispersed organic matter containing bitumens
Thermal indicators (products of thermal decomposition and oxidation of substances containing bitumens)	Indirect indicator of presence and composition of organic substances	Organic substances in soil, subsoil, and any rocks; also, coal formation products may give indicators similar to those of petroleum
IV. Inorganic Substances		
HCO_3^-	Result of influence of CO_2	Enumerated substances can be present independently, not requiring presence of petroleum and natural gas
HS^- $S_2O_3^{2-}$ SO_3^{2-} S	Possible products of petroleum reducing action and decomposition of its sulfur compounds	

TABLE 1. Geochemical indicators of petroleum (Concluded)

Geochemical indicator	Characteristic of geochemical indicator in relation to deposit	Natural occurrences and processes producing background interference at 3 m depth
IV. Inorganic Substances (Concluded)		
Cl^- Br^- $CaCl_2$ MgC_2	Indicators of deep, highly mineralized waters, often accompanying oil	Enumerated substances can be present independently, not requiring presence of petroleum and natural gas
$CaCO_3$ $MgCO_3$ $CaSO_4$	Forms by reaction of salts from deep-migrating waters with groundwater and with other waters containing SO_4^{2-}, CO_3^{2-}, and CO_2	
I	Iodine is included in composition of certain compounds contained in petroleum	
Absence of SO_4^{2-}	Possible consequence of sulfate reduction by oil and gas	Absence or small concentration of SO_4^{2-} can occur also in absence of oil; also SO_4^{2-} is known to be present in some oil bearing structures
V. Naphthenic Acids		
Naphthenic acids and their salts; phenols	Products of hydrocarbon oxidation; these are the main constituents of petroleum	-
VI. Eh Potential		
Eh potential; Reduction of rocks	Caused by reducing conditions inherent in the influence of petroleum hydrocarbons	Physicochemical conditions in surface layers (migrating H_2, CO_2, and H_2S) may influence the magnitude of Eh

Chapter VIII: ACCUMULATION AND DISPERSION OF NATURAL GAS AND PETROLEUM

Discussion on conditions of petroleum and natural-gas formation involves review of, along with other pertinent material, certain organic and inorganic theories on petroleum origin. Sokolov tends to support organic theories; inorganic origin, nevertheless, remains a possibility not yet adequately disproven. Optical activity of petroleum, so often stated to be one of the proofs of organic origin, can no longer be considered absolute. Optically active hydrocarbon compounds have been formed from optically inactive hydrocarbons by Terentyev and Klabunovsky (1951); also, optically active substances and porphyrins might have been picked up by petroleum during the course of its migration.

Of many points in support of the organic theory the following are cited: the great variety of organic components; high proportion of cyclical hydrocarbons; and significant amount of N-S-O compounds which correspond to substances of organic origin.

Petroleum source materials were considered by Mikhailovsky, as early at 1906, to consist of algae, marine animals, and the organic remains of land plants. The first step in petroleum formation is decomposition of these materials by bacterial action. The second, is burial of sediment containing the decomposition products; concurrently, the buried organic material undergoes "bituminization," a process caused by action of mineralized waters plus temperature and pressure increase with depth. Once formed, dispersed petroleum, migrates into geologic traps. Mikhailovsky's ideas have served as a basis for most current hypotheses on petroleum genesis; mention of later work includes that of several Soviet scientists, and of Trask (1932).

Studies on organic content of Recent sediments suggest relatively rapid formation of petroleum-type hydrocarbons; formation would occur in sediments early during accumulation and diagenesis stages. Smith's work (1954) is cited along with that of the following Soviet investigators: Gorskaya (1950), Weber (1955), Strakhov and Rodionov (1954), Teodorovich (1947 and 1952), Gulyayeva (1954), Dobryansky (1948), Porfiryev and Grinberg (1949), and Vassoyevich (1955).

The general mechanism of petroleum and natural gas formation in sedimentary rocks is examined through review of biochemical and geochemical theories of petroleum hydrocarbons formation. The theories visualize thermocatalytic petroleum formation, a process dependent on temperature and depth of burial. Because [geo] thermal gradients vary considerably, it follows that petroleum genesis will take place at varying depths. Some authors consider process to have occurred in two stages; biochemical followed by geochemical (physicochemical) reactions. Studies of bacterial activity indicate, however, that this process alone is incapable of producing petroleum hydrocarbons other than methane; similarly, radioactive disintegration reactions are incapable of forming petroleum. Petroleum formation at shallow depths (1 km) is a very slow process; some investigators believe that petroleum genesis requires from 1 million to 10 million years. Dobryansky (1948) believes petroleum hydrocarbons to have evolved by a series of m metamorphisms, from aromatic to naphthenic to paraffinic compounds.

Aspects of hydrocarbon formation in recent sediments are reviewed: much significance is attached to the 1954 work of Smith on hydrocarbon occurrence in Recent sediments. In the Soviet Union, Vassoyevich (1955) has also done work along these lines; he does not consider the dispersed hydrocarbons ("micropetroleum") in Recent sediments to be the same as hydrocarbons synthesized by living organisms.

General considerations on conditions of gas and oil accumulation involve discussion of gas and petroleum accumulation which have been dispersed in argillaceous, arenaceous, and carbonate rocks.

Natural-gas and petroleum accumulation during vertical migration leads to consideration of various structural-geologic conditions causing their entrapment. Bibi-Eybat oil field in the Apsheron peninsula is a good example of a multilayered oil field where migration apparently has extended vertically over considerable distance. Natural-gas and petroleum accumulation in horizontal deposits indicate that in this instance petroleum migration is not extensive, and is largely controlled by changes in lithology. Natural-gas and petroleum dispersion, as treated is primarily a discussion of factors which lead to natural gas dispersion by processes of diffusion and bulk flow. In addition, petroleum dispersion by bulk flow is mentioned.

Some of the author's main points are covered in the conclusions.

For the reader's convenience, the reviewers have included general bibliographic information, tables, and figures of the original work; by chapter:

Chapter	Tables	Figures	References
I	11	7	53 (3 American)
II	11	33	41 (4 American and 1 French)
III	2	20	47 (25 American and 1 French)
IV	2	6	30 (4 American)
V	3	1	53 (4 American and 1 German)
VI	2	3	46 (10 American and English, 4 German, 2 French, and 1 Italian).
VII	6	24	42 (3 American)
VIII	1	8	92 (16 American and 3 German).

Markovsky, A. P., chief editor, GEOLOGIC STRUCTURE OF THE U. S. S. R.: volume I, Stratigraphy, edited by N. K. Ovechkin, 588 p.; volume II, Magmatic Processes, edited by Yu. I. Polovinkina, 331 p.; volume III, Tectonics, edited by L. I. Krasny, 384 p.[1] A review by Eugene A. Alexandrov.[2]

This publication was prepared by the All-Union Geological Research Institute of the Ministry of Geology and Conservation of Mineral Resources (VSEGEI) of the Soviet Union. Participating in the preparation of these volumes were 116 geologists employed by the institute, and 41 scientists from other organizations of the Ministry of Geology, the Academy of Sciences, and the Ministry for Higher Education. The authors and editorial staff attempted to present facts in detailed, yet relatively concise,

---

[1] Geologicheskoye Stroyeniye SSSR, Gosgeoltekhizdat, Moscow, 1958. Price of volume I is 55.70 rubles; volume II, 23.15 rubles; and volume III, 29.75. In the United States three volumes are available (in Russian) for about $17.50. Volume I is supplemented by a geomorphologic and a geologic (2 sheets) map at 1:15,000,000 and 1:7,500,000, respectively.

[2] Department of Geology, Columbia University, New York.

form. Controversial points of view are considered objectively. Although it is recognized that certain differences of opinion occur where problems are interpretation, interpreted by different authors, maximum uniformity in presentation of this material seems to have been achieved.

STRATIGRAPHY

Basic Outlines of the Geomorphologic Structure of the U. S. S. R.

The major portion of the Soviet Union is composed of plains and plateaus, represented by the Russian platform, the east European plain, and the western Siberian lowland. Examples of plains developed on crystalline surfaces, are described, as well as accumulative and denudation plains and plateaus. Features of the continental bank along the Arctic coast are outlined. Mountains and highlands occupy approximately 15 percent of the territory of the Soviet Union. The highest and most extensive mountain ranges are located along the southern borders of the Soviet Union; they form an almost uninterrupted framework around the Russian and Siberian platforms. These complex elevations include the Caucasian, Crimean, Kopet-Dag, Pamir, Kamchatka, Kuril, and Sakhalin ranges, as well as the Ural, Tien-Shan, Altai, and western and eastern Sayon mountains. The mountain uplifts are classified according to the character of their basement, which may be folded, monoclinal, crystalline, or horizontally bedded.

The Geologic Regions of the Soviet Union

The age of tectonic movements was taken as the basis for differentiation of the natural elements of the geologic structure of the country; these movements caused the transformation of geosynclinal regions to platforms. The main structural elements of the Soviet Union represented by ancient platforms, generally considered to be the Russian and Siberian platforms: regions of late Proterozoic orogeny and epi-Paleozoic platforms, including the southern Urals and western Siberian lowland, extend into Kazakhstan, central Asia, the Caucasian foreland, the Stavropol plateau, the Donets basin, and northern Crimea; regions of Mesozoic orogeny and epi-Mesozoic platforms encompass, for the most part, northeastern U. S. S. R., particularly the Baikal, Amur, Sikhota-Alin, and southern Primorsky areas, as well as regions in southern and eastern Russia of Cenozoic orogeny with Recent geosynclines. Central positions are occupied by the Russian and Siberian platforms. The area separating these platforms and surrounding land, on the continent and offshore, is represented by younger folds. The Cenozoic orogenic regions are located in the south and the Far East, following the outlines of the Mesogean (Tethys) geosynclinal sea to the Pacific Ocean. The Mesozoic orogenic structures form the eastern frame of the Siberian platform; orogenic zones of Precambrian and Paleozoic age, located between the Russian and Siberian platforms, form the southern frame.

The Russian platform occupies almost the entire territory of European U. S. S. R. and extends west- and northward to Poland, Finland, and Sweden. Main structural elements of this platform are shields, anteclises, swells, syneclises, and depressions. The platform, excepting the Baltic shield and the Ukrainian massif areas is covered with sedimentary rocks; the latter range in thickness from 100 to 4,000 meters. In the northwestern areas of the platform, sedimentary rocks are of Devonian and lower Paleozoic ages, in the southern and southwestern areas, Mesozoic and Cenozoic sediments predominate.

The Siberian platform occupies the region between the Yenisei and Lena rivers; the Aldan shield and the ancient Anabar crystalline massif form its major structural elements. The Tunguska syneclise, paralleling the western border of the platform, is filled with deposits ranging in age from late Precambrian (Sinian) through Lower Triassic, inclusive. The Vilyuy syneclise located on the eastern side of the platform, is filled mainly with Mesozoic deposits.

Late Proterozoic and Paleozoic orogenic belts and epi-Paleozoic platforms occupy the area between the Russian and Siberian platforms, Kazakhstan, and central Asia. Farther to the east, the orogenic belts extend into China; the mountain ranges of western Siberia, Altai, and the Transbaikal region. The western continuation of the Ural and central Asian Paleozoic structures can be followed into the Caucasian foreland, the Donets basin, and northern Crimea. Evolutionary development of major structural features of these areas is given chronologically.

Regions of Mesozoic folding occupy vast territories of northeastern U. S. S. R., particularly the Transbaikal and Soviet far eastern areas; Mesozoic structures, as a whole, belong to the Pacific orogenic belt. Cenozoic folds and Recent geosynclines are known only in southern and eastern U. S. S. R. The southern structures are related to the Mediterranean geosynclinal belt; the eastern, to the Pacific geosynclinal belt.

Stratigraphy

Stratigraphic study of sedimentary deposits outcropping in the Soviet Union, is reviewed historically from the end of the 18th century to the present; stratigraphic criteria which serve as guides for exploration of new mineral deposits, are examined. At present, Russian stratigraphers are concentrating on unifying all

available stratigraphic data for the country and are preparing general correlations over the entire Soviet Union.

In the first volume of this work, the outline of stratigraphy was compiled from a large number of publications and manuscripts: Each system is described on a regional basis, except for the oldest (Precambrian) formations which are undifferentiated. In general, the following major geologic and geographic regions are considered in the description of systems and, infrequently, smaller stratigraphic divisions: 1) Russian platform and the Donets basin; 2) the Urals and Novaya Zemlya; 3) the Carpathians, Crimean, and Caucasian mountains; 4) central Asia; 5) the geosynclinal regions of Kazakhstan; 6) the western Siberian lowland and the Turgay depression; 7) mountains and intermontane depressions of western Siberia; 8) the Siberian platform; 9) the Taymyr peninsula and Soviet arctic islands; 10) the Transbaikal region; 11) the Far East; 12) the northeast; and 13) Sakhalin and Kamchatka.

Precambrian intrusives and metamorphosed sediments extending far to the southeast over the greater part of the Soviet Union, form the foundation of the Russian platform. In the northeast, outcrops of granitic intrusions, including the unique rapakivi granites, and nonmetamorphosed epicontinental sediments deposited on the borders of the foreland comprise the Karalia and Kila peninsula terrain. Other Precambrian outcrops, mainly schists, are evident in the Ukrainian massif and the cores of ranges in Kazakhstan, central Asia, Taymyr and the Soviet arctic islands, Transbaikal, and other areas. For the most part, Paleozoic sediments are represented by Devonian through Permian marine deposits. The Old Red sandstone with marine intercalations occurs north of Moscow. In central Russia, the continental facies of Baltic sandstones is replaced by marine facies. Hercynian deposits, coal measurements of the Donets basin, are typically geosynclinal in the Urals. Permo-Carboniferous marine deposits are extensive; then occur throughout the Caucasus, central Asia, the Kuznets basin, the Sikhota Alin mountains, and Vostok [Ed.: North East].

The Alpine Triassic extends into the Carpathians, the Crimea, and the Caucasus. Liassic seas did not cover the Russian platform; far to the south, only, are traces of the oldest Jurassic seas. The Cretaceous although thin, is widespread. During the Cenozoic, marine sediments from the Mesogean sea throughout southern Russia, and in other areas, continental sediments were deposited; the latter, Quaternary glacial, and nonglacial deposits.

Description of each system includes an introduction, characteristics of deposits from separate regions, correlation of principal cross sections, summarization of major mineral deposits associated with formations of that system, and main problems involved in further study of the system. Regional stratigraphic descriptions of each system were written by separate authors. They include information on lithology, change of lithology of formations within specific areas under study, source of sedimentary material, and index fossils. Evolution of sedimentary basins is analyzed paleogeographically and tectonically. Correlation charts accompanying each system are less extensive than charts prepared by the Committee on Stratigraphy of the National Research Council in the United States.

Appendix to Volume I

In 1957, a geologic map of the U. S. S. R., on the scale of 1:7,500,000, was published (in 91 colors) prior to the publication of the first volume; it was edited by D. V. Nalivkin. This represents the handiest and most elaborate map of a large country accompanying a book. The legend reflects the lower, middle, and upper divisions of each system; shown on the map, are certain stages of the Devonian, Permian, and all stages of the Tertiary periods. Adequately translated, this map should be a valuable contribution to the study of world geology.

The second map on the scale of 1:15,000,000, outlines the geomorphologic structure of the Soviet Union: Flatlands and plateaus, mountains and highlands folded and crystalline basements, elevations, and deeps are represented. The map, compiled by G. S. Ganeshin and S. V. Epshteyn, geomorphologic text in volume I. This map is equally as useful as a supplement to the entire three-volume work; major topographic features of the earth's surface are indicated.

MAGMATIC PROCESSES

The relation of petrogenetic processes in time and space are summarized in the introduction to this volume by Yu. I. Polovinkina, who excellently presents the account of achievements of Soviet scientists in this field, and summarizes the essence of Russian petrologic philosophy.

Enormous granitoid massifs of varying composition, associated with migmatites, are known to occur in the Soviet Union; migmatites have been studied extensively in the Aldan and Baltic shields, in the Ukraine, and in the Urals. It is suggested that many granitoids were formed in situ, and of metasomatic origin. Geologic age of the granitoids ranges from Precambrian to Cenozoic. The anorthoclase-bearing granitoids of the main Caucasian range and the Pambaksky mountains of Armenia should be mentioned among the younger Tertiary rocks, as well as various granitoids from the extreme northeastern areas: Kamchatka, the Kuriles, Sakhalin, and the Koryaksky upland.

Basic magma is represented by spilitic formations, which are Silurian in the Urals; Precambrian in Karelia, the Ukraine, and Kazakhstan; and Mesozoic in the Crimea. Basalt effusives occur in the Transbaikal region, Armenia, the eastern Sayon mountains, Tuva, and Kamchatka. The Mesozoic trap formation occupies almost the entire Siberian platform. The Urals represent a classic region of basic and ultrabasic intrusive rocks which contain platinum-bearing and gabbro-peridotitic belts. Gabbroid and ultrabasic rocks form the ophiolitic belts of the Caucasus, Kamchatka, the Kalbin range, and Sayan-Altai mountain system, the Ukraine, and other regions. Ultrabasic intrusions and associated mineralization outcropping in the Kola peninsula have been the subject of careful studies. Of great interest are the large gabbro-anorthosite bodies within Proterozoic formations of the Aldan shield, the Dzhugdzur and Stanovoy ranges, and smaller massifs of the Ukraine. In recent years, kimberlites have been discovered in the Siberian platform; at least some of these are diamond bearing rocks.

Feldspathoid rocks, of varying composition are widespread in the Kila peninsula, the coastal region surrounding the Azov sea, the Urals, Kazakhstan, the Kuznets basin, Tannu Tuva, eastern Siberia, Transbaikal, and Minusinsk basin, Aldan, Sakhalin, and Taymyr. Shonkinites and other alkaline gabbroic rocks have been found in Khibiny, northern Tien-Shan mountains, Talassky Alatau, and Aldan. Camptonites and monchiquites occur in the Donets basin, the Ukrainian crystalline massif, Khibiny, and Berdyansk. Alkaline basaltic rocks have been found in Tien-Shan, the Transcaucasian region, and the Far East.

Boreholes drilled to establish the nature of deep-seated structures, have yielded some information on magmatic phenomena occurring below the sedimentary cover; areas within the Precambrian basement of the Russian platform and in the Paleozoic basement the western Siberian lowland were investigated.

Evolution of magmatic processes in the Soviet Union is considered in relation to structural evolution of the earth's crust, from the historical aspect, during the Precambrian, lower Paleozoic, Mesozoic, and Cenozoic magmatic epochs. Almost all descriptions of the regions were prepared using data from field studies conducted by the authors. The petrographic terms, proposed by A. N. Zavaritsky in 1955, are used where agreement could not be reached on the use of other terms. Mineralogic composition is indicated only in descriptions of rare rocks; chemical characteristics of complexes are given in general form without analytical data. Characteristics of magmatic complexes are considered with reference to the corresponding evolution of the region in which they occur, accompanying metamorphism, and endogenetic mineralization.

Magmatic processes are intimately related to tectonics: association of definite magmatic complexes with different evolutionary stages of tectogenesis is one of the basic principles in the study of magmatic rocks; a second basic principle is the general trend of development in magmatic processes and their irreversibility. The history of the evolution of magmatic processes within the Soviet Union is analyzed according to these principles.

Platforms and labile belts are considered in the analysis of magmatic processes, as two basic types of crustal-structure elements. Orogenic region, geosyncline, and geosynclinal region are used almost as synonyms of labile belt; the terms, geosyncline and orogenic region, are applied to the earlier and the later periods respectively, of labile belt evolution. A labile belt embodies not only zones of geosynclinal downwarping, but also the adjacent and peripheral geanticlinal zones. The term magmatic complex, as used in this work, corresponds to a natural group of paragenetically associated rocks characterized by: peculiarities of composition, definite localization during development of the labile belt, conditions of formation, and character of metallogeny. Material recorded in the field indicates that this definition may be applied not only to associations of intrusive rocks, but to effusive rocks and mixed groups as well, where both intrusive and effusive rocks are paragenetically associated. Magmatic cycle, as used here, indicates the entire association of magmatic phenomena during labile belt evolution, beginning with the incipient stage and terminating with the platform-formation period.

Derivatives of basic and ultrabasic magma; spilitic and keratophyre-spilitic-effusive and ophiolitic-intrusive complexes, develop during early stages of labile-belt evolution. Diorite-granodiorite complexes of higher acidity, are formed toward the end of the early stages. Plagiogranites and diorites represent evidently, granitoidal differentiates of basic magma. These rocks are genetically associated with the early stages of labile-belt evolution. In many regions, however, relation of these rocks to granitoids of the middle stage is established. During the middle stage, large granitoid batholiths develop concomitant to folding, at subsidence of folding, or immediately thereafter. The more basic granitoids form small, prebatholithic intrusions. Moderately acid granitoids are developed earlier than acid and ultra-acid granites.

The late and conclusive stage of labile-belt evolution is characterized by intermediate and acid effusives, and by near-surface intrusives of the same composition; the intrusives may be more alkaline. Large masses of batholithic

granitoids are formed. During the conclusive stages of magmatic process, basic and ultra basic intrusions are emplaced again.

Magmatic processes of platforms are generally less well studied than those operative in labile belts. Basic magmas dominate to a considerable degree whereas derivatives of granitoids magmas play a relatively subordinated role. Mesozoic traps of the Siberian platform and Cambrian traps of the Russian platform are both magmatic formations of this type. Another feature of the platform type of magmatic activity is the more intensive differentiation of intrusive and effusive formations; from the effusives, a complicated series of derivatives ranging from picritic porphyrites through basalts to phonolitic porphyrites may result. Presence of alkaline derivatives and kimberlites is a characteristic feature of the platforms. Most characteristic of platform magmatic activity is the intimate relation of intrusives and effusives, the hypabyssal or even subvolcanic character of intrusive bodies. Lava effusives on platforms, predominantly terrestrial, are rarely subaqueous.

All types of magmatic activity characteristic of labile belts and platforms are outlined and analyzed according to four major geologic-epoch groupings: Precambrian, lower Paleozoic, upper Paleozoic, and Mesozoic and Cenozoic. Summarization for each magmatic epoch is presented in the form of concise tables. Information on regional petrology is given in detail; and, on mineralization accompanying each stage of magmatic activity. Earlier studies on petrologic phenomena in the areas considered; are credited; some sources date back to the middle 19th century.

It is concluded that some of the igneous rocks are associated predominantly with formations of definite geologic age. Magmatic formations are related to tectonic zones with a definite type of development. Archean and Proterozoic magmatic activity is recognized in the Soviet Union, particularly in the Baltic shield area where ancient amphibolites, granulites, granites, peridotites, keratophyres, and other types crop out. The Ukrainian massif is composed, generally, of Archean and lower Proterozoic pyroxenites, granodiorites, gabbros, metasomatic granites, and rapakivis. Precambrian magmatic activity in Kazakhstan and the Altai-Sayan system is confined relatively to upper Proterozoic granitoid intrusives. Upper Proterozoic diabase occurs in the Yenisei area.

Spilites are the most common expression of lower Paleozoic magmatic activity in the Urals; diabase predominates in Kazakhstan; and, porphyrites, tuffs, granites, and gabbro-peridotites occur in the Tien-Shan range. Upper Paleozoic magmatic activity is represented in part, by Devonian andesite-basalts on the Russian platform. Upper Carboniferous nepheline-syenites occur in the Donets basin area. Upper Paleozoic granitoids crop out in many areas including the Great Caucasus and the Urals. Among the igneous components of Tien-Shan are upper Paleozoic porphyrites; of Pamir, diorites; and of the Altai-Sayan system, alaskite.

Representative of Mesozoic and Cenozoic magmatic activity are: Permo-Triassic liparites in the Turgay region; upper Mesozoic basalt and andesite in Kazakhstan; Neogene and Quaternary basalt in Tuva; Mesozoic granite and quartz diorite in Pamir; Neogene andesite- and trachy-basalts, as well as Mesozoic monzonite, diorite, and lamprophyres in the Transbaikal region; and Cenozoic granitic intrusives and extrusives, including Quaternary dacite and liparite extrusives, and basaltic and andesitic lavas in the Far East.

Much attention is paid to the role of deep faults. The review of magmatic processes in the Soviet Union considers their relation to regional geotectonic evolution. The editor admits that certain regional petrographic studies are incomplete: these studies should be conducted simultaneously with the geologic survey, on the scale of 1:200,000.

Correlation of magmatic processes occurring in different regions is impossible without an elaborate study of magmatic formations. Although spilitic (keratophyre-spilitic), ophiolitic, andesite-basaltic, liparite-dacitic, trap, diorite-plagiogranitic, granodiorite-granitic, nepheline-syenitic, alkaline basaltoids, and others have been roughly established; it is admitted that these formations have not been studied adequately, especially with respect to their geologic position, tectonic relation, petrographic composition, cause of changes in composition, role of metallogeny, and many other features. Future studies will be concerned mainly with regional tectono-magmatic analysis. Metallogenic-forecast maps will be compiled on the basis of regional petrographic investigations and study of magmatic formations. An additional problem concerns outline and study of petrographic and metallogenic provinces of the Soviet Union.

TECTONICS

The first part of the third volume is a review by region of tectonics of the Soviet Union; included are descriptions of ancient platforms, folded regions, and younger platform structures. In the second part, basic features of orogenic development are discussed including activity during the Archean and Proterozoic eras; Paleozoic, Mesozoic, and Cenozoic eras; and Recent orogenic activity.

Within the boundaries of the Soviet Union, major structural elements are represented by

platforms (the Russian, and Siberian); numerous folded regions of different ages, particularly the present-day mountain ranges, Kamchatka and other regions of contemporaneous volcanism; island arcs; and deep-sea depressions.

At the present time, studies in tectonics follow the path blazed some 75 years ago by Russian geologists. In the early 1930's, a series of much-discussed schemes of tectonic structure were elaborated and made public by Tetyayev, Arkhangelsky, Shatskiy, and others. Tectonic maps were published in 1955 on the scale of 1:500,000, and, in 1956, on the scale of 1:2,-500,000.

Results of geophysical studies, deep drilling for exploration of regional geologic structure, and application of aerial photography have been used in detailed studies of structural geology. Special attention is paid to those recent tectonic movements responsible for present surface-relief features. This branch of structural geology has practical application in engineering geology and in prospecting for placer deposits.

The regional review of tectonics does not cover uniformly the entire Soviet Union. Tectonics of regions such as the eastern Carpathians, Crimea, the Caucasus, the Urals, and, to a certain extent, the Russian platform, are described briefly: literature already published covers these regions. Emphasis is placed on Paleozoic through Recent crustal movements in Asiatic U. S. S. R., particularly in the eastern and Pacific coastal regions. Data on stratigraphy, magmatic processes, and tectonics serve as a basis for interpretation, historically, of geologic and tectonic evolution.

The editor of this (third) volume admits the disagreement of different authors concerning application of tectonic terms; also accepted are those appearing on the tectonic map of U. S. S. R., on the scale of 1:5,000,000, published in 1956. Approximately 40 authors participated in preparation of material for the tectonic volume, thus involving differing approaches to tectonic problems and terminology; in certain cases, where terms had been ascribed to particular authors, no changes were made. A special commission of the U. S. S. R. Academy of Sciences is responsible, now working on unification of tectonic terminology.

The most extensive structures of planetary magnitude [Ed.: Apparently analogous to first-order geographic features.] are called belts, for example, the Mediterranean and Pacific belts. Lesser, folded structures of a regional, more or less independent nature are termed fold regions; these regions may be subdivided into fold systems. Epochs of folding are classified according to geologic chronology, that is in terms of early Paleozoic, late Paleozoic, Mesozoic, and Cenozoic. In some reviews, Caledonian, Hercynian, and Alpine are used also to date tectonic activity. Stable uplifts within fold (geosynclinal) region boundaries covered by a relatively thin sedimentary sequence or relatively stripped of sediments, are called middle massifs. The terms "platform mass" or "rigid mass," are applied to little-studied areas where structures of middle-massif type are assumed to exist. Major branches of orogenic systems adapted to the contours of middle massifs are "branches" of an orogenic (geosynclinal) region. Intermontane downwarping corresponds approximately to the "relict geosyncline." Mega-anticlinoria and megasynclinoria include anticlinoria. Uplifts within the ancient platform structures are called shields (for example: Baltic, Aldan), or crystalline massifs (for example: Ukrainian, Anabar). There is a tendency to apply to however, the Aldan shield and the Anabar crystalline massif the term anteclise (Spizharsky). In general, anteclise designates an uplifted area between syneclises. Downwarpings are marginal, intraplatform, foreland, inherited, and superimposed.

Each major orogenic region is illustrated by a black and white tectonic map on a separate plate. Orogenic evolution previously discussed, is interpreted according to the structural features of the area, analysis of sedimentary facies (functions of orogenic movements), magmatic activities with associated metamorphism and metallogenic mineralization, and volcanism.

CONCLUSIONS

No major works on the geology of the Soviet Union have been published since the 1930's. Except the more voluminous Geology of the U. S. S. R., edited by P. Ya Antropov, these three volumes are the most up-to-date summary of all geologic data available. For at least another decade, it will remain the best available reference book on geology of Russia. An economic geologist will find all three volumes of interest; some information is included on mineral deposits and metallogeny. A search through the pages of all three volumes would not yield information on location and type of mineralization of Russian uranium deposits; uranium still remains classified in Soviet literature.

The editors and authors to avoid overloading this work, did not include reference lists in their contributions. References to certain outstanding scientists are made in the text; these, however, do not substitute for conventional bibliographic lists. Despite the concomitant increase in size, addition of an alphabetical index to this work would be desirable. There is no doubt that a foreign reader with an adequate reading ability in Russian, will find this work to be a great help in studying regional geology and theoretical aspects of petrogenesis and tectonics,

as understood and presented by our Russian colleagues. It would not be practical to recommend a translation of this voluminous work. In addition to geological texts available on various individual regions, a more concise text on the geology of Russia is needed.

[Ed.: Nalivikin is preparing a more concise work on the geology of the Soviet Union which Tomkeieff will translate.]

SOVIET BLOC INTERNATIONAL GEOPHYSICAL YEAR INFORMATION: U. S. Dept. of Commerce, Office of Technical Services, December 12, 1958, p. 5-9, 10-14.[1] Information on Soviet bloc activities in the International Geophysical Year program are abstracted or translated in full from foreign-language publications and are published by the Office of Technical Services. The reports of Soviet gravimetric, glaciologic, and arctic and antarctic investigations reprinted here are the three earth-science contributions to the publication containing information on developments in six scientific disciplines.

PROBLEMS ON REDUCTIONS OF GRAVITY DATA

The problem involving reduction of gravity data was encountered by Ye. B. Adzhimamudov [1] in compilation of gravimetric maps for the territory of Armenia. Two particular aspects of this problem are considered, namely: Use of a statistical reduction, and use of differential density in the introduction of Bouguer corrections.

Glenn's reduction, introducing both topographic reductions for nearby zones and isostatic reductions for the remainder, was discarded in favor of a more simplified reduction proposed by Ye. N. Lyustikh, in the following order: 1) local topographic reduction, 2) statistical reduction, and 3) Bouguer's reduction (less correction for relief). The author followed Lyustikh's method to compile maps of gravitational anomalies using Bouguer's reduction (for average density of the intermediate layer: $\sigma = 2.67$), and statistical reduction.

Corrections for local relief were calculated at four points located in different relief conditions, to explain the possible magnitude of influence which relief might exert on the gravitational field; also, this was done to ascertain the expediency of using statistical reduction.

Comparative values of Bouguer anomalies for local relief, Bouguer anomalies with corrections for local relief, and statistical anomalies are given in a table. This presentation shows the usual Bouguer anomalies to differ much less from Bouguer anomalies with corrections for local relief, than from the statistical (with the exception of the one point: 4) the magnitude of this divergence depends on conditions of relief, not on altitude of individual points. B. K. Balavadze [2] also confirmed this fact.

An objection to the use of Bouguer anomalies is based on the argument that this method does not take into account the effect of rock lying above sea level; because the average density of rock in the intermediate layer is not known with sufficient accuracy, introduction of Bouguer corrections into values of certain anomalies would inject an arbitrary element. In Bouguer corrections, however, of the total mass lying above sea level, only the "normal" mass is eliminated; the effects of anomalous masses are retained. Objections relevant to introduction of usual Bouguer reductions lack validity where, as in this case, one value for average density is used for the intermediate layer; the stated objections relate, rather, to the method of calculating Bouguer anomalies using a value of actual density for each point. The latter method assumes knowledge of the density throughout the region being studied, over a geologic profile of an area taken from the earth's surface down to sea level; this information, in many cases, is the particular aim of the investigation.

On the assumption that actual density of the intermediate layer were taken successfully into consideration, an anomaly would be obtained reflecting the distribution of masses located only below sea level. Thus, certain geologic structures would show the sea-level surface to be divided into two parts; accordingly, there would be only partial representation on a gravimetric map. Consequently, introduction of actual density cannot be justified from this viewpoint.

GLACIOLOGICAL WORK ON THE FEDCHENKO GLACIERS

The IGY program of the Academy of Sciences of Uzbek S. S. R. included investigations on the Fedchenko glacier [3]. Organized in 1957, the expedition was staffed by scientists and technical workers from the V. I. Romanovsky institute of mathematics and mechanics, associates of Leningrad and Moscow universities, the Institute of Geography of the U. S. S. R. Academy of Sciences, and Chinese and Polish scientists.

Under exceptionally unfavorable meteorologic and glacial conditions, the expedition traveled to Fedchenko glacier by way of the nearly inaccessible Tanymas and Seldara river valleys. Shortly after its arrival at the glacier, the expedition set up two new scientific stations, augmenting the hydrometeorologic observatory previously established in the central part of the glacier. One of the new stations was established

[1] PB 131632-44.

in the firn region of the glacier, at an altitude of 4,900 meters (m); it is the highest winter station in the U. S. S. R. The other station was located on the glacier terminus, at an altitude of 3,000 m. These two stations were named Vitkovsky glacier (upper station) and Fedchenko glacier (lower station).

In addition to organization of the winter stations, seasonal work on the glacier was in progress. Expeditionary teams have explored the lower and upper areas of the Fedchenko glacier and its larger tributaries: the Kashal-Ayan, the Bibachny, the Maly Yanymas, and Lednik (glacier). Seven traverse lines of direction were extended to determine ice movement rate. Drilling through the ice to determine thickness and structure peculiarities and temperature pattern of subsurface layers, was the first work to be done. Teams of scientists from Leningrad university conducted meteorologic, actinometric, and hydrologic observations on the glacier itself and on surrounding regions.

The winter stations are continuing work already started in connection with the IGY program. During the entire wintering-over period, regular radio communications were maintained; meteorologic data from the winter stations were transmitted four times per day to the general synoptic network. [Ed.: Complete translation].

DEVELOPMENT OF GLACIATION IN THE ANTARCTIC

The first party of the Soviet Complex Antarctic Expedition wintered in the Antarctic during the 1956-1957 season [4]. Thickness of the ice sheet was measured on the continent and on the adjoining islands of Drygalski, Mill, and Bowman; a portable 12-trace seismic station, made by the Swedish firm ABEM, was used to measure depth by registering initial reflected waves. The average propagation speed of longitudinal waves was considered to equal 3,750 m per second. This speed was obtained by core sampling an 86-m drill hole, and calculated using the reflected-wave hodograph of an uninterrupted 1,750-meter profile.

Ice-thickness measurements taken of the Antarctic ice sheet along the Mirnyy-Pionerskaya profile enabled scientists to construct a cross section extending over 100 kilometers (km). (the cross-section diagram appears in the original article.) The cross section shows clearly that 154-m thickness at the glacier boundary in the Mirnyy area, increasing toward Pionerskaya, reaches 1,650 m at a distance of 100 km; in other words, there is a tenfold increase in thickness. With the exception of the 75-km point, the subglacial bed is below sea level along the entire length of the profile, in relation to sea level its average depth is 225 m.

Along the indicated profile the glacier surface rises toward the south; at 100 km, it reaches an altitude of 1,405 m above sea level. The nature of the surface varies over the entire profile; a dense network of "movement crevasses" covers the marginal area of the glacier from Mirnyy to a distance of 20 km. The crevasses, perpendicular to the main direction of glacier movement, bear witness to the great speed of this movement. Toward the south, indications of rapid movement disappear and no crevasses are observed beyond the 20-km point.

Snow-measurement observations, conducted by expedition members L. D. Dolgushin and Yu. M. Model, proved annual precipitation, which forms a snow-accumulation layer on the glacier surface, to decrease gradually toward the south. Maximum accumulation of precipitation, fallen or carried over as drifting snow, occurs in the area between the 4- and 20-km points. There, the average snow accumulation reaches 166 centimeters (cm) during the winter; while from 40 to 50 cm only, of snow accumulation, with an average density of 0.42 grams (g) per cubic centimeter, is recorded in the area between the 75- and 100-km points. Thickness of snow accumulation decreases, accordingly, by approximately one-third or one-fourth, over a distance of 100 km from the coast into the interior; but, the amount of snow accumulation is clearly in contrast to glacier thickness as indicated by the profile. In this area, there is no ablation, by melting, of snow; even at the peak of the summer season, temperature rarely increases above the freezing point; the water forming, in such cases, appears only as interlaid ice previously infiltrated into the snow.

Heat balance in this area is sharply negative; only in a narrow 2-km coastal zone does melting play a more important part in glacier ablation.

Contrast between snow accumulation and glacier thickness may be explained as follows: Velocity of glacier movement is much greater near the glacier edge than in its interior regions; velocity of marginal areas must be great enough to cause removal not only of fallen snow, but of ice masses moving out of interior regions. As ice approaches the glacier terminus, it breaks off as icebergs and is carried into the open sea. If movement velocity were uniform along the entire profile, resulting difference in accumulation would lead to an increase in ice thickness at the marginal areas.

Formerly, it was assumed that average-elevation range of the Antarctic subglacial bed was approximately from 600 to 700 m; in agreement with the average elevation of continental surfaces on our planet. According to measurements made by the Soviet, Norwegian-British-Swedish, and U. S. expeditions, one may assume, at present, that the Antarctic central-glacier area has enormous thickness, reaching from 3,000 to 4,000 m; accordingly, in the central

parts of east Antarctica, the subglacial bed is at, or below, the world ocean level. Consequently, by assuming the average ice thickness to be from 2,200 to 2,500 m, and the extend of glacier area to be 13 million km^2, it is possible to estimate Antarctic ice reserves to range in volume from 28 to 32 million km^3. Melting of this quantity of ice would raise the world ocean surface by approximately 71 to 80 m.

In connection with the preceding statements, ice measurements made on Drygalski, Mill, and Bowman islands are of special interest: Drygalski Island is 20 km long, 10 km wide, and of 430 m maximum thickness; situated on a flat submarine shelf, the shallowest part of Davis Bank, its appearance suggests a huge cupola-shaped ice block. Cross sections of the island and Antarctica, with respect to general features, show similarity to one another; common to both are the cupola shape and decreasing ice thickness toward the margins. One may observe also a series of concentric crevasses near the island shores, a proof that ice movement as it approaches the margins, increases in velocity. Precipitation amount, apparently, is uniform throughout the island area; during the winter of 1956, a layer of fallen snow 120 cm thick, was measured on Drygalski Island; there were no signs of intense melting on the surface.

"Feeding," by precipitation, of the island glacier occurs in a very unique manner: moist sea air coming into direct contact with the cold island surface, causes intense hoar-frost formation. During the night of December 2-3, 1956, scientists on Drygalski Island observed extremely rapid formation of a thick hoar-frost layer on the island surface and on the wings of an airplane. The frost layer formed during a 2- or 3-hour period, attaining thickness from 3 to 4 millimeters. It should be noted that open-sea areas, or more correctly, huge polynya [Ed.: leads], are preserved all year in the vicinity of Drygalski Island, thereby providing for a regime of year-round "feeding."

A similar situation is observed on Mill and Bowman islands, despite the difference between their environmental conditions and those of Drygalski Island. Because the islands partially adjoin the Shackleton Ice Shelf, only half their coastline borders on open sea, as a result, the seaward-facing slope receives a larger amount of precipitation than does the slope opposite, and again, ice movement is more active on the seaward slope.

Conditions on these islands, snow accumulation and ablation, indicate that it is possible for independent glaciation nuclei to develop in Antarctic waters. Factors which might lead to ice-island formation from ice nuclei could be: Settling of a large iceberg on a bank, preservation of some portion of a broken-up shelf glacier moved down to a bank during its growth process, or some other condition initiating formation of a future ice island around an ice nucleus in the open sea.

It would be incorrect to state that formation of similar islands has no connection with the existence of Antarctica; only the presence of the huge Antarctic glacier could create favorable conditions necessary to formation of these cupola-shaped islands. Their existence and development, observed at this time, are proof that present conditions in Antarctica are favorable toward development of glaciation. Reduction and disappearance of these islands will be the first indication of Antarctic-glacier retreat and, subsequently, disappearance. Insofar as these islands represent small replicas, or working models, of Antarctica, they will react faster than the continental glacier to factors initiating reduction of glaciation in the Southern Hemisphere.

It is necessary, therefore, to conduct stationary research in order to determine exact dimensions, conditions governing accumulation, and ice balance of the cupola-shaped islands at present. During the next IGY, repetition of previous measurements conducted on these islands will make it possible to obtain more exact information on trends in development of Southern Hemisphere glaciation.

STUDY ON THE ELASTIC PROPERTIES OF ARCTIC SEA ICE

In the Cape Schmidt region, seismic methods were used to investigate elastic properties of Arctic sea ice. Observations were made in 1957 during a 6-week period extending from the middle of May to the end of June.

Research was conducted by the Arctic Institute, I. S. Peschansky laboratory, in conjunction with the Leningrad university Chair of Physics of the Earth's Crust. Seismic observations were made along with investigations of physicomechanical, such as structural and thermic, ice properties.

Explosions and mechanical impact were used to stimulate seismic-wave propagation in the ice. Elastic waves were recorded by means of an 8-trace electronic oscillograph and a seismic station; the latter consisted of a type MPO 2-trace oscillograph and transitorized amplifiers. Local and average values of Young's modulus were obtained for Arctic ice under natural conditions as were temperature relationships of elastic modulus.

REFERENCES

1. Adzhimamudov, Ye. B., K VOPROSU O REDUKTSIYAK SILY TYAZHFSTI [PROBLEM ON REDUCTIONS OF GRAVITY DATA]:

Akademiya Nauk Arm SSR, Izvestiya, Seriya Geologicheskikh i Geograficheskikh Nauk, v. 11, no. 4, p. 73-75, 1958.

2. Balavadze, B. K., GRAVITATSIONNOYE POLE I STROYENIYE ZEMNOY KORY-GRUZZII [THE GRAVITATIONAL FIELD AND THE STRUCTURE OF THE EARTH'S CRUST IN GEORGIA]: Akademiya Nauk GSSR, Izd., 1957.

3. Aleyev, B. G., GLYATSIOLOGICHESKIYE RABOTY NA LEDNIKE FEDCHENKO [GLACIOLOGICAL WORK ON THE FEDCHENKO GLACIER]: Akademiya Nauk SSSR, Vestnik, 1958, no. 10, p. 57.

4. Kapitsa, A. P., K VOPROSU O TENDENTSII RAZVITIYA OLDENENIYA MATERIKA ANTARKTIDY [ON THE QUESTION REGARDING THE TENDENCY OF GLACIATION DEVELOPMENT OF THE ANTARCTIC CONTINENT]: Nauchnyye Doklady Vysshey Shkoly, Geologo-Geograficheskiye Nauki, 1958, no. 1, p. 48-52.

5. Linkov, Ye. M., IZUCHENIYE UPRUGIKH SVOYSTV LEDYANOGO POKROVA V ARKTIKE [STUDY OF ELASTIC PROPERTIES OF ICE COVER IN THE ARCTIC]: Leningradskogo Universiteta, Vestnik, no. 4, Seriya Fiziki i Khimii, 1958, no. 1, p. 17-22.